

## IDENTIFICATION

FS1-0025122

## REVISION

1.0

AREVA Front End BG  
Fuel BL

TOTAL NUMBER OF PAGES: 177

**AREVA TN-B1 ATRIUM-11 Fuel Assembly Shipping Container Drop Analyses****ADDITIONAL INFORMATION:**

TN B1

PROJECT		DISTRIBUTION TO	PURPOSE OF DISTRIBUTION
HANDLING			
CATEGORY	TEP - Technical Report		
STATUS			

This document is electronically approved. Records regarding the signatures are stored in the Fuel BU Document Database. Any attempt to modify this file may subject employees to civil and criminal penalties. EDM Object Id: 090121678084f8e2 Release date (YYYY/MM/DD): 2016/01/04 23:41:06 [Western European Time]

Role	Name	Date (YYYY/MM/DD)	Organization
Writer	TUPPER Lawrence	2015/12/28 19:13:49	AREVA Inc.
Reviewer	ELLIOTT Kevin	2016/01/04 20:50:00	AREVA Inc.
Approver	TUPPER Lawrence	2016/01/04 23:40:57	AREVA Inc.

**RELEASE DATA:****SAFETY RELATED DOCUMENT:**

Y

**CHANGE CONTROL RECORDS:**

This document, when revised, must be reviewed or approved by the following regions:

France: N

USA: Y

Germany: N

**Exportkennzeichnung** AL: 0E001 ECCN: 0E001


Die mit "AL ungleich N" gekennzeichneten Güter unterliegen bei der Ausfuhr aus der EU bzw. in der gemeinschaftlichen Verbringung der europäischen bzw. deutschen Ausfuhr genehmigungspflicht. Die mit "ECCN ungleich N" gekennzeichneten Güter unterliegen der US-Reexport genehmigungspflicht. Auch ohne Kennzeichen, bzw. bei Kennzeichen "AL: N" oder "ECCN: N", kann sich eine Genehmigungspflicht, unter anderem durch den Endverbleib und Verwendungszweck der Güter, ergeben.

**Export classification** AL: 0E001

ECCN: 0E001

Goods labeled with "AL not equal to N" are subject to European or German export authorization when being exported within or out of the EU. Goods labeled with "ECCN not equal to N" are subject to US reexport authorization. Even without a label, or with label "AL: N" or "ECCN: N", authorization may be required due to the final whereabouts and purpose for which the goods are to be used.



N° FS1-0025122	Rev. 1.0	TEP - Technical Report	
	Page 2/177		

## REVISIONS

REVISION	DATE	EXPLANATORY NOTES
1.0	See 1 <sup>st</sup> page release date	Report ATKINS-NS-DAC-ARV-15-02 "AREVA TN-B1 ATRIUM-11 Fuel Assembly Shipping Container Drop Analyses". This report was created by ATKINS Nuclear Solutions US, under Purchase Order 1015036950 of 7/13/2015

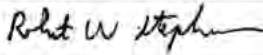
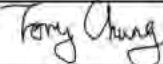
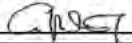



N° FS1-0025122	Rev. 1.0	<div style="text-align: center;">  </div>
	Page 3/177	

**TEP - Technical Report**



## Design Analyses and Calculation

Design Analysis and Calculation (DAC) No:		Rev. No.:		Page No.:		Total Pages:	
ATKINS-NS-DAC-ARV-15-02		Final		1		87	
DAC Title:							
AREVA TN-B1 ATRIUM-11 Fuel Assembly Shipping Container Drop Analyses							
Scoping	<input type="checkbox"/>	Preliminary	<input type="checkbox"/>	Final	<input checked="" type="checkbox"/>	Unverified Assumptions?	Yes <input type="checkbox"/> No <input checked="" type="checkbox"/>
Objective:							
<p>The purpose of this calculation is to confirm that the AREVA ATRIUM-11 Fuel Assemblies shipped within a TN-B1 Shipping Container during transportation can structurally withstand the free drops that are required by 10CFR71.71; Normal Condition of Transportation (NCT) and 10CFR71.73; Hypothetical Accident Condition (HAC) without breaching the containment boundary caused by structural failure or plastic instability. The minimum factor of safety for the ATRIUM-11 Fuel Assembly is 1.4.</p> <p>The analyses are performed using the LSDYNA finite element dynamic analysis program. The finite element model and the material properties are validated using the instrumented 30-ft (9-meter) drop test performed on the RAJ-II Certification Test Unit (CTU) at room temperature. The RAJ-II CTU has the identical geometry and total gross weight (930 kg) as the AREVA TN-B1 shipping container. The weight of the fuel contents used in the CTU test is 560 Kg. The maximum weight of the ATRIUM-11 Fuel Assembly is 684 kg. The un-instrumented container drop test with fuel weight of 684 kg was performed at National Transportation Research Center (NTRC) in Oak Ridge, Tennessee. The results are used to compare with the damages of the analytical model. The validated finite element model with the design weight is used to simulate the structural performance of the container under NCT (1.2 meter drop) and HAC (9 meter drop) at -40°F and 150°F. The temperature conditions analyzed are more conservative than the code required value between -20°F and 100°F. The calculated accelerations are used to confirm that the ATRIUM-11 Fuel Assembly shipped inside the AREVA TN-B1 shipping container retains shape and still complies with the ASME Code structural requirements.</p>							
Results:							
<p>The predicted accelerations of the accident and normal conditions drops at -40°F and 150°F are calculated and confirm that the structural integrity of the ATRIUM-11 fuel assembly is preserved with a factor of safety greater than 1.4.</p>							
Preparer (Print):		Preparer (Sign):		Date:			
Robert W. Stephenson P.E.				12/18/15			
Reviewer (Print):		Reviewer (Sign):		Date:			
Tony Chung, P.E.				12/18/15			
Project Lead Engineer/Manager (Print):		Project Lead Engineer/Manager (Sign):		Date:			
A. Bruce DeWald, Jr.				12/18/15			
		<div style="text-align: center;">  </div> <p>This calculation is prepared by Atkins Nuclear Solutions US for AREVA under AREVA Contract ANP003.</p>					
						Page 1 of 87	





## Design Analyses and Calculation

Rev.	Date	Revision Description/Reason
0	12/25/2015	Original Issue





## Design Analyses and Calculation

### Table of Contents

<b>TABLE OF CONTENTS .....</b>	<b>3</b>
<b>1. INTRODUCTION .....</b>	<b>5</b>
1.1 BACKGROUND/PURPOSE .....	5
1.2 LIMITS OF APPLICABILITY .....	6
<b>2. CONCLUSIONS .....</b>	<b>6</b>
<b>3. DESCRIPTION OF TN-B1 PACKAGE .....</b>	<b>7</b>
3.1 TN-B1 PACKAGE INTRODUCTION .....	7
3.2 STRUCTURAL DESIGN OF TN-B1 PACKAGE .....	10
3.3 WEIGHTS OF CONTAINER AND PAYLOADS .....	13
3.4 CODE REQUIREMENTS AND COMPLIANCES .....	14
3.5 IMPACT VELOCITIES .....	20
<b>4. COMPUTER CODES USED IN DAC .....</b>	<b>20</b>
<b>5. ASSUMPTIONS &amp; OPEN ITEMS .....</b>	<b>21</b>
5.1 ASSUMPTIONS .....	21
5.2 OPEN ITEMS .....	21
<b>6. ACCEPTANCE CRITERIA .....</b>	<b>21</b>
6.1 BIASES AND UNCERTAINTIES .....	22
6.2 AREA OF APPLICABILITY (AOA) .....	22
<b>7. CALCULATIONS .....</b>	<b>23</b>
7.1 TN-B1 SHIPPING CONTAINER FINITE ELEMENT MODEL .....	23
7.2 MODELING ASSUMPTIONS .....	29
7.3 MATERIAL PROPERTIES .....	30
<b>8. EVALUATION RESULTS .....</b>	<b>54</b>
8.1 VALIDATION OF FINITE ELEMENT MODEL .....	54
8.2 ACCELERATION RESULTS OF LSDYNA SIMULATED DROPS: NORMAL CONDITIONS OF TRANSPORT (NCT) .....	63
8.3 ACCELERATION RESULTS OF LSDYNA SIMULATED DROPS: HYPOTHETICAL ACCIDENT CONDITIONS (HAC) .....	67
8.4 REANALYSIS OF ATRIUM-11 FUEL ASSEMBLY REGULAR SHIPMENT .....	81
8.5 REANALYSIS OF ATRIUM-11 SINGLE FUEL ASSEMBLY SHIPMENT .....	82
8.6 PUNCTURE ANALYSIS .....	83
<b>9. DISCUSSION AND SUMMARY .....</b>	<b>83</b>
<b>10. REFERENCES .....</b>	<b>86</b>
<b>APPENDIX A MATERIAL PROPERTIES DERIVATION .....</b>	<b>1</b>
A.1 ZIRCALOY-2 .....	1
A.2 AISI 304 (SUS 304) GRADE STAINLESS STEEL .....	25
A.3 BALSA (SHOCK ABSORBER) .....	40
A.4 PAPER HONEYCOMB .....	44





## Design Analyses and Calculation

A.5 LUMBER (HEMLOCK) .....	47
A.6 ALUMINA SILICATE .....	49
A.7. POLYETHYLENE FOAM .....	50
<b>APPENDIX B RECONFIRMATION OF ATRIUM-11 FUEL ASSEMBLY STRUCTURAL INTEGRITY .....</b>	<b>1</b>
B.1 INTRODUCTION .....	1
B-2 AMPLIFIED ACCELERATION TIME HISTORIES .....	2
B.3 ACCEPTANCE CRITERIA .....	5
B.4 FINITE ELEMENT MODELS .....	5
B.5 PLASTIC STABILITY EVALUATION RESULTS .....	6
B.6 FUEL ASSEMBLY STRUCTURAL STABILITY CONCLUSION .....	9
<b>APPENDIX C. SHIPPING WITH A SINGLE FUEL ASSEMBLY IN THE TN-B1 CONTAINER .....</b>	<b>1</b>
C.1. INTRODUCTION .....	1
C.2 THE AMPLIFIED ACCELERATION TIME HISTORIES .....	3
C.3 ACCEPTANCE CRITERIA .....	4
C.4 FINITE ELEMENT MODELS .....	4
C.5 PLASTIC STABILITY EVALUATION RESULTS .....	6
C.6 FUEL ASSEMBLY STRUCTURAL STABILITY CONCLUSION .....	7
<b>APPENDIX D PIN PUNCTURE EVALUATION .....</b>	<b>1</b>
D.1 CODE REQUIREMENTS .....	1
D.2 PIN PUNCTURE ANALYSIS METHODOLOGY .....	1
D.3 PUNCTURE AND PENETRATION RESULTS .....	2
D.4 CONCLUSION OF PIN PUNCTURE .....	5
<b>APPENDIX E LISTING OF INPUT FILES .....</b>	<b>1</b>
<b>APPENDIX F VENDOR DATA SHEETS .....</b>	<b>1</b>
F.1 PRODUCT DATA SHEET OF ALUMINA SILICATE .....	1
F.2 POLYPLANK EXT DATA SHEET .....	2
F.3 DATA SHEET FOR ZIRCALOY .....	3





## Design Analyses and Calculation

### 1. INTRODUCTION

#### 1.1 Background/Purpose

The AREVA ATRIUM-11 Fuel Assemblies are designed to be shipped in the AREVA TN-B1 Container. Using the instrumented RAJ-II Certified Test Unit (CTU) drop test acceleration results [Ref. 1] which was performed under room temperature, the ATRIUM-11 Fuel Assemblies, shipped within a TN-B1 Shipping Container, have been structurally analyzed [Ref. 2] to comply with the code requirements of 10CFR71.73 [Ref. 3] of a 30-ft drop.

The structural acceptance criteria of fuel bundle under impact require that the structural elements of the fuel to maintain plastic stability. The structural elements include the fuel cladding and spacers. The criteria for fuel bundle stability evaluation is established based on the acceptance criteria of the Plastic Instability Load Analysis as discussed in ASME Boiler and Pressure Vessel Code, Subsection III, Appendix F, Section F-1341.4 [Ref. 5]. The ASME Code states that the load should not exceed 70% of the plastic instability load. The criterion for the minimum safety factor for the Atrium-11 fuel bundle stability evaluation is therefore considered to be 1.4 ( $=1/0.7$ ). The above criteria have been quantified by applying a scale factor of 1.4 to the acceleration time histories from the RAJ-II container drop test results [Ref. 1] so that the minimum factor of safety is 1.4.

The purpose of this calculation is to confirm that the AREVA ATRIUM-11 Fuel Assemblies shipped within a TN-B1 Shipping Container can structurally withstand the free drops that are required by 10CFR71.71; Normal Condition of Transportation (NCT) 4 ft (1.2 meter) drop, and 10CFR71.73; Hypothetical Accident of Transportation (HAC) 30 ft (9 meter) for temperatures of -40°F and 150°F. In addition to the required drops for NCT and HAC, sensitivity studies are performed on the variation of fuel weights, the slap down angles, and the effect of shipping a single fuel assembly. Following the Plastic Instability Load Analysis Methodology specified above, the factor of safety for the ATRIUM-11 Fuel Assembly is determined to be greater than 1.4.

The analyses are performed using the LSDYNA finite element analysis software [Ref. 4]. The finite element model of the shipping container and the material properties are validated using the instrumented 30-ft drop test performed on the RAJ-II Certified Test Unit (CTU) at room temperature [Ref. 1]. The RAJ-II CTU has the identical material, geometry and gross weight of 930 kg as the AREVA TN-B1 shipping container. The simulated weight of the fuel contents in the CTU is 560 kg. The design weight of the ATRIUM-11 Fuel Assembly is 684 kg. The validated finite element model is then used to predict the peak accelerations of the container dropped under NCT and HAC at -40°F and 150°F. The temperature conditions analyzed are more conservative than the code required value between -20°F and 100°F. Using the same design weight, the un-instrumented container drop tests were performed at National Transportation Research Center (NTRC) in Oak Ridge, Tennessee. The results of the NTRC test are also used to compare with the deformation of the analytical model.

According to TN-B1 SAR Rev. 3 [Ref. 7], Section 2.1.4, the applicable ASME Boiler and Pressure Vessel





## Design Analyses and Calculation

Codes [Ref. 5] for the material strengths are

1. Section III, Subsection ND for the containment boundary which includes the fuel cladding.
2. Section III, Subsection NG for the criticality control structure which includes the fuel assembly cages and clips.
3. Section VIII for the non-containment components which include the container shells.

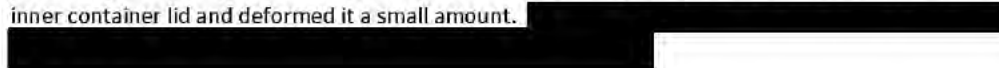


The development of the material properties used in the analyses is presented in Appendix A.

In Appendix B, analyses of the ATRIUM-11 fuel assembly for the regular fuel shipment (2 fuel assemblies) using the finite element model from Ref. 2 and calculated inner container acceleration time histories from the HAC drops are performed to reconfirm the structural integrity of the fuel assembly.

In Appendix C, analyses of the ATRIUM-11 fuel assembly for the reduced weight shipment (one fuel assembly) using the same finite element model from Ref. 2 and calculated acceleration time histories at the fuel from the HAC are performed to reconfirm the structural integrity of the fuel assembly.

The puncture analysis is performed for hot temperature condition and presented in Appendix D. The puncture pin did not penetrate the outer container. It deformed the lid inward and it contacted the inner container lid and deformed it a small amount.



### 1.2 Limits of Applicability

The TN-B1 package has been developed to transport un-irradiated fuel for Boiling Water Reactors and Pressurized Water Reactors. The cladding of the fuel provides the primary containment for the radioactive material. The inner and outer containers provide both thermal protection as well as mechanical protection from drops or accident conditions. The applicability of this report is limited to the prediction of the accelerations of the inner container during code required drops at temperatures of -40°F and 150°F; for the sole purpose of protecting the ATRIUM-11 fuel assemblies. There is no implied determination of structural integrity of the closure bolts, shipping clamps and the water tightness of the lid seals. The damages to the above items were already confirmed by the CTU drop tests [Ref. 1].

## 2. CONCLUSIONS

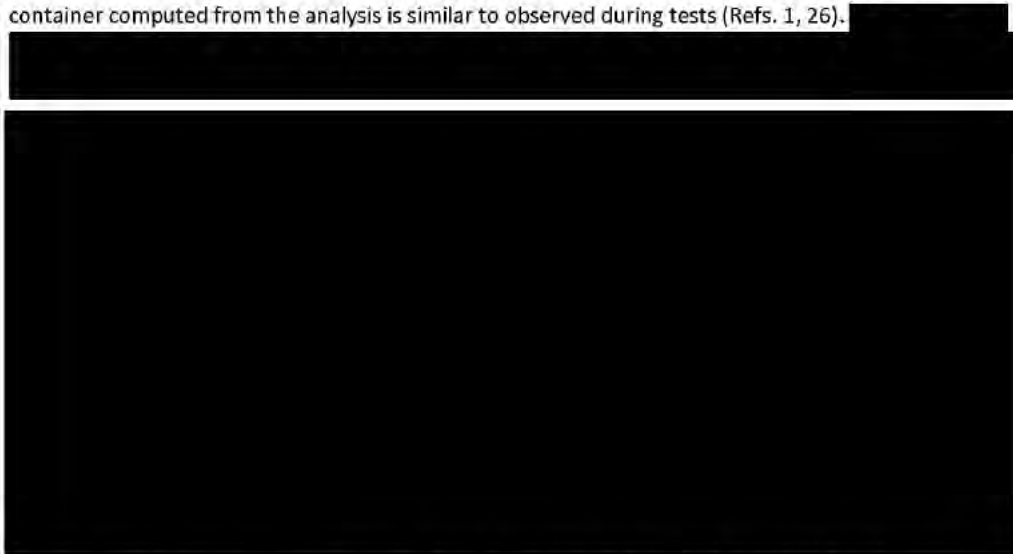
The predicted accelerations of the accident and normal conditions drops at -40°F and 150°F are calculated and confirm that the structural integrity of the ATRIUM-11 fuel is preserved with a factor of safety greater than 1.4.





## Design Analyses and Calculation

The validation study performed to confirm the finite element model used in the TN-B1 evaluation shows reasonable agreement with actual drop tests. The overall deformation and damage to the container computed from the analysis is similar to observed during tests (Refs. 1, 26).



The container and the detailed fuel assembly analyses confirm that the ATRIUM-11 Fuel Assemblies shipped within the AREVA TN-B1 shipping container deform but still maintain cladding integrity and structural stability while complying with the 10CFR and ASME structural code requirements.

### 3. Description of TN-B1 Package

#### 3.1 TN-B1 Package Introduction

The RAJ-II container [Ref. 6] is illustrated in Figures 3-1 through 3-4 below. The dimensions are in millimeter. The description of the package and the illustrations are taken from AREVA TN-B1 Safety Analysis Report, Rev. 3 [Ref. 7].



**ATKINS**

## Design Analyses and Calculation

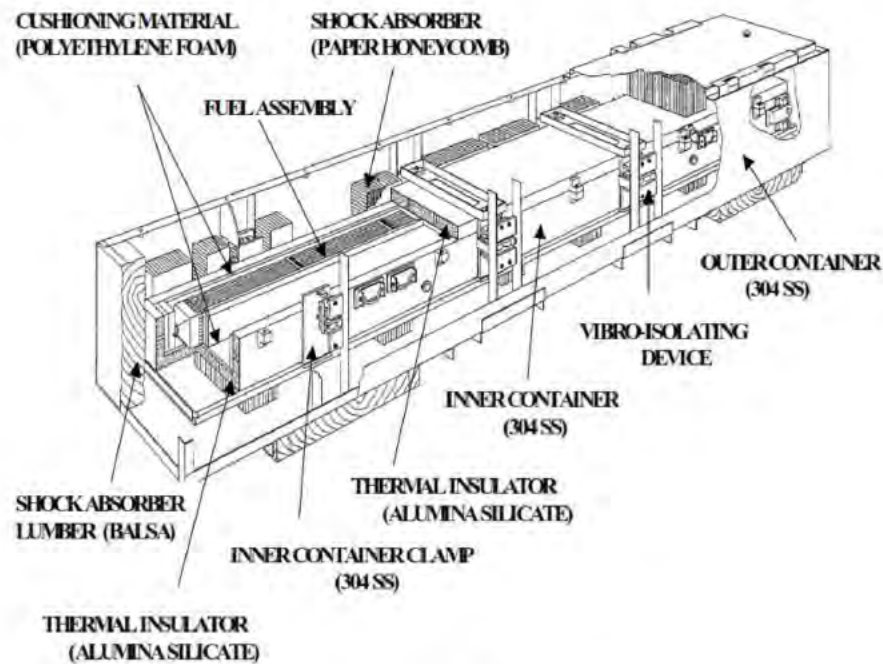


Figure 3-1 TN-B1 Package Assembly

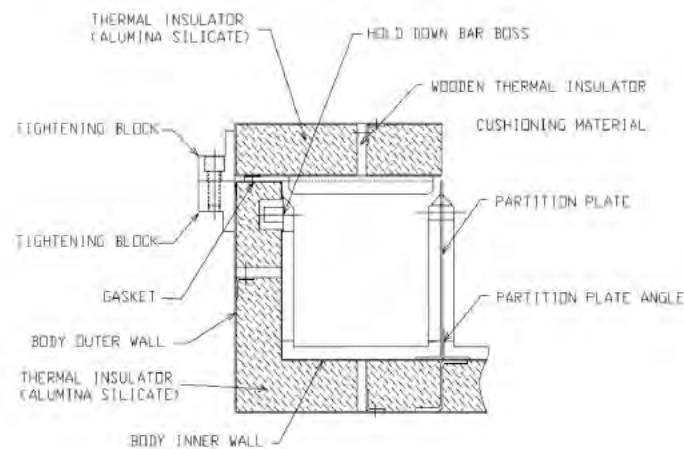


Figure 3-2 Cross Section of Inner Container





### Design Analyses and Calculation

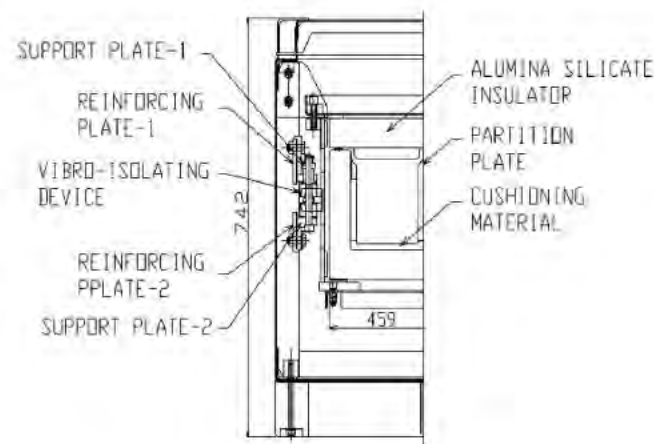


Figure 3-3 Cross Section of Outer Container

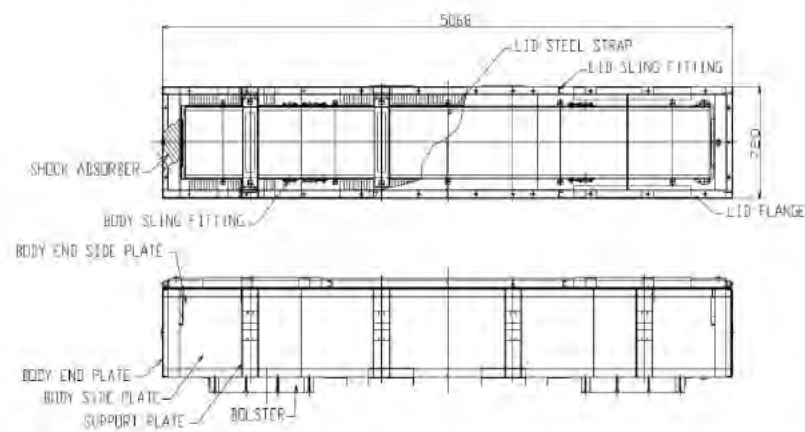
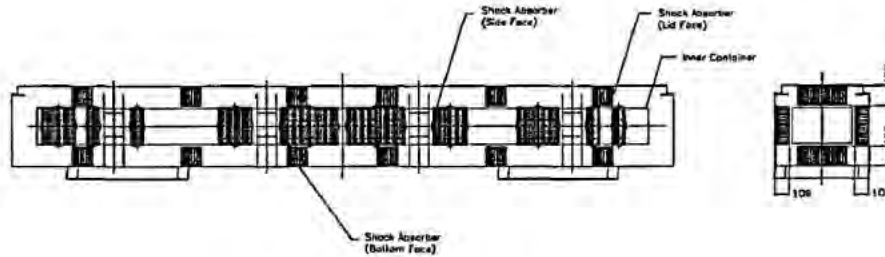


Figure 3-4 Top View of Inner Container (top figure) and Side View of Outer Container (bottom figure)





## Design Analyses and Calculation



**Figure 3-5 Shock Absorber Geometry**

The finite element model of TN-B1 package is derived from the RAJ-II package (revision 9 of NRC CoC 9309, Ref. 8) and has the identical structural design. The only difference in the current analyses is to provide justification to use the container for packaging and transporting ATRIUM-11 fuel elements.

The integrity of the fuel is maintained by the protective outer package, the insulated inner package and the fuel rod cladding through both Normal Conditions of Transport (NCT) and Hypothetical Accident Conditions (HAC) deformations. A variety of full-scale engineering development tests [Ref. 1] were included as part of the certification process. Ultimately, two full-scale Certification Test Units (CTUs) were subjected to a series of free drops and puncture drops. No accelerometers were attached to the CTU. The drop tests were performed at ambient temperature.

The payload within each TN-B1 package consists of a maximum of two un-irradiated Boiling Water Reactor (BWR) fuel assemblies or individual rods (BWR, Uranium Carbide, or generic Pressurized Water Reactor (PWR) contained in a cylinder, protective case or bundled together and positioned in one or both sides of the inner container.

### **3.2 Structural Design of TN-B1 Package**

The packaging is comprised of one inner container and one outer container both made of stainless steel (SUS304 same as AISI304). The inner container is comprised of a double-wall stainless steel sheet structure with alumina silicate thermal insulator filling the gap between the two walls to reduce the flow of heat into the contents in the event of a fire. Foam polyethylene cushioning material is placed on the inside of the inner container for protection of the fuel assembly. The outer container is comprised of a stainless steel angular framework covered with stainless steel plates. Inner Container Clamps are installed inside the outer container with a vibro-isolating device between to alleviate vibration occurring during transportation.

Additionally, balsa wood and a honeycomb resin impregnated kraft paper (hereinafter called "paper honeycomb") are placed as shock absorbers to reduce shock due to a Horizontal Drop of the package. In addition to the packaging described above, the fuel rod clad and ceramic nature of the fuel pellets provide primary containment of the radioactive material. The balsa wood is the primary energy





## Design Analyses and Calculation

dissipating component during the end drop configuration. The paper honeycomb is the primary energy dissipating component during the Horizontal Drop configuration.

### 3.2.1 Inner Container (IC)

The structure of the inner container is shown in Figure 3-2 and Figure 3-4 (top view). The inner container is comprised of three parts; an inner container body, an inner container end lid (removable), and an inner container top lid (removable). These components are fastened together by bolts made of stainless steel through tightening blocks. The inner container body is fitted with six sling fittings and the inner container lid is fitted with four sling fittings as shown in Figure 3-4. The inner container body has a double wall structure made of stainless steel. Its main components are an outer wall, inner wall and alumina silicate thermal insulator.

The outer wall is made of a 1.5 mm (0.0591 in) thick stainless steel sheet formed to a U-shape that constitutes the bottom and sides of the inner container body. A total of 14 stainless steel tightening blocks are attached on the sides of the outer wall, seven per side, to fasten the inner container lid and the inner container end lid by bolts. Additionally, six stainless steel sling fittings are attached on the sides (three on each side) for handling.

The inner wall of the inner packaging is formed into U-shape with 1.0 mm (0.0391 in) thick stainless steel sheet. The inner packaging is partitioned down the center with 2.0 mm (0.0787 in) thick stainless steel sheet welded to the bottom of the packaging. Foam polyethylene is placed on the inner surface of the inner wall where the fuel assemblies are seated. The void space between the outer and inner steel sheeting is filled with an alumina silicate thermal insulation 48 mm (1.89 in) thick.

### 3.2.2 Outer Container (OC)

The structure of the outer container is shown in Figure 3-3. The outer container is comprised of three parts: a container body, a container lid and inner container hold clamps made of stainless steel and fastened together using stainless steel bolts. Two tamper-indicating device attachment locations are provided, one on each end, of the outer container.

#### 3.2.2.1 OUTER CONTAINER BODY

The outer container is made from a series of stainless steel angles (50 mm x 50 mm x 4 mm)(1.97 inch x 1.97 inch x 0.157 inches) that make the framework. Welded to the framework are a bottom plate and side plates; both made of 2 mm (0.079 inch) thick stainless steel. Sling holding angles for handling with a crane and protective plates for handling with a forklift are welded on the outside of the container body. A total of eight sets of support plates are welded on the inside of the outer container body for installing the inner container hold clamps. Additionally, shock absorbers made of 146 mm (5.75 in) wood are attached to each end and paper honeycomb shock absorbers are attached to the bottom and sides for absorbing shock due to a drop. The geometry of the shock absorber is shown in Figure 3-5. The shock absorbers are 157 mm (6.18 in) thick on the top of bottom and 108 mm (4.25 in) thick on the sides.





## Design Analyses and Calculation

### 3.2.2.2 OUTER CONTAINER LID

The outer container lid is comprised of a lid flange and a lid plate made of stainless steel. Stainless steel lid sling fittings are welded four places on the top surface of the outer container lid. A paper honeycomb shock absorber, 157 mm (6.18 in) thick by 160 mm (6.30 in) wide and 380 mm (14.96 in) long is attached to the bottom side of the lid similar to the attachment at the bottom of the container. The outer container lid has holes for bolts in its flange so that it can be fastened to the outer container body by the stainless steel bolts.

### 3.2.2.3. INNER CONTAINER HOLD CLAMP (LOCATED ON OUTER CONTAINER)

The inner container hold clamp consists of an inner container receptacle and a vibro-isolating device. The inner container receptacle consists of an inner container support plate, a support frame, a bracket and an inner container hold clamp fastener made of stainless steel. The receptacle guides the inner container to the correct position. The inner container receptacle is fitted with the vibro-isolating device through the gusset attached to the bracket. The vibro-isolating material is attached on the upper and lower side of the gusset. Shock mount fastening bolts go through the center of each piece of vibro-isolating rubber. The bolts at both ends are tightened so that the vibro-isolating rubber pieces press the gusset. There are four sets (eight pieces) of the vibro-isolating devices mounted on the outer container. Finally, a variety of stainless steel fasteners are used.





## Design Analyses and Calculation

### 3.3 Weights of Container and Payloads

The weight comparisons of the RAJ-II CTU [Ref. 1], GNF-Drop Test [Ref. 26] and the TN-B1 package (this report) are tabulated below.

**Table 3.3-1 Weight Distribution of the Packaging**

Packaging and Item description	CTU	Reference	TN-B1 (LSDYNA Analyses)	Note
Instrumented Drop Test [Ref. 1] and FEM validation				
Weight of inner container	308 kg	Ref. 1, page (B)-A.2		
Weight of Outer container	622 kg	Ref. 1, page (B)-A.2		
Gross weight of packaging	930 kg	Ref. 1, page (B)-A.2		
Fuel contents (Ballast)	280 kg x2	Ref. 1, page (B)-A.2		
Total weight of package	1490 kg	Ref. 1, page (B)-A.2		
Drop Test performed by NTRC At Oak Ridge, Tennessee [Ref. 26]				
Gross weight of packaging	930 kg	Ref.26, Table 2-8		
Fuel contents (Ballast)	684 kg	Ref.26, Table 2-8		
Total weight of package	1614 kg	Ref.26, Table 2-8		
TN-B1 Analyses (LSDYNA Simulation in this report)				
Weight of inner container		Ref. 7, Table 2-1	308 kg	
Weight of Outer container		Ref. 7, Table 2-1	622 kg	
Gross weight of packaging		Ref. 7, Table 2-1	930 kg	
Fuel contents (Rigid Mass)		Ref. 7, Table 2-1	684 kg	
Total weight of package		Ref. 7, Table 2-1	1614 kg	
Sensitivity Studies performed in this report				
upper bound fuel content weight studied		Section 3.3		weight sensitivity study
lower bound fuel content weight studied		Section 3.3		weight sensitivity study





## Design Analyses and Calculation

According to Ref. 9, Section 3.2, the weight of uranium dioxide pellets (per fuel assembly) varies from 235 kg (type 8x8 fuel) to 281 kg (type 11x11 fuel). The maximum fuel content of 684 kg is based on the design weight of 275 kg per fuel assembly for type 10x10 fuel. The fuel contents weights are shown in the table below.

**Table 3.3-2 Fuel Content weight Comparison**

Description	Fuel Assembly Materials			
	Type 8x8	Type 9x9	Type 10x10	Type 11x11
1. Fuel characteristic				
2. Maximum weight of uranium dioxide pellets (per fuel assembly)	235 kg	240 kg	275 kg	281 kg
3. Maximum number of fuel assembly per packaging	2	2	2	2
4. Weights of Other components	134 kg*	134 kg*	134 Kg	134*
5. Estimated Fuel content Weight	604 Kg*	614 Kg*	684 kg	696 Kg*

\*estimated

Therefore, the fuel content can vary from 696 kg (type 11x11 fuel) to 604 kg (type 8x8 fuel). Based on the design maximum weight of 684 kg, the possible weight variation is +2% to -12%. For the weight sensitivity study on the most limiting drops that generate the highest impact loads or deformation, the weight variation of +5% to -15% is used. Therefore, two fuel weights of 720 kg and 580 kg are used to perform the fuel weight sensitivity study.

### 3.4 Code Requirements and Compliances

The current task is performed to meet the code structural requirements of the following.

#### A. Normal Condition of Transport (NCT) per 10CFR71.71

1. **Reduced external pressure at 3.5 psia:** The fuel rods are pressurized with helium to a maximum pressure of 1.1145 MPa (absolute pressure (161.7 psia) helium at ambient temperature (T=293°K) prior to sealing. Hence, the Maximum Normal Operating Pressure (MNOP) at the maximum normal temperature of 350°K (=170°F) is 192.9 psia (Section 3.4.2, Ref. 7). At code specified hot temperature of 100°F (=38°C = 311°K), the internal pressure is:

$$IP = 161.7 \times \frac{311}{293} = 171.6 \text{ psia}$$





## Design Analyses and Calculation

- With the reduced external pressure of 3.5 Psia, the differential pressure of  $(171.6 - 3.5 =) 168.1$  psig is bound by the MNOP differential pressure of  $(192.9 - 14.7 =) 178.2$  psig.
2. **Increased external pressure of 20 psia:** Since the primary containment boundary of the shipping package is the cladding of the fuel rods, the pressurization that could be seen by the containment boundary is far below the normal conditions the fuel experiences while in service. No more analysis is necessary for this task.
  3. **Vibration,** in terms of g-value, this is bounded by the drop analyses, no more analysis is necessary.
  4. **Water spray;** per Ref. 7, Section 2.6.6, the materials of construction of the TN-B1 package are such that the water spray test identified in 10 CFR 71.71(c)(6) will have a negligible effect on the package.
  5. **Free drops:** 8 drop analyses are performed. To comply with the 10CFR Code, two end drops, two horizontal drops and two corner drops for cold condition and similar drops for hot condition are planned. However, the two corner drops are bound by the end drop and horizontal drop, therefore they are not performed. LSDYNA software is used to perform the analyses.
  6. The maximum package weight of 1614 kg (Table 3.3-1) dictates that the free drop distance is 4-ft, per 10CFR 71.71 (c)-(7). The packaging is greater than 50 kg; no corner drops are required for the NCT. The configurations of the drops are listed in Table 3.4-1 below.
  7. **Penetration:** This is bound by the much more limiting case of a 40-inch drop of the entire package onto a puncture bar during HAC drop accident; reported in Appendix D. The drop of the 6 kg bar will not damage the outer container.

The drop analyses and case numbers for NCT are listed in the following table. Because the focus of the drop analyses is to determine the bounding acceleration value, the drop cases at hot ambient temperature are bounded by the drop cases at cold ambient temperature at which the stiffness of the package material is higher than that at hot ambient temperature which results in greater acceleration values.

		Page 15 of 87
--	--	---------------





## Design Analyses and Calculation

**Table 3.4-1 Code-Compliant Drop Analyses Cases for Normal Condition of Transportation**

Case ID	Drop Description	Drop Height, ft	Ambient Temperature °F	Drop Orientation (degree of primary axis from Horizontal Surface)	Note
NCT01	Top End Drop	4	-40	270	
NCT02	Bottom End Drop	4	-40	90	
NCT03	Horizontal Drop on Lid	4	-40	0	
NCT04	Horizontal Drop on Side	4	-40	0	
NCT05	Top End Drop	4	150	270	Bound by Case NCT01
NCT06	Bottom End Drop	4	150	90	Bound by Case NCT02
NCT07	Horizontal Drop on Lid	4	150	0	Bound by Case NCT03
NCT08	Horizontal Drop on Side	4	150	0	Bound by Case NCT04

### B. Hypothetic Accident Condition (HAC) of transport per 10CFR71.73

1. **Free drops:** this includes 6 drop orientations each for both cold and hot conditions. Per 10CFR71.73, the cold and hot temperatures are specified as -20°F and 100°F. However, temperatures of -40°F and 150°F are conservatively used in the analysis. The drop orientations include 2 end drops, 2 Horizontal Drops (2 planes of the TN-B1 package), 2 corner drops (long side corner and short side corner). The total is **12 drop cases**. The configurations of the drops are listed in Table 3.4-2 below.
2. **Crush test:** Per 10CFR71.73 (c)-(2), the crush test is required only when the specimen (the combined weight of container and the fuel) has a mass not greater than 500 kg (1100 lb). The combined weight of TN-B1 container and the fuel content (1614 kg) is greater than 500 kg; therefore it is not required to perform the crush test.
3. **Pin puncture:**  
 Subpart F of 10 CFR 71 requires performing a puncture test in accordance with the requirements of 10 CFR 71.73(c)(3). The puncture test involves a 1-meter (40-inch) free drop of a package onto the upper end of a solid, vertical, cylindrical, mild steel bar mounted on an essentially unyielding, horizontal surface. The bar must be 150 mm (6 inches) in diameter, with the top surface horizontal and its edge rounded to a radius of not more than 6 millimeter (0.25 inch). The package is to be oriented in a position for which maximum damage will occur. The length of the bar used was approximately 1.5 meters (60 inches). The ability of the TN-B1 package to adequately withstand this specified puncture drop condition at room temperature





## Design Analyses and Calculation

has been demonstrated via drop test of the full-scale RAI-II CTUs [Ref. 26] ad discussed in the next section.

To properly select a worst-case package orientation for the puncture drop event, items that could potentially compromise containment integrity of the TN-B1 package must be clearly identified. For the TN-B1 package design, the foremost item to be addressed is the ability of the containment (fuel bundles) to remain leak-tight. Shielding integrity is not a controlling case for the reasons described in Chapter 5.0 of SAR Rev. 3 [Ref. 7]. Criticality safety is conservatively evaluated based on measured physical damage to the outer container walls as described in SAR Rev. 3[Ref. 7], Section 6.0.

Previous drop tests in [Ref. 1] have shown that, at room temperature, the 1-meter drop onto the puncture bar did not penetrate the outer wall or damage the fuel. Based on this previous tests and other experience as specified in [Ref. 7], an oblique and horizontal puncture drop orientations centered over the fuel were chosen as the most damaging and simulated in this report.

This task is to reanalyze the pin puncture at elevated ambient temperature of 150°F, where the stiffness of the packaging material is the lowest. Based on SAR Ref. 3 [Ref. 7], the "worst-case" puncture drop as required by 10 CFR 71.73(c)(3) was analyzed on the package with the lid down and 25 degrees from horizontal. The angle was chosen based on experience with other packages and the TN-B1. The puncture bar was aimed at the CG of package to maximize the energy imparted to the package. The configuration of this drop is shown in Figure D.3-1. As reported in Appendix D. The puncture pin did not penetrate the outer container. It deformed the lid inward and it contacted the inner container lid and deformed it a small amount. The outer lid total deformation was less than 12 cm (4.7 inches) and the inner container lid deformed less than 5 cm (2.0 inches).

4. **Immersion:** Subpart F of 10 CFR 71 requires performing an immersion test for fissile material packages in accordance with the requirements of 10 CFR 71.73(c)(5). The criticality evaluation presented in [Ref. 7], Chapter 6.0 assumes optimum hydrogenous moderation of the contents, thereby conservatively addressing the effects and consequences of water in-leakage.

In addition to the code requirements, the following analyses are also performed.

1. A sensitivity study is performed on the effects of package weight variation on the resulted peak accelerations. Selected from one end drop orientation and one Horizontal Drop orientation under cold temperature, the package weight is varied by +/- 10%. The drop analyses have been performed that consisted of 4 extra drop cases for the sensitivity study. The configurations of the drops are also listed in Table 3.4-2 below.
2. A sensitivity study on the effects of shallow angle drops (slap down) is performed. Three horizontal drops with cold temperature have been performed for 5-degree, 10-degree and 15-degree drop angles off the horizon surface. The configurations of the drops are also listed in Table 3.4-2 below.





## Design Analyses and Calculation

The drop analyses and case numbers for HAC are listed in the following table. Similar to the bounding cases for the NCT cases, the drop cases for HAC at hot ambient temperature are bounded by the drop cases at cold ambient temperature. At cold temperatures the stiffness of the package material is greater than that at hot ambient temperature, and this results in higher acceleration value. However, the HAC analysis cases at 150°F are performed for completeness and to demonstrate the effect of temperature on the container response.





## Design Analyses and Calculation

Table 3.4-2 Code-Compliant Drop Analyses Cases for Hypothetical Accident Condition

Case ID	Drop Description	Drop Height, ft	Ambient Temperature °F	Drop Orientation (degree of primary axis from Horizontal Surface)
HAC01	Top End Drop	30	-40	270
HAC02	Bottom End Drop	30	-40	90
HAC03	Side Drop on Lid	30	-40	0
HAC04	Side Drop on Side	30	-40	0
HAC05	Corner Drop on Lid	30	-40	83
HAC06	Corner Drop on Side	30	-40	83
HAC07	Top End Drop	30	150	270
HAC08	Bottom End Drop	30	150	90
HAC09	Side Drop on Lid	30	150	0
HAC10	Side Drop on Side	30	150	0
HAC11	Corner Drop on Lid	30	150	83
HAC12	Corner Drop on Side	30	150	83
HAC13	Bottom End Drop, Heavy Load	30	-40	90
HAC14	Bottom End Drop, Light Load	30	-40	90
HAC15	Horizontal Drop on Side shell, Heavy Load	30	-40	0
HAC16	Horizontal Drop on Side shell, Light Load	30	-40	0
HAC17	5° Shallow Angle Horizontal Drop on Side Shell	30	-40	5
HAC18	10° Shallow Angle Horizontal Drop on Side Shell	30	-40	10
HAC19	15° Shallow Angle Horizontal Drop on Side Shell	30	-40	15

Note: The pin-puncture case is presented in Appendix D.





## Design Analyses and Calculation

### 3.5 Impact Velocities

The evaluations for normal conditions of transport and hypothetical accident conditions are performed using the finite element analysis program LSDYNA. The finite element model of the TB-B1 container is discussed in detail in Section 7.1. The drop heights are simulated using equivalent impact velocities as follows.

The dynamic boundary conditions are the impact velocities described as follows.

- a. For a drop from a height of 30-ft (HAC), the impact velocity is

$$V_o = \sqrt{2 \times g \times h} = \sqrt{2 \times 386.4 \times 360} = 527.45 \text{ in/sec.}$$

where

$$g = \text{gravitational constant} = 386.4 \text{ in/sec}^2$$

$$h = \text{drop height} = 30\text{-ft} = 360 \text{ inches}$$

- b. For a drop from a height of 40-in (HAC steel cylinder penetration test), the impact velocity is:

$$V_o = \sqrt{2 \times g \times h} = \sqrt{2 \times 386.4 \times 40} = 175.8 \text{ in/sec.}$$

In the above equation, the drop height,  $h = 40\text{-in}$

- c. For a drop from a height of 4-ft (NCT), the impact velocity is:

$$V_o = \sqrt{2 \times g \times h} = \sqrt{2 \times 386.4 \times 48} = 192.6 \text{ in/sec.}$$

In the above equation, the drop height,  $h = 4\text{-ft} = 48\text{-in.}$

The inertia load of gravity is applied at all times.

Drop analyses required by 10 CFR71.73 specify temperatures at  $-20^\circ\text{F}$  (Cold Condition) and  $100^\circ\text{F}$  (hot condition). However, the analyses are conservatively performed with material properties corresponding to  $40^\circ\text{F}$  and  $150^\circ\text{F}$ .

### 4. COMPUTER CODES USED IN DAC

The LSDYNA finite element analysis program [Ref. 10] is used for the drop analyses of TN-B1 Container. LSDYNA is a dynamic simulation finite element analysis program with non-linear material and geometry capability. The LSDYNA program is verified in Ref. 11 following Atkin's QA program.





## Design Analyses and Calculation

### 5. ASSUMPTIONS & OPEN ITEMS

#### 5.1 Assumptions

There are no unverified assumptions in this calculation. Other design assumptions used, if any, has been noted and referenced as needed in the body of the calculation.

#### 5.2 Open Items

There are no open items.

### 6. ACCEPTANCE CRITERIA

The acceptance of the fuel assembly under drop conditions is to comply with the relevant ASME pressure and Boiler Vessel Codes. According to TN-B1 SAR Rev. 3 [Ref. 7], Section 2.1.4, the applicable ASME Boiler and Pressure Vessel Codes [Ref. 5] to the material strengths are

1. Section III, Subsection ND for the containment boundary which includes the fuel cladding.
2. Section III, Subsection NG for the criticality control structure which includes the fuel assembly cages and clips.
3. Section VIII for the non-containment components which include the container shells.

Since the fuel cladding is the containment boundary Per Ref.7, the container is not classified as the containment boundary and it is treated as the acceleration control component during transportation and the impact drops. The relevant structural acceptance criteria for the plastic stability of fuel bundle are:

- a. During normal and accident temperature and pressure conditions, the fuel bundle cladding remains stable without gross deformation or collapse that could cause a criticality incident.
- b. During the accident drop scenario, the geometry of the fuel bundle remains safe and would not cause criticality.

The acceptance criteria for fuel bundle stability evaluation is established based on the acceptance criteria of the Plastic Instability Load Analysis as discussed in ASME Code Subsection III, Appendix F, Section F-1341.4 [Ref. 5]. The ASME Code states that the load should not exceed 70% of the plastic instability load. The criterion for the minimum safety factor for the Atrium-11 fuel bundle stability evaluation is considered to be 1.4 (1/0.7). The above criteria are quantified by applying a scale factor of 1.4 to the acceleration time histories derived from the simulated RAJ-II container drops. As the resulted fuel assembly remains stable and without plastic cladding failure, then the minimum factor of safety is 1.4.

As reported in Section 8 of the calculation, the bounding acceleration for the inner container is found to be 335 g that occurs for the end drop configuration. The peak acceleration for the side drop on the





## Design Analyses and Calculation

side is found to be 260 g. In order to fulfill the requirement that the factor of safety on cladding integrity and plastic collapse is greater than 1.4, the fuel assemblies are reanalyzed using the above methodology by subjecting them to the maximum bounding acceleration calculated from the drop analyses of the TN-B1 container. The factor of safety of 1.4 is achieved by multiplying the bounding accelerations by a factor of 1.4. The structural acceptance criteria are therefore established as follows.

1. The fuel cladding integrity, limited by the ultimate strain, shall be maintained with a factor of safety of 1.4.
2. The fuel rod structural stability against plastic collapse is greater than 1.4
3. The maximum strain of other components in the fuel assembly is less than the ultimate strain
4. The structural integrity of the overall fuel elements shall be maintained

### 6.1 Biases and Uncertainties

There are no known biases or unaccounted uncertainties in this calculation.

### 6.2 Area of Applicability (AOA)

The accident drop simulation is applicable only to the extent that the ATRIUM-11 fuel assembly is packaged in the standard TN-B1 container with the total payload weight of two ATRIUM-11 fuel assemblies. The packing material facing the Lower Tie Plate and the Top handle of the ATRIUM-11 fuel bundle is made of Balsa wood with a minimum thickness of 5.8-inches and its grain direction must be parallel to the longitudinal axis of the fuel bundle as shown in the applicable TN-B1 licensing drawings. The inner container of the TN-B1 holds the ATRIUM-11 fuel bundle. The sides of the fuel bundle are surrounded with packing material made of Polyethylene foam (Polyplank) [Ref. 24].





## Design Analyses and Calculation

### 7. CALCULATIONS

#### 7.1 TN-B1 Shipping Container Finite Element Model

The container LSDYNA finite element model used for the evaluation includes the outer container, inner container, fuel load, and shock absorbing materials between the inner and outer containers and between the fuel and inner container. Generally, shell elements are used to represent the stainless steel structural of the inner and outer containers, and solid 3D brick elements are used to model the various wood components and other shock absorber blocks. Welds are not included in the model, and the connections between joined parts are considered to be solid (with merged nodes). The geometry of the container model is determined from the AREVA drawings [Ref. 6].

The two fuel assemblies are modeled as rigid rectangular blocks with a square cross-section and defined with the \*MAT\_RIGID material specification as the structural response of the fuel itself is not an objective of the analysis. Nominal densities are provided for the various materials in section 7.3, but are adjusted as required for some components to provide the correct masses for the inner and outer containers and the fuel assemblies. The TN-B1 overall finite element model and various components are shown in Figures 7.1-1 through 7.1-4.

The interaction between all components is included with a single surface contact definition for all container parts, and a surface to surface contact definition for the container and rigid impact plane.

For all drop analyses, impact of the container is on a rigid plane located just below the outer container. The rigid plane, defined with a \*MAT\_RIGID material specification, is modeled as a rectangular surface generated with shell elements and fixed in space. The rigid impact surface lies in the x-y plane, with the negative z-axis as the vertical drop direction. The complete model is assigned an initial velocity corresponding to the drop height (see Section 3.4) and the LSDYNA simulation commences at a time just before impact with the rigid plane. The different drop orientations of the model with respect to the rigid plane are illustrated in Figure 7.1-5 through 7.1-10. The terms "Vertical Drop" and "End Drop" are used interchangeably in this report. The terms "Horizontal Drop" and "Side Drop" are used interchangeably in this report.



**ATKINS**

**Design Analyses and Calculation**

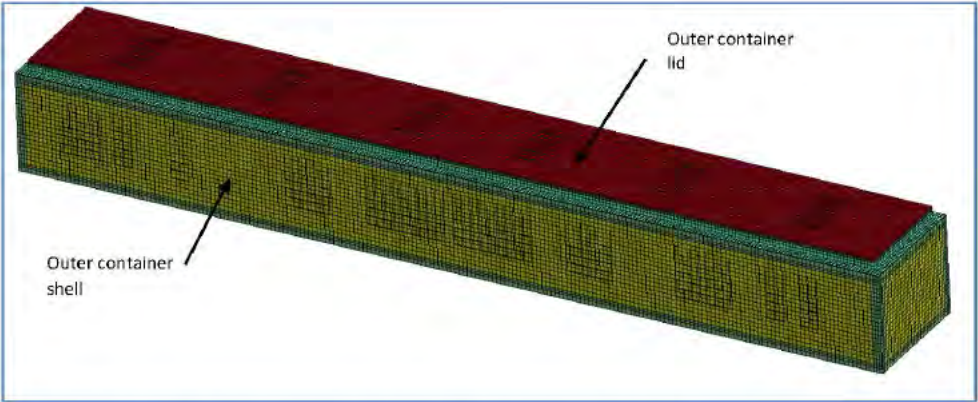


Figure 7.1-1 Complete TN-B1 Shipping Container Finite Element Model

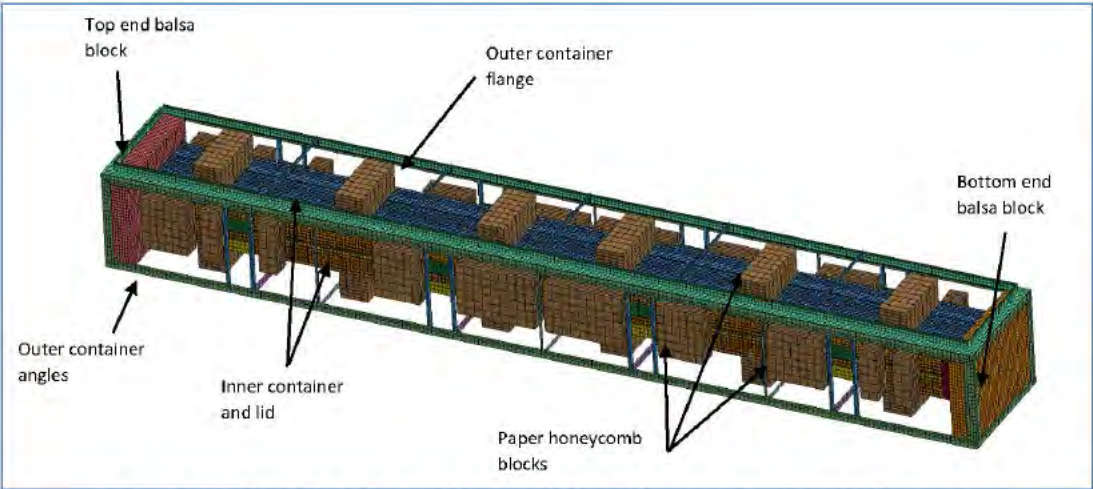


Figure 7.1-2 TN-B1 Finite Element Model with Outer Container Shell and Lid Removed.





Design Analyses and Calculation

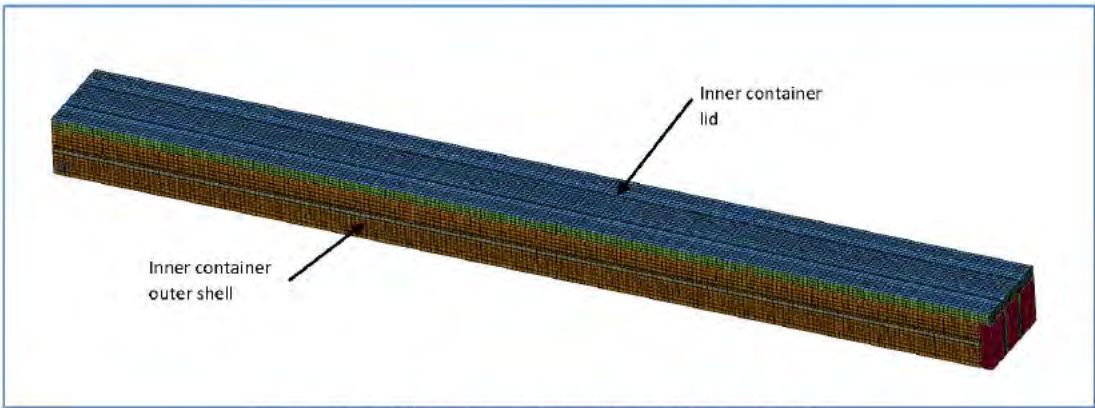


Figure 7.1-3 TN-B1 Inner Container Finite Element Model

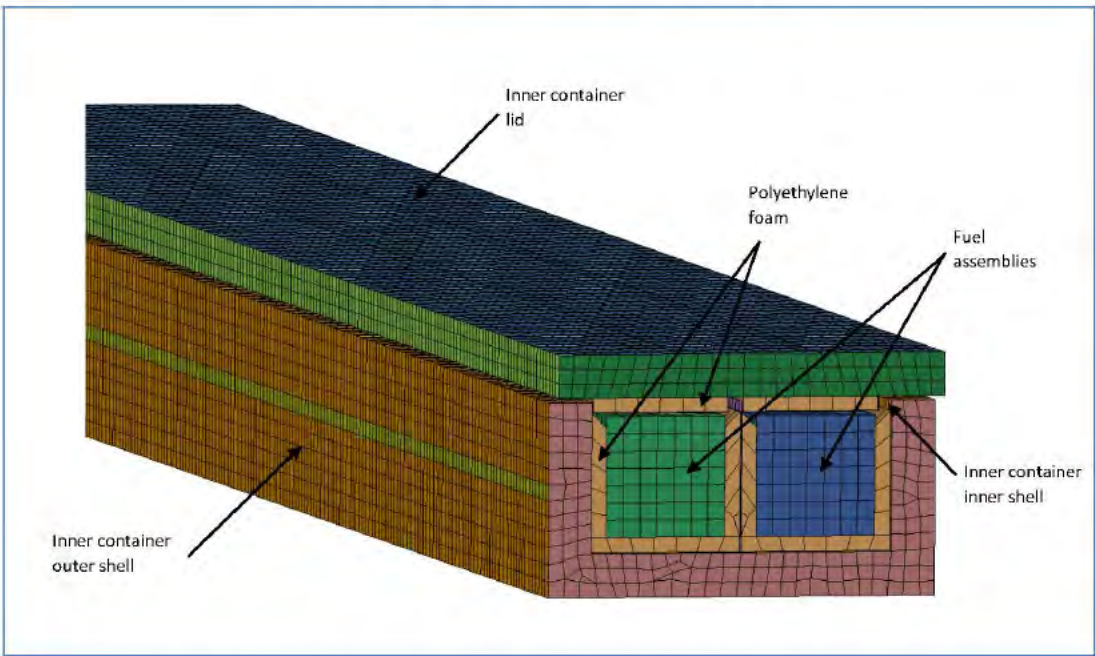


Figure 7.1-4 TN-B1 Inner Container Finite Element Model with End Removed



**ATKINS**

### Design Analyses and Calculation

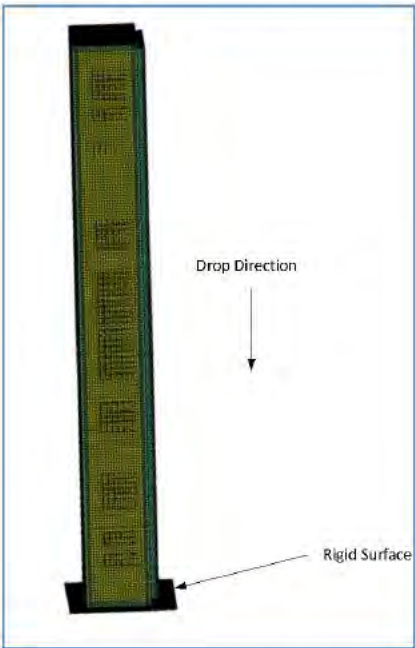


Figure 7.1-5 Orientation for Top and Bottom End Drop

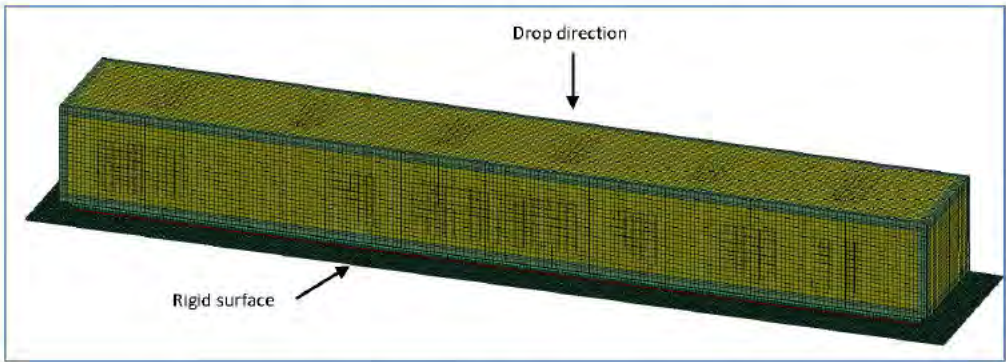


Figure 7.1-6 Orientation for Horizontal Drop on Lid



**ATKINS**

# Design Analyses and Calculation

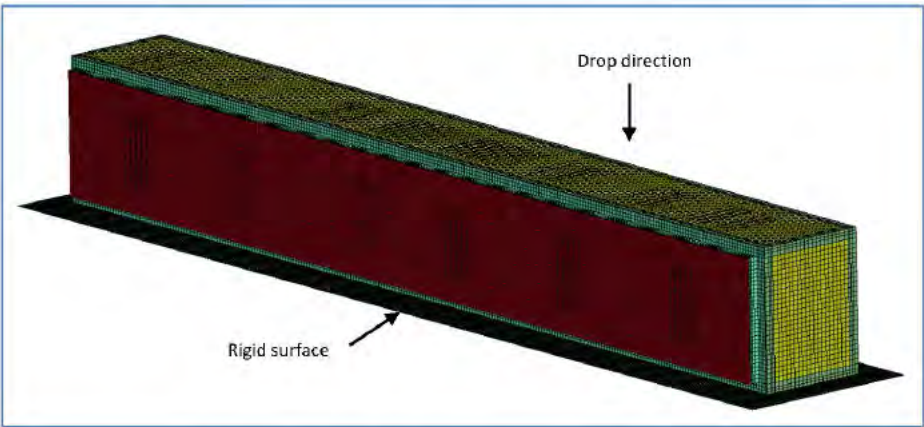


Figure 7.1-7 Orientation for Horizontal Drop on Side Shell

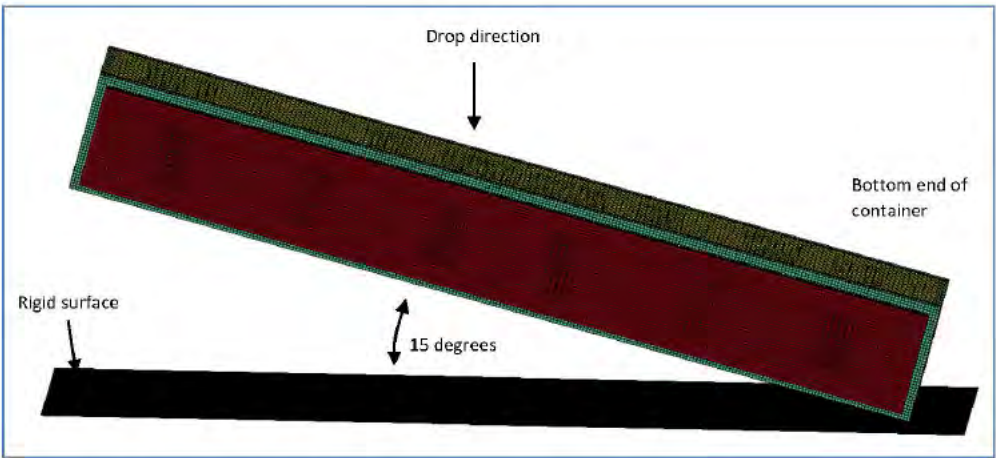


Figure 7.1-8 Orientation for 15° Shallow Angle from Horizontal Drop on Side (5° and 10° Angles Similar)



ATKINS

## Design Analyses and Calculation

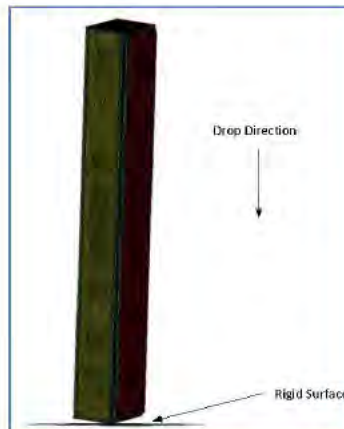


Figure 7.1-9 Bottom Corner Drop on Lid

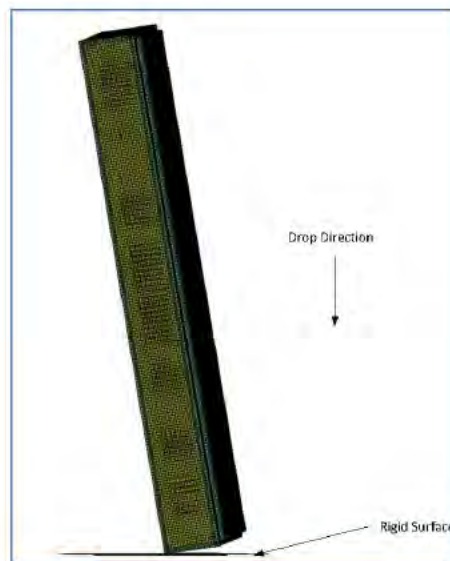


Figure 7.1-10 Bottom Corner Drop on Side





## Design Analyses and Calculation

### 7.2 Modeling Assumptions

The main modeling assumptions are listed below.

- [Redacted]
- [Redacted]
- [Redacted]
- [Redacted]





## Design Analyses and Calculation

•



### 7.3 Material Properties

The derivations of the material properties are presented in Appendix A. The summary of the material properties are presented in this section.

#### 7.3.1 Zircaloy-2

This material is used only for the fuel rod cladding of the fuel assembly, which served as the containment boundary. According to TN-B1 SAR Rev. 3 [Ref. 7], Section 2.1.4, the applicable ASME Boiler and Pressure Vessel Codes for the material strength of Fuel Cladding is Section III, Subsection ND [Ref. 5].

The Zircaloy Material Properties with dependency on temperature are derived based on *NUREG/CR-6150 EGG-2750 MATPRO - A Library of Materials Properties for Light-Water-Reactor Accident Analysis* [Ref. 12]. The ultimate strain is taken from [Ref. 13]. The detailed derivation of the stress strain curves are presented in Appendix A.1. The property presented in this section corresponds to dynamic property. The Zircaloy material is modeled in LSDYNA as \*MAT\_PIECEWISE\_LINEAR\_PLASTICITY (Type 24). The cladding is modeled as shell elements.

The mechanical properties of Zircaloy are presented in Table 7.3.1-1 below. The data for the stress-stress curves of the zircaloy used in the LSDYNA program in compliance with ASME Boiler and Pressure Vessel Codes Section III [Ref. 5] are presented in Table 7.3.1-2 below.





## Design Analyses and Calculation

**Table 7.3.1.1 Summary of Material Properties for Zircaloy**

Temperature = -40 degree F				
Poisson's ratio =0.3				
Density = 6.5 gm/cm <sup>3</sup> (Ref. 7, Table 2-3)				
Strain Rate	.001	.1	1	10
Modulus of Elasticity, psi	1.393 x 10 <sup>7</sup>			
Yield Stress, psi	1.106 x 10 <sup>5</sup>	1.222 x 10 <sup>5</sup>	1.285 x 10 <sup>5</sup>	1.351 x 10 <sup>5</sup>
Yield Strain	0.0079	0.0088	0.0092	0.0097
Ultimate Stress, psi	1.401 x 10 <sup>5</sup>	1.537 x 10 <sup>5</sup>	1.609 x 10 <sup>5</sup>	1.685 x 10 <sup>5</sup>
Ultimate Strain	0.15	0.15	0.15	0.15

Temperature = 70 degree F				
Poisson's ratio =0.3				
Density = 6.5 gm/cm <sup>3</sup> (Ref. 7, Table 2-3)				
Strain Rate	.001	.1	1	10
Modulus of Elasticity, psi	1.345 x 10 <sup>7</sup>			
Yield Stress, psi	9.46 x 10 <sup>4</sup>	1.048 x 10 <sup>5</sup>	1.103 x 10 <sup>5</sup>	1.161 x 10 <sup>5</sup>
Yield Strain	0.0070	0.0078	0.0082	0.0070
Ultimate Stress, psi	1.292 x 10 <sup>5</sup>	1.417 x 10 <sup>5</sup>	1.484 x 10 <sup>5</sup>	1.554 x 10 <sup>5</sup>
Ultimate Strain	0.16	0.16	0.16	0.16

Temperature = 150 degree F				
Poisson's ratio =0.3				
Density = 6.5 gm/cm <sup>3</sup> (Ref. 7, Table 2-3)				
Strain Rate	.001	.1	1	10
Modulus of Elasticity, psi	1.309 x 10 <sup>7</sup>			
Yield Stress, psi	8.586 x 10 <sup>4</sup>	9.520 x 10 <sup>4</sup>	1.002 x 10 <sup>5</sup>	1.056 x 10 <sup>5</sup>
Yield Strain	0.0066	0.0073	0.0076	0.0081
Ultimate Stress, psi	1.222 x 10 <sup>5</sup>	1.340 x 10 <sup>5</sup>	1.403 x 10 <sup>5</sup>	1.469 x 10 <sup>5</sup>
Ultimate Strain	0.17	0.17	0.17	0.17





## Design Analyses and Calculation

**Table 7.3.1.2 Stress Strain Data for Zircaloy**

Temperature = -40 degree F				
Poisson's ratio =0.3				
Stress, psi				
Strain Rate	0.001	0.1	1	10
Strain =0.02	1.191 x 10 <sup>5</sup>	1.306 x 10 <sup>5</sup>	1.368 x 10 <sup>5</sup>	1.432 x 10 <sup>5</sup>
Strain =0.04	1.260 x 10 <sup>5</sup>	1.381 x 10 <sup>5</sup>	1.446 x 10 <sup>5</sup>	1.515 x 10 <sup>5</sup>
Strain =0.06	1.302 x 10 <sup>5</sup>	1.427 x 10 <sup>5</sup>	1.494 x 10 <sup>5</sup>	1.565x 10 <sup>5</sup>
Strain =0.15	1.401 x 10 <sup>5</sup>	1.537 x 10 <sup>5</sup>	1.609 x 10 <sup>5</sup>	1.685x 10 <sup>5</sup>
Ultimate Strain				

Temperature = 70 degree F				
Poisson's ratio =0.3				
Stress, psi				
Strain Rate	0.001	0.1	1	10
Strain =0.02	1.05 x 10 <sup>5</sup>	1.151 x 10 <sup>5</sup>	1.206 x 10 <sup>5</sup>	1.262 x 10 <sup>5</sup>
Strain =0.04	1.125 x 10 <sup>5</sup>	1.234 x 10 <sup>5</sup>	1.292 x 10 <sup>5</sup>	1.353 x 10 <sup>5</sup>
Strain =0.06	1.172 x 10 <sup>5</sup>	1.285 x 10 <sup>5</sup>	1.345 x 10 <sup>5</sup>	1.409x 10 <sup>5</sup>
Strain =0.16	1.292 x 10 <sup>5</sup>	1.417 x 10 <sup>5</sup>	1.484 x 10 <sup>5</sup>	1.554x 10 <sup>5</sup>
Ultimate Strain				

Temperature = 150 degree F				
Poisson's ratio =0.3				
Stress, psi				
Strain Rate	0.001	0.1	1	10
Strain =0.02	0.9689x 10 <sup>5</sup>	1.062 x 10 <sup>5</sup>	1.112 x 10 <sup>5</sup>	1.165 x 10 <sup>5</sup>
Strain =0.04	1.045 x 10 <sup>5</sup>	1.145 x 10 <sup>5</sup>	1.199 x 10 <sup>5</sup>	1.256 x 10 <sup>5</sup>
Strain =0.06	1.091 x 10 <sup>5</sup>	1.197 x 10 <sup>5</sup>	1.253 x 10 <sup>5</sup>	1.312 x 10 <sup>5</sup>
Strain =0.17	1.222 x 10 <sup>5</sup>	1.340 x 10 <sup>5</sup>	1.403 x 10 <sup>5</sup>	1.469x 10 <sup>5</sup>
Ultimate Strain				





## Design Analyses and Calculation

### 7.3.2 AISI 304 (SUS 304) Grade Stainless Steel

#### 7.3.2.1 MECHANICAL PROPERTIES OF SS304 AND APPLICABLE CODES

The 304 stainless steel is used in the following components; fuel cage (304L, plates), container shells and container frames (304, plates).

The plates are modeled as shell elements in LSDYNA program.

According to TN-B1 SAR Rev. 3 [Ref. 7], Section 2.1.4, the applicable ASME Boiler and Pressure Vessel Codes [Ref. 5] to the components are

1. Section III, Subsection NG for the criticality control structure which includes the fuel assembly cages and clips (i.e. SS304L).
2. Section VIII for the non-containment components which include the container shells (i.e. SS304).

The material properties for Type 304 and 304L stainless steel, taken from ASME Boiler and Pressure Code, Section II, Part D, 2010 Ed. [Ref. 14], are presented in Table 7.3.2-1 and 7.3.2-2 below. The densities are nominal values. In the LSDYNA input file, the densities are adjusted so that the total mass equal to the design weight of the fuel bundle and containers. The stresses listed below are engineering stress.

**Table 7.3.2.1-1 Mechanical Properties of 304 (SA-240) at temperature of interest**

Property	-40°F	70°F	150°F	Reference
Modulus of Elasticity, E, ksi	28,900	28,300	27,800	Ref. 14, Table TM-1
Ultimate Tensile Stress, $S_u$ , ksi	75	75	72.5	Ref. 14, Table U
Yield Stress, $S_y$ , ksi	30	30	26.7	Ref. 14, Table Y-1
Poisson's ratio	0.31			Ref. 14, Table PRD
Density, (lb/in <sup>3</sup> )	0.29			Ref. 14, Table PRD





## Design Analyses and Calculation

**Table 7.3.2.1-2 Mechanical Properties of 304L (SA-240) at temperature of interest**

Property	-40°F	70°F	150°F	Reference
Modulus of Elasticity, E, ksi	28,900	28,300	27,800	Ref. 14, Table TM-1
Ultimate Tensile Stress, S <sub>u</sub> , ksi	70	70	67.6	Ref. 14, Table U
Yield Stress, S <sub>y</sub> , ksi	25	25.0	22.7	Ref. 14, Table Y-1
Poisson's ratio	0.31			Ref. 14, Table PRD
Density, (lb/in <sup>3</sup> )	0.29			Ref. 14, Table PRD

The derivations of stress strain curves in compliance with each applicable code are presented in Appendix A2. These requirements are summarized in the table below.

**Table 7.3.2.1-3 Applicable Structural Codes for the Stainless Steel 304 and 304L**

Component Description	Usage	Material	Applicable Codes
Fuel Assembly Cages	criticality control	SS304L	ASME B&PV Code, Section III, Subsection NG
Container Shell	non-Containment components	SS304	ASME B&PV Code, Section VIII





## Design Analyses and Calculation

### 7.3.2.2 STRESS STRAIN CURVE FOR STAINLESS STEEL IN COMPLIANCE WITH THE ASME B&PV CODE, SECTION III, SUBSECTION NG

The stress strain curves data for SS304L at temperature of interest presented in this section are derived based on equations in [Ref. 27].

Table 7.3.2.2-1 Stress Strain Value of SS304L at -40°F

Strain	stress, psi
0	0
0.000144	4166.7
0.00029	8333.3
0.000457	12500.0
0.000728	16666.7
0.001347	20833.3
0.002865	25000.0
0.005037	32336.4
0.009192	39672.7
0.017563	47009.1
0.032512	54345.5
0.056484	61681.8
0.091988	69018.2
0.141581	76354.5
0.207866	83690.9
0.293485	91027.3
0.401110	98363.6
0.510000	105700.0





## Design Analyses and Calculation

Table 7.3.2.2-2 Stress Strain Value of SS304L at Room Temperature

Strain	stress, psi
0	0
0.000147	4166.7
0.000296	8333.3
0.000466	12500.0
0.000740	16666.7
0.001362	20833.3
0.002883	25000.0
0.005095	32336.4
0.009289	39672.7
0.017700	47009.1
0.032689	54345.5
0.056701	61681.8
0.092244	69018.2
0.141877	76354.5
0.208202	83690.9
0.293860	91027.3
0.401525	98363.6
0.510000	105700.0





## Design Analyses and Calculation

Table 7.3.2.2-3 Stress Strain Value of SS304L at 150°F

Strain	stress, psi
0	0
0.00014	3783.3
0.00027	7566.7
0.00043	11350.0
0.00070	15133.3
0.00131	18916.7
0.00282	22700.0
0.00503	29916.0
0.00923	37132.0
0.01764	44348.0
0.03263	51564.0
0.05664	58780.0
0.09219	65996.0
0.14182	73212.0
0.20815	80428.0
0.29381	87644.0
0.40148	94860.0
0.51000	102076.0





## Design Analyses and Calculation

### 7.3.2.3 STRESS STRAIN CURVE FOR STAINLESS STEEL IN COMPLIANCE WITH THE ASME B&PV CODE, SECTION VIII

The stress strain curves data at temperature of interest based on the Table 7.3.2.1-1 and the equations in ASME Boiler and Pressure Vessel Code, Section VIII, Div 2, Annex 3.D (Ref. 15) are tabulated as follows.

Table 7.3.2.3-1 Stress-Strain Data of SS304 at -40° F

Strain	Stress psi
0.0	0.0
0.0015	24000.0
0.0022	27000.0
0.0034	30000.0
0.0074	34868.0
0.0182	39735.9
0.0395	44603.9
0.0625	49471.9
0.0815	54339.8
0.0997	59207.8
0.1189	64075.8
0.1397	68943.7
0.1623	73811.7
0.1869	78679.7
0.2133	83547.6
0.2417	88415.6
0.2720	93283.6
0.3044	98151.5
0.3387	103019.5
0.3751	107887.5
0.4136	112755.4
0.4541	117623.4
0.5541	117623.4





## Design Analyses and Calculation

Table 7.3.2.3-2 Stress-Strain Data of SS304 at 70°F

Strain	Stress psi
0.0	0.0
0.0016	24000.0
0.0023	27000.0
0.0035	30000.0
0.0075	34868.0
0.0183	39735.9
0.0396	44603.9
0.0626	49471.9
0.0817	54339.8
0.0999	59207.8
0.1191	64075.8
0.1399	68943.7
0.1626	73811.7
0.1871	78679.7
0.2136	83547.6
0.2420	88415.6
0.2723	93283.6
0.3047	98151.5
0.3391	103019.5
0.3755	107887.5
0.4139	112755.4
0.4544	117623.4
0.5544	117623.4





## Design Analyses and Calculation

Table 7.3.2.3-3 Stress-Strain Data of SS304 at 150° F

Strain	Stress psi
0.0	0.0
0.0015	21538.5
0.0022	24230.8
0.0033	26923.1
0.0077	31885.7
0.0205	36848.4
0.0443	41811.0
0.0670	46773.7
0.0859	51736.3
0.1048	56699.0
0.1251	61661.6
0.1473	66624.3
0.1713	71586.9
0.1972	76549.6
0.2251	81512.2
0.2550	86474.9
0.2868	91437.6
0.3206	96400.2
0.3563	101362.9
0.3941	106325.5
0.4340	111288.2
0.4758	116250.8
0.5758	116250.8





## Design Analyses and Calculation

### 7.3.2.4 STRAIN RATE EFFECTS

At high strain rate, as in the case of dynamic impact condition, the yield stress increases and this tends to strengthen the material. The strain-rate sensitivity data of 304 and 304L, taken from "Impact tensile testing of stainless steels at various temperatures" D.K. Morton and R. K. Blandford, March 2008, INL/EXT-08-14082 [Ref. 16], is listed in Table 7.3.2.4-1 below. The strain rate sensitivity data for 304 and 304L at temperature of -40°F is the same as that at temperature -20°F.

**Table 7.3.2.4-1 The Strain-rate Sensitivity of 304/304L**

Strain Rate	Temperature, °F				
	-20	70	150	300	600
5	1.333	1.235	1.211	1.166	1.043
10	1.361	1.278	1.254	1.210	1.094
22	1.428	1.381	1.358	1.316	1.217
25	1.445	1.407	1.384	1.342	1.247

### 7.3.3 Balsa (Shock Absorber)

This wood is used as a Shock Absorber for the following applications.

Item 26 of Outer Container Main Body Assembly (Dwg 105E3738, Rev. 7)

The Balsa wood is used primarily as shock absorber in the oblique and End Drop orientation. Based on TN-B1 SAR Rev. 3 [Ref. 7], Table 2-3, the compressive strength of the Balsa wood at ambient temperature is 16 MPa. The density of the Balsa wood is 0.18 g/cm<sup>3</sup>. Therefore

The compressive strength is

$$\sigma = 16 \text{ MPa} = 2321 \text{ psi}$$

The nominal density of the Balsa wood, as defined in TN-B1 SAR Rev. 3 [Ref. 7], Table 2-3, is

$$\rho = 0.18 \text{ g/cm}^3 = 11.24 \text{ lb/ft}^3$$

The derivation of the compressive stress vs. volumetric strain is presented in Appendix A.3 and summarized in the table below.





## Design Analyses and Calculation

**Table 7.3.3-2 Stress Strain Data Developed for Balsa Wood ( $\rho=180\text{kg/m}^3$ )**

Volumetric Strain	Stress, psi
0.000	0.000
0.020	1,500
0.040	2,000
0.100	2,250
0.150	2,300
0.600	2,400
0.700	2,600
0.770	4,000
0.800	6,000

**a. EFFECTS OF TEMPERATURE ON THE STRENGTH OF Balsa WOOD**

The derivation of the temperature correction factors, applied to the Balsa Wood material properties at room temperature that are used as input to the LSDYNA program, is presented in Appendix A.3 and summarized in the table below.

**Table 7.3.3-3 Correction Factors for Compressive Strength of Balsa Wood at Extreme Temperatures**

at degree C		-20			150
at degree F					
interpolated and extrapolated	-40	-4	70	150	302
Scale from research, [Ref. 30, Section 3.3.3]	1.61	1.55	1.42	1.27	1.00
New scale to be used in LSDYNA input	1.140	1.09	1.00	0.899	

**b. POISSON'S RATIO**

The Balsa Wood is modeled using the LSDYNA material model crushable foam (Material 63 and 163). After the initial limiting stress (the threshold of plastic deformation), the material model generally is uncoupled between the axial direction and the radial or tangential directions. Therefore, the use of a plastic Poisson's ratio of  $\nu=0.0$  is recommended. In this calculation, a small value of  $\nu=0.01$  is used to represent the marginal effect.





## Design Analyses and Calculation

### c. DYNAMIC EFFECTS ON STRESS-STRAIN CURVE OF Balsa Wood

Since there is no readily available published data on dynamic effects of balsa wood under impact, this calculation relies on the benchmark drop test performed on the RAJ-II container to make material property adjustment to reflect the dynamic effect on the compressive strength of the Balsa Wood. The strength correction factor will be developed from the benchmark runs at ambient temperature then applied to the LSDYNA runs for cold and hot temperature.

The Balsa Wood is modeled using the LSDYNA material model of Crushable\_Foam.

### 7.3.4 Paper Honeycomb

This is used as shock absorber for the following applications.

1. Items 1, 2, 3, 4, 5 of Outer Container Shock Absorber Assembly (Dwg 105E3741, Rev. 1)
2. Item 4 of Protective Case (Dwg 105E3773, Rev. 1)

This material is used as shock absorber primarily during the two side drop orientations. Based on TN-B1 SAR Rev. 3 [Ref. 7] Table 2-3, the static initial peak stress of the Paper Honeycomb at ambient temperature is 2.35 MPa. The density of the Paper Honeycomb is 0.06 g/cm<sup>3</sup>. Therefore

The initial peak stress is

$$\sigma = 2.35 \text{ MPa} = 342.3 \text{ psi}$$

The density of the Paper Honeycomb is

$$\rho = 0.06 \text{ g/cm}^3 = 3.746 \text{ lb/ft}^3 \text{ or } \rho = 60 \text{ kg/m}^3$$

The derivation of the load-deflection curve for honeycomb material is detailed in Appendix A.3. The graphical representation of the load-deflection curve is presented following the load-deflection data table. The actual value of the crush strength is corrected by benchmarking the predicted acceleration g values against the drop test result. Because the load-deflection curve behaves so much like orthotropic crushable foam, and the other material properties of a true honeycomb are not known or relevant, the honey comb in the container is therefore modeled using the LSDYNA material model of Crushable\_Foam.





## Design Analyses and Calculation

Table 7.3.4-1 Load Deflection Data Developed for Paper Honeycomb

Volumetric Strain	Stress, psi
0.000	0
0.020	390
0.040	350
0.100	340
0.200	343
0.300	343
0.500	343
0.700	343

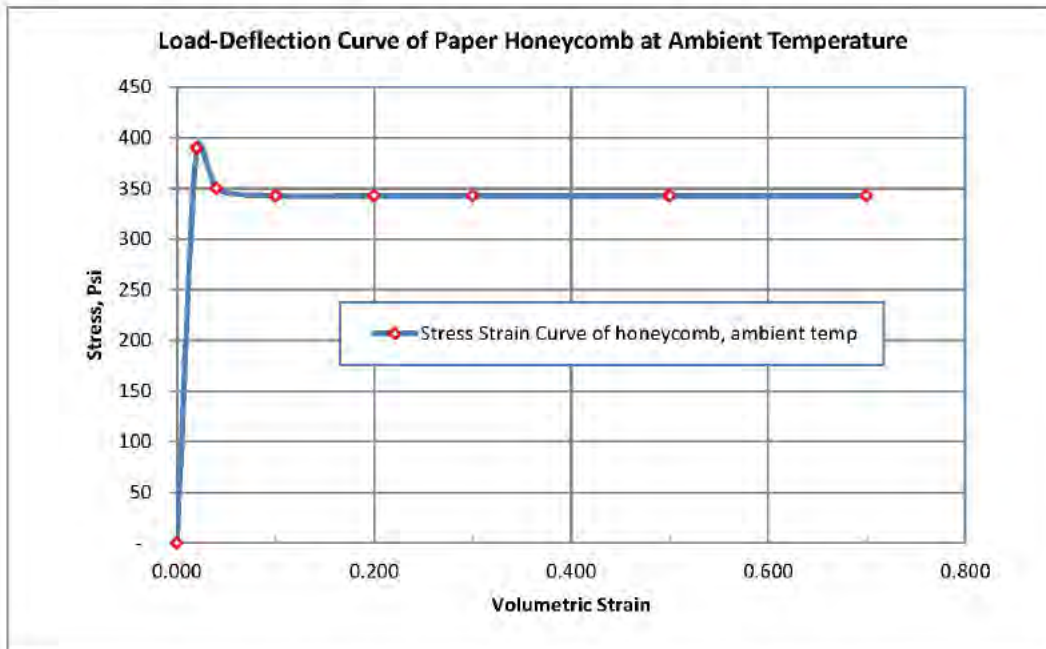


Figure 7.3.4-1 Load-Deflection Curve Developed for Paper Honeycomb





## Design Analyses and Calculation

### a. POISSON'S RATIO

The deformation of the honeycomb material generally is uncoupled between the axial direction and the lateral directions. A small value of  $\nu=0.01$  is used to represent the marginal effect of Poisson's ratio.

### b. EFFECTS OF TEMPERATURE ON THE STRENGTH OF PAPER HONEYCOMB

Several studies on the effects of temperature on the strength of paper were reported in [Ref. 17]. Between  $-25^{\circ}\text{C}$  and  $175^{\circ}\text{C}$ , the elastic modulus of paper decreases at an average rate of 0.3% per degree C. The ultimate strength of paper decreases at a rate comparable to the tensile modulus. Therefore, it is reasonable to assume that between  $-40^{\circ}\text{F}$  and  $150^{\circ}\text{F}$ , the change in paper honeycomb strength is comparable; recognizing that the test data for temperature below  $-25^{\circ}\text{C}$  ( $-13^{\circ}\text{F}$ ) is lacking. At cold temperature ( $-40^{\circ}\text{F}$ ), the stiffness correction factor (CF) applied to the honeycomb material property of room temperature is

$$\text{CF} = 1 + 0.003 \times (70 + 40) \times 5/9 = 1.18$$

Where

0.003 = rate of change for the elastic modulus per degree C (=0.3%)

(70+40) = temperature span between  $-40^{\circ}\text{F}$  to room temperature ( $70^{\circ}\text{F}$ ) =  $110^{\circ}\text{F}$

5/9 = conversation factor between  $^{\circ}\text{F}$  to  $^{\circ}\text{C}$

At hot temperature ( $150^{\circ}\text{F}$ ), the stiffness correction factor (CF) applied to the honeycomb material property of room temperature is

$$\text{CF} = 1 - 0.003 \times (150 - 70) \times 5/9 = 0.86$$

Where

0.003 = rate of change for the elastic modulus per degree C (=0.3%)

(150-70) = temperature span between  $150^{\circ}\text{F}$  to room temperature ( $70^{\circ}\text{F}$ ) =  $80^{\circ}\text{F}$

5/9 = conversation factor between  $^{\circ}\text{F}$  to  $^{\circ}\text{C}$

Therefore, the correction factors for the honeycomb strength for cold and hot temperature are 1.18 and 0.86, respectively.

### c. DYNAMIC STRENGTH OF THE HONEYCOMB MATERIAL

Since there is no readily available published data on dynamic effects of paper honeycomb under impact, this calculation relies on the benchmark drop test performed on the RAI-II container to make material property adjustment to reflect the dynamic effect on the compressive strength of the paper honeycomb. The strength correction factor is developed from the benchmark runs at ambient temperature then applied to the LSDYNA runs for cold and hot temperature.

		Page 45 of 87
--	--	---------------





## Design Analyses and Calculation

### 7.3.5 Lumber (Hemlock)

This wood is designated on the license drawing and used as thermal insulator for the following applications.

1. Items 24, 25, 26, 27 of Inner Container Main Body Assembly (Dwg 105E3745, Rev. 8)
2. Item 13 of Inner Container Lid (Dwg 105E3747, Rev. 4).
3. Item 7 of Inner Container End Lid (Dwg 105E3748, Rev. 2)

#### a. THE ELASTIC MODULUS AND DENSITY FOR COMPACTED HEMLOCK

The Hemlock is used as thermal insulator; therefore there is no structural value intended for the Hemlock. If other types of wood are used, there should not be a significant difference in the resulted peak acceleration value when the container is accidentally dropped during transportation. During the end drop orientation, the Hemlock is not in the load path of the fuel bundle except its own weight. During the side drop orientation, the Hemlock plates provide support for the fuel rod bundle. Therefore the hemlock is treated as elastic material. The loading on the Hemlock is compression perpendicular to grain direction. The properties of the Hemlock are taken from Ref.18, Table 4-3b. There are 3 species of Hemlock wood published in [Ref. 18]. For this calculation, the Hemlock wood (Western Hemlock) with the strongest modulus is conservatively selected (that could produce the greatest acceleration during impact).

Specific gravity = 0.45 from [Ref. 18], Table 4-3a, 12% moisture content

Density =  $0.45 \text{ gm/cm}^3 = 0.016 \text{ lb/in}^3$

The compressive stress parallel to grain = 7200 psi

The compressive stress perpendicular to grain = 550 psi

The modulus of elasticity in the parallel to grain direction =  $1.63 \times 10^6 \text{ lbf/in}^2$ .

Normally, the modulus of elasticity in the perpendicular to grain direction takes the same reduction as the compressive stress; therefore the modulus of elasticity in the perpendicular to grain direction is:

$$E = 1.63 \times 10^6 \text{ lbf/in}^2 \times 550/7200 = 125 \times 10^3 \text{ lbf/in}^2$$

#### b. POISSON'S RATIO

Per [Ref. 18], Table 4-2, the Poisson's ratio in the perpendicular to grain direction (Radial to Tangential direction) is

$$\mu_{RL} = 0.442$$





## Design Analyses and Calculation

### c. *EFFECT OF TEMPERATURE ON THE ELASTIC MODULUS*

According to Ref. 30, section 3.3.3, The temperature effect is similar to all wood material. Therefore, the same temperature effect applied to the Balsa Wood in Section 7.3.3 is also applicable to Hemlock wood.

Similarly, the resulted compressive stress increase is 14% ( $\approx 1.14-1$ ) more for temperature at  $-40^{\circ}\text{F}$  and 10% less ( $\approx 1-0.899$ ) for temperature at  $150^{\circ}\text{F}$ . The same temperature correction factors for the modulus of elasticity (compression perpendicular to grain) are presented in the following Table.

**Table 7.3.5-1 Correction Factors for Compressive Strength of Hemlock Wood at extreme Temperatures**

at degree C [endnote 17]		-20			150
at degree F	-40	-4	70	150	302
interpolated and extrapolated					
Scale from research, Ref. 8	1.61	1.55	1.42	1.27	1.00
New scale to be used in LSDYNA input	1.140	1.09	1.00	0.899	

### d. *DYNAMIC EFFECT ON ELASTIC MODULUS*

There is no published literature of experiment data on the dynamic effect on elastic modulus of Hemlock wood. The dynamic effect of Hemlock is not considered.

The Hemlock wood is modeled using \*Mat\_elastic. The strips are modeled as brick elements.

### 7.3.6 Alumina Silicate

This is used as thermal insulator for the following applications.

1. Items, 28, 29, 30, 31, 32, 33, 34, 35 of Inner Container Main Body Assembly (Dwg 105E3745, Rev. 8)
2. Items 14, 15 of inner container Lid (Dwg 105E3747, Rev 4)
3. Items 8, 9 of Inner Container End Lid (Dwg 105E3748, Rev 2)

#### a. *THE ELASTIC MODULUS AND DENSITY OF ALUMINA SILICATE*

The Alumina Silicate is used as thermal insulator; therefore there is no structural value intended for the Alumina Silicate. During the end drop orientation, the Alumina Silicate is not in the load path of the fuel bundle except its own weight. During the side drop orientation, the Alumina Silicate blocks provide support for the fuel rod bundle and the Hemlock plates. The loading on the Alumina Silicate is compression. The density and compressive strength of the material are given in Table 2-3 of TN-B1 SAR Rev. 3.

Density = 0.25 gm/cc

		Page 47 of 87
--	--	---------------





## Design Analyses and Calculation

$$\text{Density} = 0.009 \text{ lb/in}^3$$

The compressive strength = 294 kPa = 42.6 psi. A search on the internet found a commercial product provided by Zircar [Ref. 19] closely matches the density and strength of the Alumina Silicate. The product data sheet is attached in Appendix F. According to the Zircar data sheet, the compressive strength is the properties expressed parallel to thickness at 10% compression. Therefore the modulus of elasticity is

$$E = 42.6 \text{ psi}/0.1 = 426 \text{ psi.}$$

### **b. POISSON'S RATIO**

There is no data available on the Poisson's ratio. Since this is a ceramic fiber material with porous interior (as demonstrated by very low density), the deformation of the ceramic material generally is uncoupled between the axial direction and the radial or tangential directions. Therefore, the use of a Poisson's ratio of  $\nu=0$  is recommended.

### **c. EFFECT OF TEMPERATURE ON THE ELASTIC MODULUS**

The ceramic material is suitable for extreme high temperature service up to 2600°F. The mechanical strength is not expected to change significantly between -40°F and 150°F. Therefore, the material property remains constant for this calculation.

### **d. DYNAMIC EFFECT ON ELASTIC MODULUS**

There is no published literature of experiment data on the dynamic effect on elastic modulus of alumina silicate. Therefore, the dynamic effect of alumina silicate is not considered.

The alumina silicate is a ceramic fiber with a rigid outer surface and unbound interior space. It is modeled in LSDYNA using material model Crushable\_Foam. Since the material is loaded to less than 10% strain, it behaves elastically in this container application.

### **7.3.7 Polyethylene Foam**

This is used as shock absorber for the following applications.

1. Items 36, 37, 38, 39, 40, 41 of Inner Container Main Body Assembly (Dwg 105E3745, Rev. 8)
2. Item 16 of Inner Container Lid (Dwg 105E3747, Rev 4)

#### **a. THE LOAD-DEFLECTION CURVE AND DENSITY OF POLYETHYLENE FOAM**

The density and compressive strength of the material are given in AREVA FS1-0014159 TN-B1 Rev. 3 [Ref. 7], Table 2-3.

$$\text{Specific gravity} = 0.144$$





## Design Analyses and Calculation

Density =  $0.068 \text{ gm/cm}^3 = 0.00246 \text{ lb/in}^3 = 4.3 \text{ lb/ft}^3$  (PCF). The nominal weight is 4 PCF.

This is the Type III material specified in [Ref. 20]. Noting that the licensing drawings allow the option of using heavier weight foam, such as 9 PCF foam. Per [Ref. 24], the average compressive strength of the 9-PCF foam at 25% strain is 46 psi, resulting in more energy-absorbing capability than the 4-PCF foam. Therefore, the use of the 4 PCF foam material is more conservative in the analysis and bounding.

Per AREVA FS1-0021899 Rev. 1, Section 3.5, the compressive strength is 0.2MPa at 50% strain.

$$\sigma_{50\%} = 0.2 \text{ MPa} = 29 \text{ psi}$$

Per [Ref. 24], for the Type III foam (4 PCF), the average compressive strength at 25% strain is 16 psi.

$$\sigma_{25\%} = 16 \text{ psi}$$

This material is modeled using LSDYNA material model Crushable\_Foam in the calculation.

### b. POISSON'S RATIO

There is no data available on the Poisson's ratio. Since this is a foam material with porous interior (as demonstrated by very low density), the material deformation is generally uncoupled between the axial direction and the radial or tangential directions. Therefore, the use of a Poisson's ratio of  $\nu=0$  is recommended.

### c. EFFECT OF TEMPERATURE ON THE ELASTIC MODULUS

The mechanical strength is not expected to change significantly between  $-40^\circ\text{F}$  and  $150^\circ\text{F}$ . Therefore, the material property remains constant for this calculation.

The polyethylene foams are modeled as brick elements using material model \*Crushable\_foam.

### d. DYNAMIC EFFECT ON ELASTIC MODULUS

Based on a test sample of 50 mm thick x 125 mm x 125mm to ASTM D1596 standard [Ref. 21], the Load-Deflection curve of the dynamic cushioning properties for the Type III foam taken from Figure 2 of [Ref. 20] is shown in the figure below.



ATKINS

## Design Analyses and Calculation

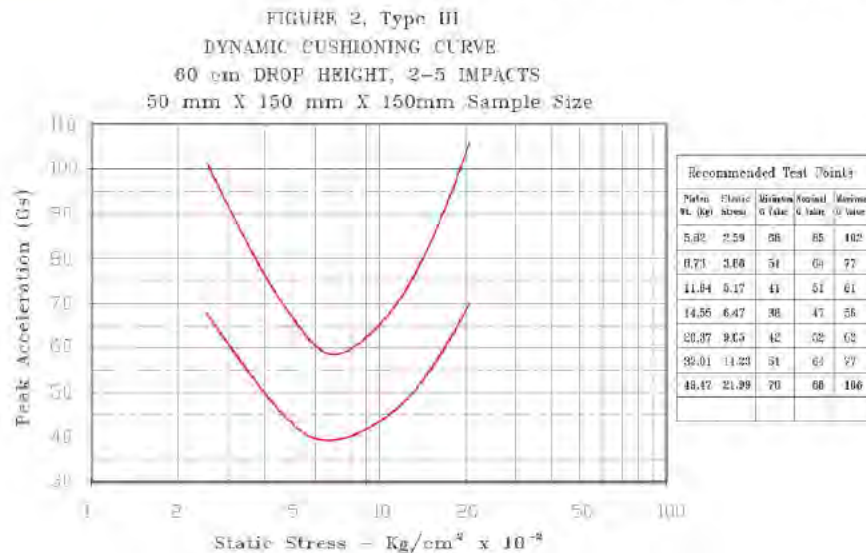


Figure 7.3.7-1 Dynamic Cushioning Curve for Polyethylene, Type III

According to the test procedure described in [Ref. 22], the shock performance of cushion materials is measured using instrumented impacts resulting in a cushion curve such as that shown in Figure 7.3.7-1. The cushion curve describes the level of deceleration transmitted through a given thickness of material as a function of static stress (loading) on the cushion and the drop height.

Procedures for running a cushion curve are covered by ASTM D1596, D4168, and similar MIL Specs. They are basically a matter of dropping a guided platen of predetermined mass onto a cushion of known thickness and area from a given drop height. The amount of deceleration transmitted through the cushion is measured by an accelerometer mounted on the platen or test block. The results are displayed on an oscilloscope or similar readout device.

The procedure results in cushion curves, such as those in Figure 7.3.7-1, with peak deceleration on the vertical axis and static stress on the horizontal axis (static stress = weight/bearing area). Each curve should be drawn from a minimum of 5 test points (static stress levels) and each test point is the average of the last 4 of 5 (the first impact data point is discarded. The average of No 2 to No 5 impacts as indicated on the above figure) deceleration readings from the cushion material. Most cushion curves have the general shape of those in Figure 7.3.7-1 above. The left-hand portion of the curve shows a relatively high deceleration transmitted through the cushion. In this area the static stress is relatively low because of the light weight on the cushion; the object (the platen in the cushion test) does not have sufficient force to deflect the cushion and the result is a rigid or "stiff" impact. The effect resembles dropping a product onto a rigid surface. In the center portion of the curve (where the cushion is being used effectively), the falling object has sufficient force to deflect the cushion and





## Design Analyses and Calculation

cause the deceleration to be spread over a longer period of time. The result is a lower deceleration level. On the right-hand portion of the curve, the cushion material is stressed beyond its optimum design limit and the specimen continues to penetrate through the cushion (it bottoms out) and impacts with the surface on which the cushion is resting. Thus, it approaches using no cushion at all resulting in, once again, high deceleration levels. It is desirable to use the cushion in the lower portion of the curve where its performance is optimum. When the product limiting acceleration, weight and design drop height are known, the usable range of cushion area can be determined for a given cushion material and thickness.

Assuming the Load-deflection curve of the cushion is linear; using the formula in Page 10 of [Ref. 22], the deflection of the cushion can be calculated as follows.

$$X = 2 \times H / (G - 2) \quad \text{Equation (a)}$$

Where:

X = cushion dynamic deflection in cm (or inches)

H = drop height in cm (or inches) = 60 cm

G = the required deceleration level (g's)

Remember that this exercise gives the theoretical dynamic deflection necessary, not the overall cushion thickness. In general, cushion materials such as expanded polystyrene and polyethylene foam will compress approximately 40 to 70% of their total thickness before "bottoming out" starts to occur. More flexible materials such as polyurethane foam will compress up to 80% of total thickness before beginning to bottom out.

A typical compressive Load-Deflection curve for the polyethylene foam taken from [Ref. 23] is shown in the figure below.

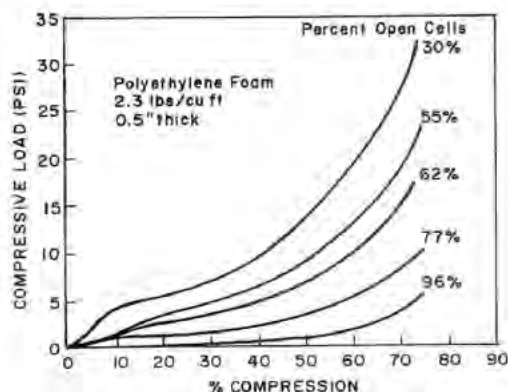
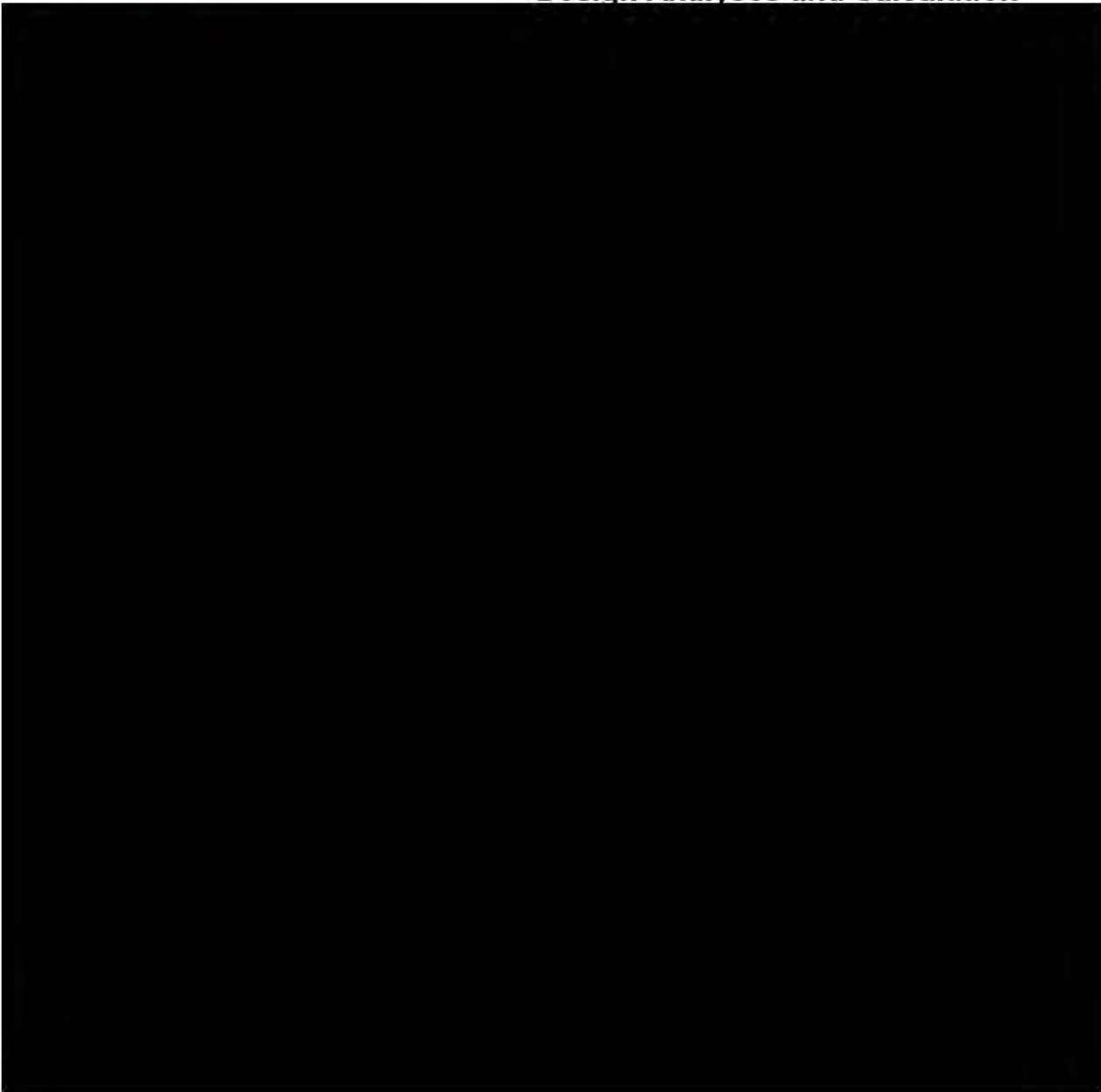


Figure 7.3.7-2 Compressive Load Versus Compression of Different Fraction Open Cells.



**ATKINS**

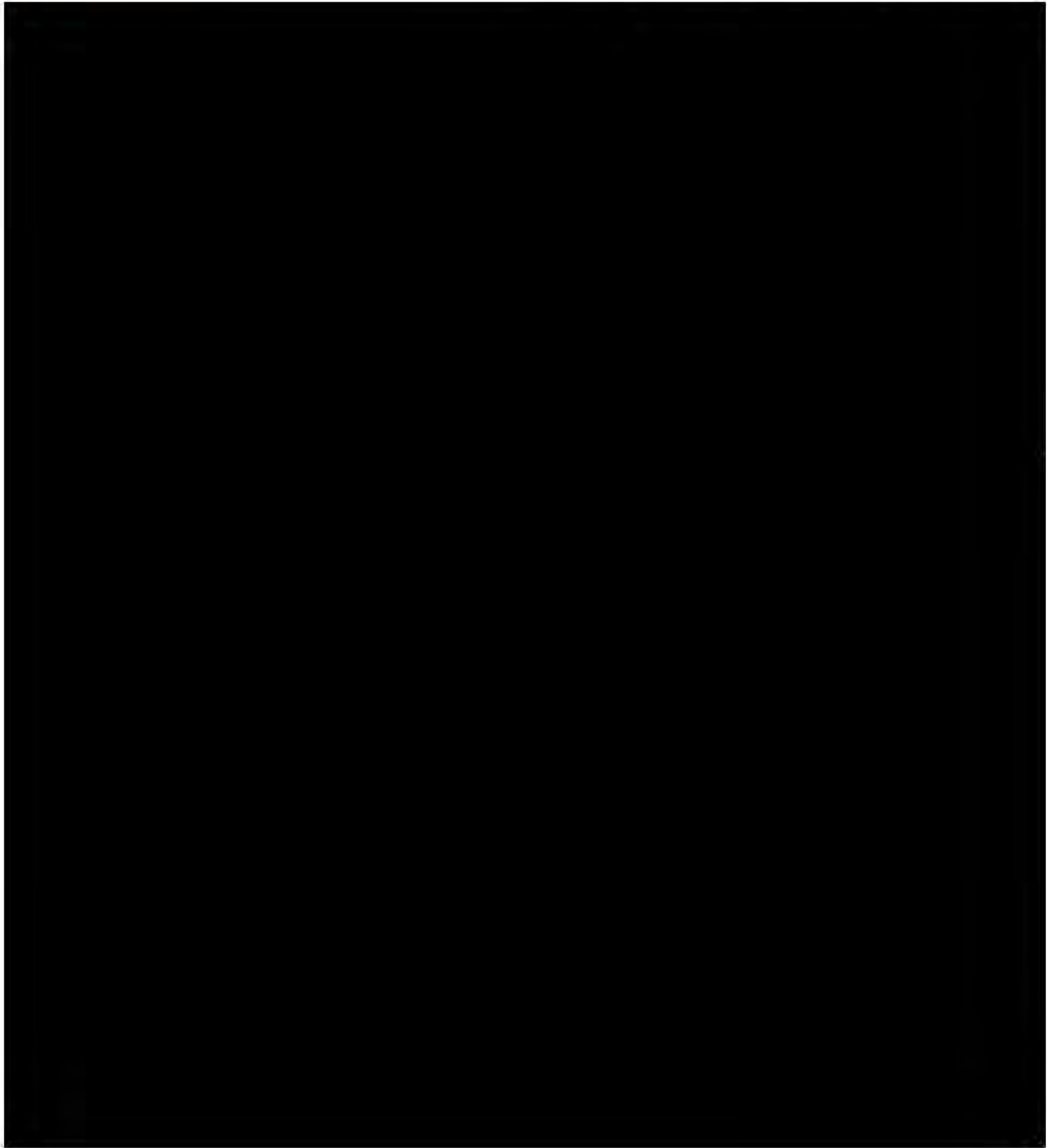
**Design Analyses and Calculation**







Design Analyses and Calculation







## Design Analyses and Calculation

### 8. Evaluation Results

#### 8.1 Validation of Finite Element Model

##### 8.1.1 Comparison with GNF-Japan RAF-II Drop Tests

Two analysis drop cases are performed using the developed LSDYNA finite element analysis model and specified material properties for validation with the actual 30-ft drop tests performed on the RAF-II Certified Test Unit (CTU) at room temperature by GNF-Japan [Ref. 1]. The RAF-II CTU has the identical material properties and geometry as the AREVA TN-B1 shipping container. For the drop tests, the total package weight is given as 1490 kg, which corresponds to a fuel assembly weight of 560 kg. This is less than the AREVA ATRIUM-11 fuel assembly weight of 684 kg to be shipped in the TN-B1 container, and this is accounted for in the analysis by adjusting the density of the rigid body representing the mass of the fuel elements in the model to match the test weight of 1490 kg. This is the only modification made to the finite element model. Material properties at room temperature are assigned to the model components to agree with the test conditions. The designations of the two analysis drop cases for material validation are listed in the table below.

**Table 8.1.1-1 Designation of Analysis Drop Cases for Material Validation**

Case ID	Drop Orientation
HAC-V1	HAC free drop, vertical bottom end
HAC-V2	HAC free drop, horizontal side drop on lid



**Table 8.1.1-2 Comparison of Acceleration Results from GNF-Japan Drop Tests (Ref.1) and LSDYNA Simulations**

Drop Orientation	Sensor Location	Drop Test G	Case ID	LSDYNA G
HAC free drop, vertical bottom end	Inner container outer shell	303	HAC-V1	
HAC free drop, horizontal side drop on lid	Inner container outer shell	194	HAC-V2	

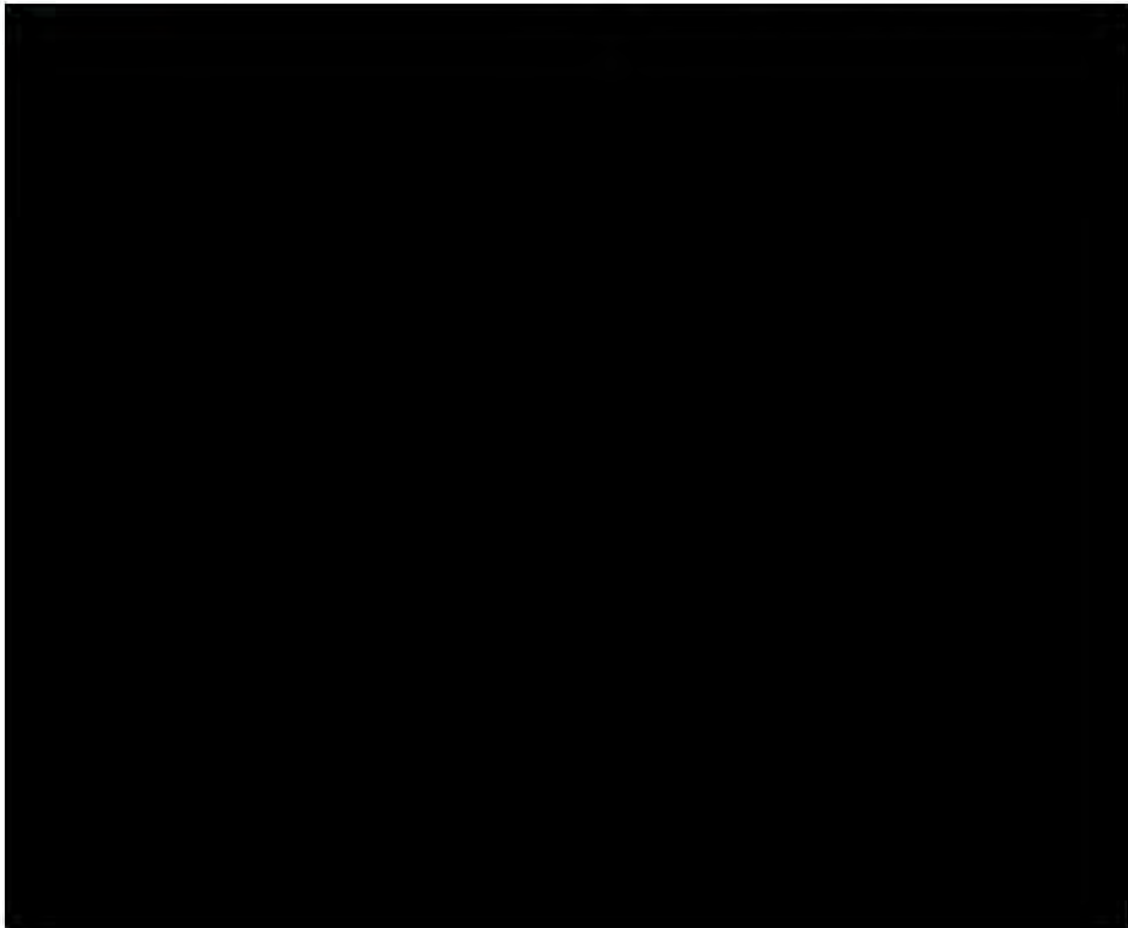
Damage to the RAF-II CTU from the drop tests is documented in Ref. 1. For the end drop and horizontal drop on the lid, a comparison of deformation test results with results calculated from the LSDYNA simulations is given in Table 8.1-3.

		Page 54 of 87
--	--	---------------





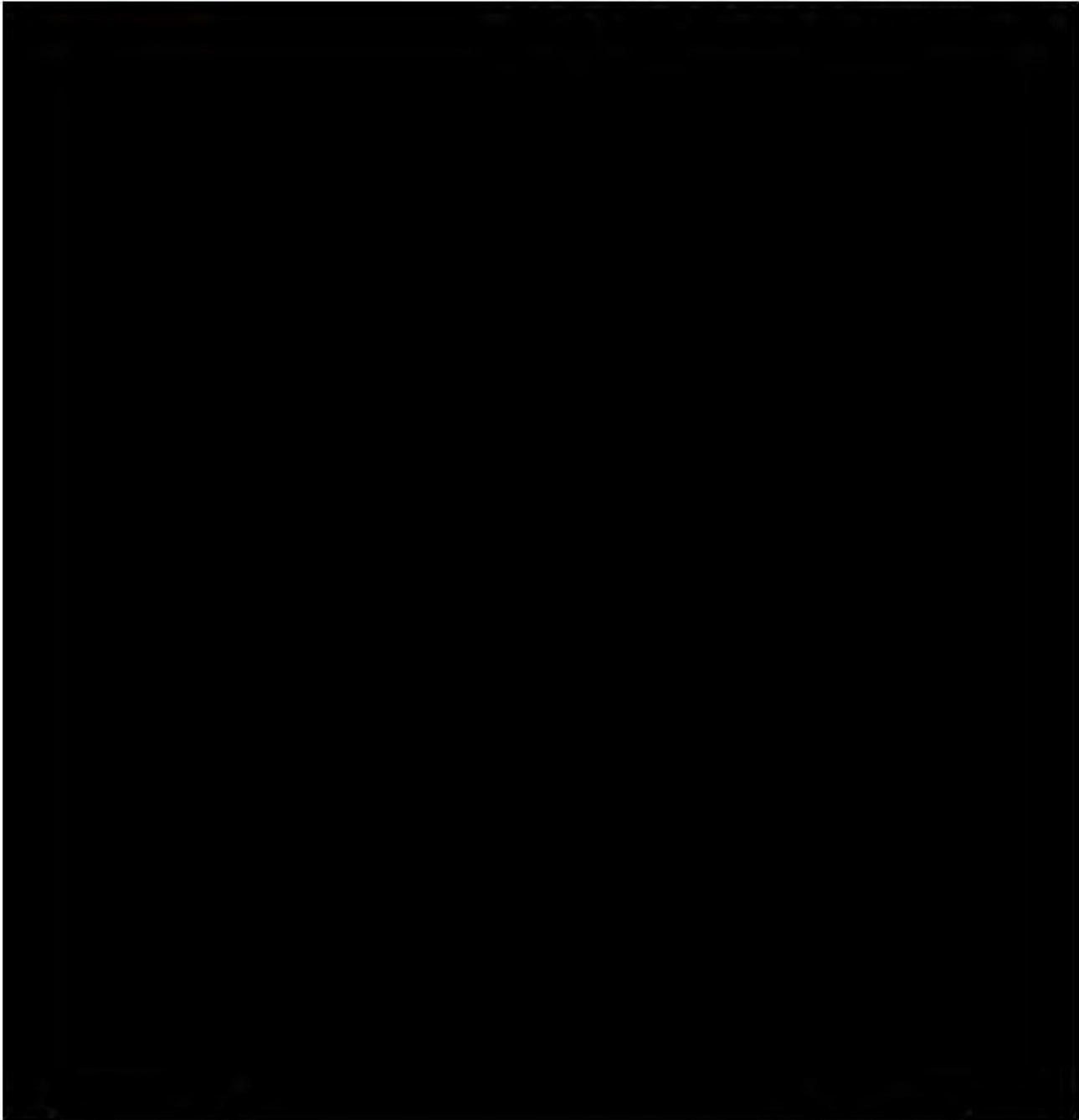
Design Analyses and Calculation





**ATKINS**

**Design Analyses and Calculation**





**ATKINS**

**Design Analyses and Calculation**

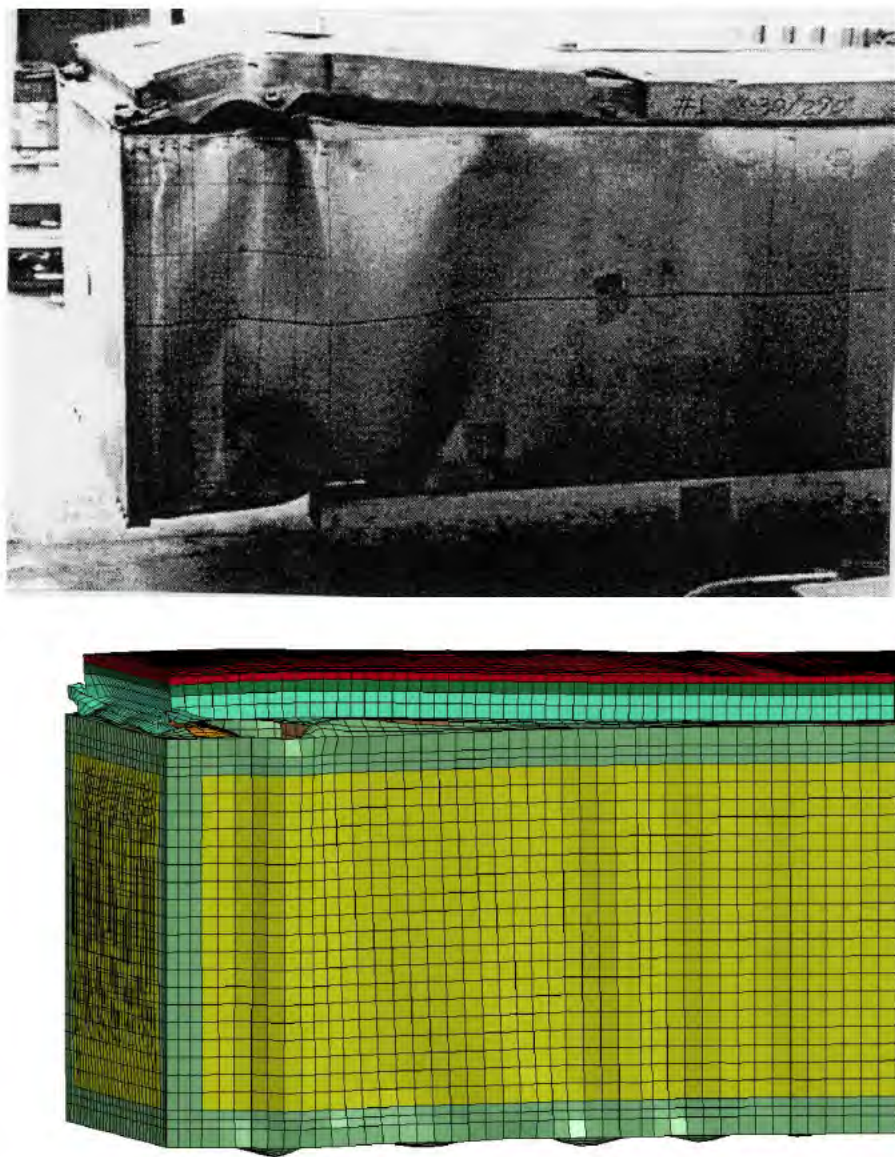


Figure 8.1.1-3 Comparison of Container Deformation from GNF-Japan Drop Test (top, Ref. 1) and LSDYNA Simulation (bottom), Bottom End Drop



**ATKINS**

**Design Analyses and Calculation**

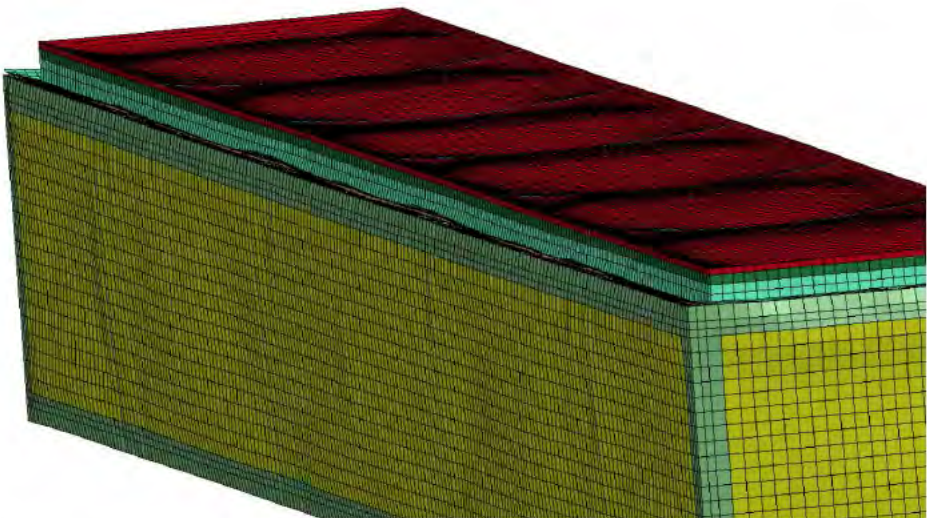
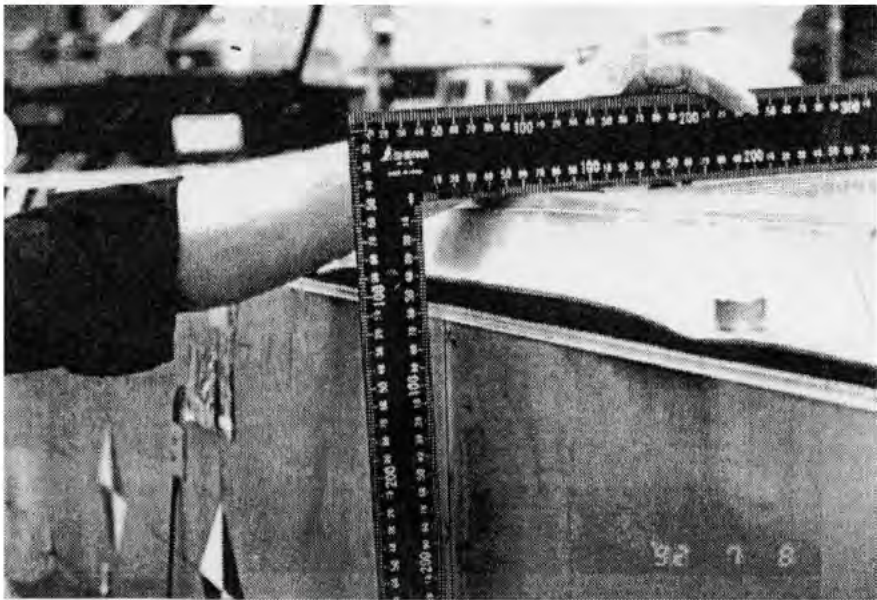


Figure 8.1.1-4 Comparison of Container Deformation from GNF-Japan Drop Test (top, Ref. 1) and LSDYNA Simulation (bottom), Horizontal Side Drop on Lid

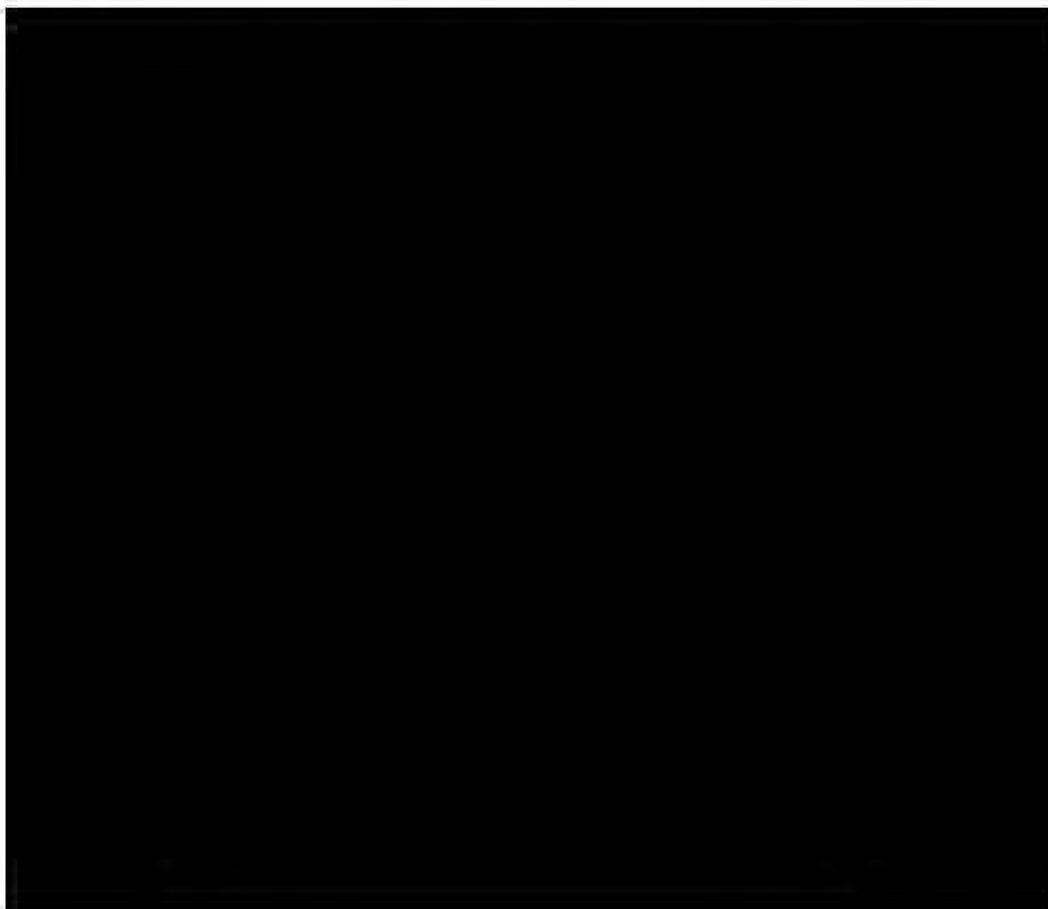




## Design Analyses and Calculation

### 8.1.2 Comparison with NTRC RAF-II Drop Tests

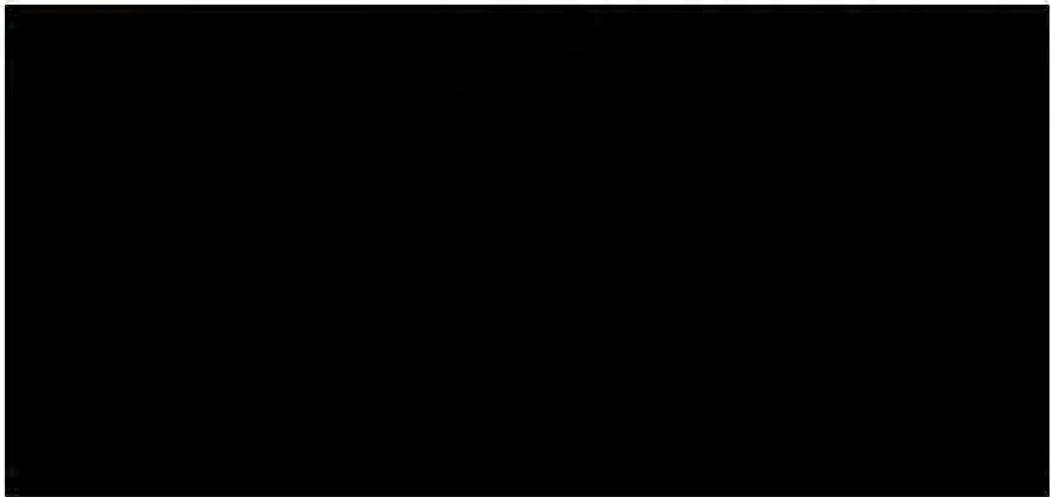
Testing of the same RAF-II container package for two 30-ft drop orientations was also performed at the National Transportation Research Center (NTRC) in Oak Ridge, Tennessee [Refs. 25, 26]. In these drop tests, mock up fuel assemblies were used to represent the fuel mass (ATRIUM-10 design). The total package weights of the two certified test units were 1616 kg for CTU-1 and 1622 kg for CTU-2. These weights are higher than those used in the drop test and LSDYNA analysis comparisons summarized above in section 8.1.1, and are attributed primarily to higher fuel contents weights of 684 kg for CTU-1 and 685 kg for CTU-2.







Design Analyses and Calculation





**ATKINS**

## Design Analyses and Calculation

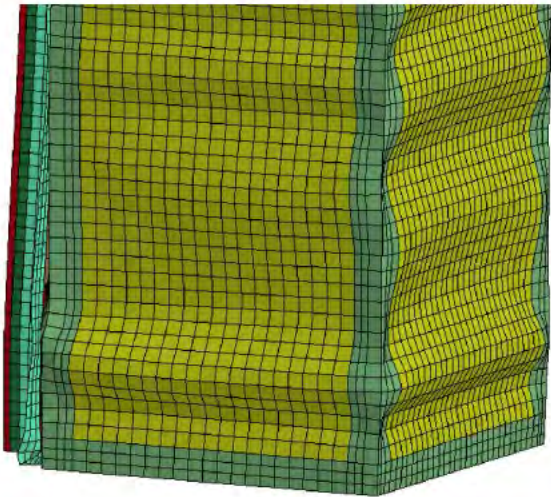


Figure 8.1.2-1 Comparison of Container Deformation from NTRC Drop Test (top, Ref. 26) and LSDYNA Simulation (bottom), Bottom End Drop



ATKINS

Design Analyses and Calculation

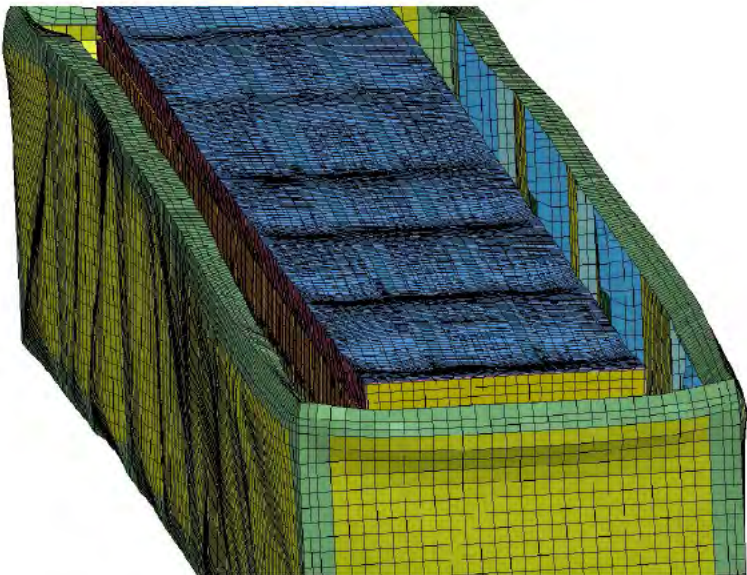


Figure 8.1.2-2 Comparison of Container Deformation from NTRC Drop Test (top, Ref.26) and LSDYNA Simulation (bottom), 15-Degree Slap Down Drop on Lid, Inner Container Lid Deformation





Design Analyses and Calculation



Secondary Impact End



Primary Impact End

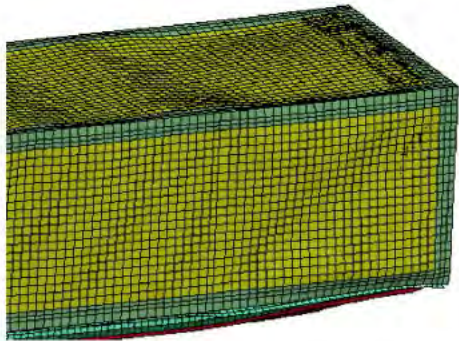
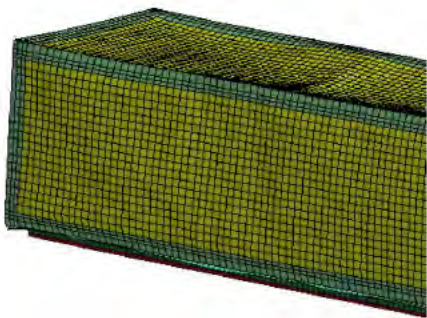


Figure 8.1.2-3 Comparison of Container Deformation from NTRC Drop Test (top, Ref. 26) and LSDYNA Simulation (bottom), 15-Degree Slap Down Drop on Lid, Outer Container Deformation

8.2 Acceleration Results of LSDYNA Simulated Drops: Normal Conditions of Transport (NCT)





**ATKINS**

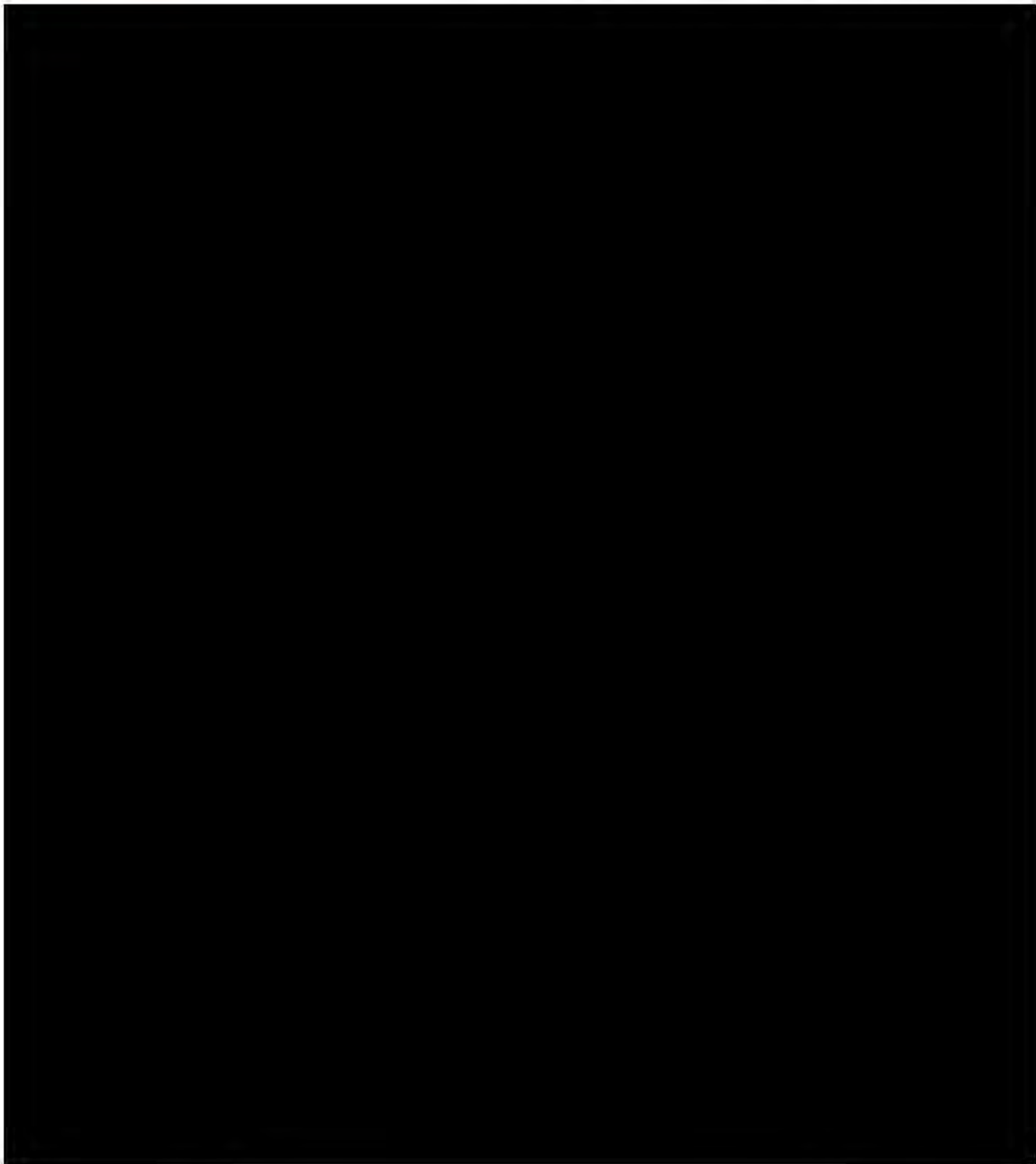
## Design Analyses and Calculation







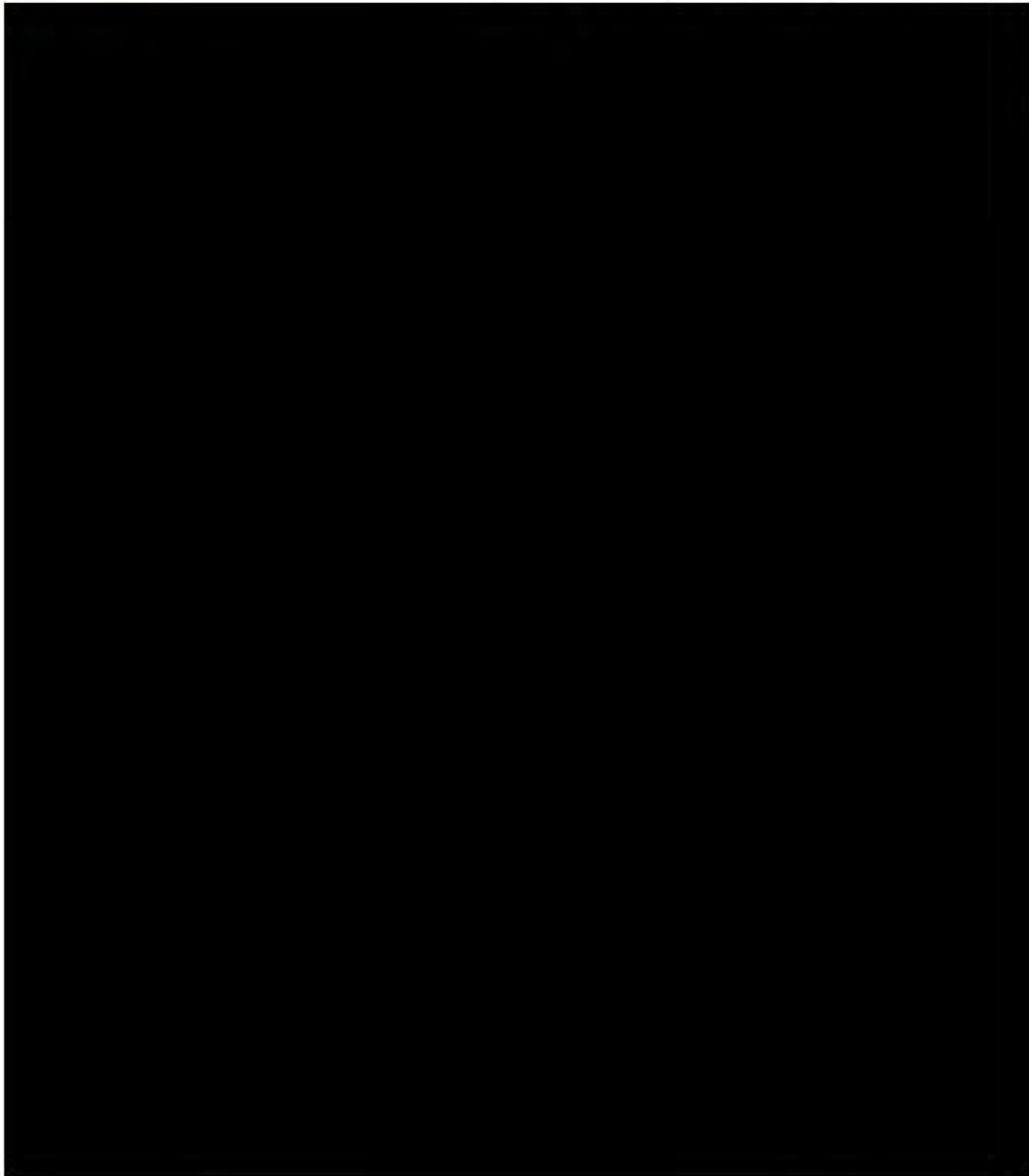
Design Analyses and Calculation







Design Analyses and Calculation







## Design Analyses and Calculation

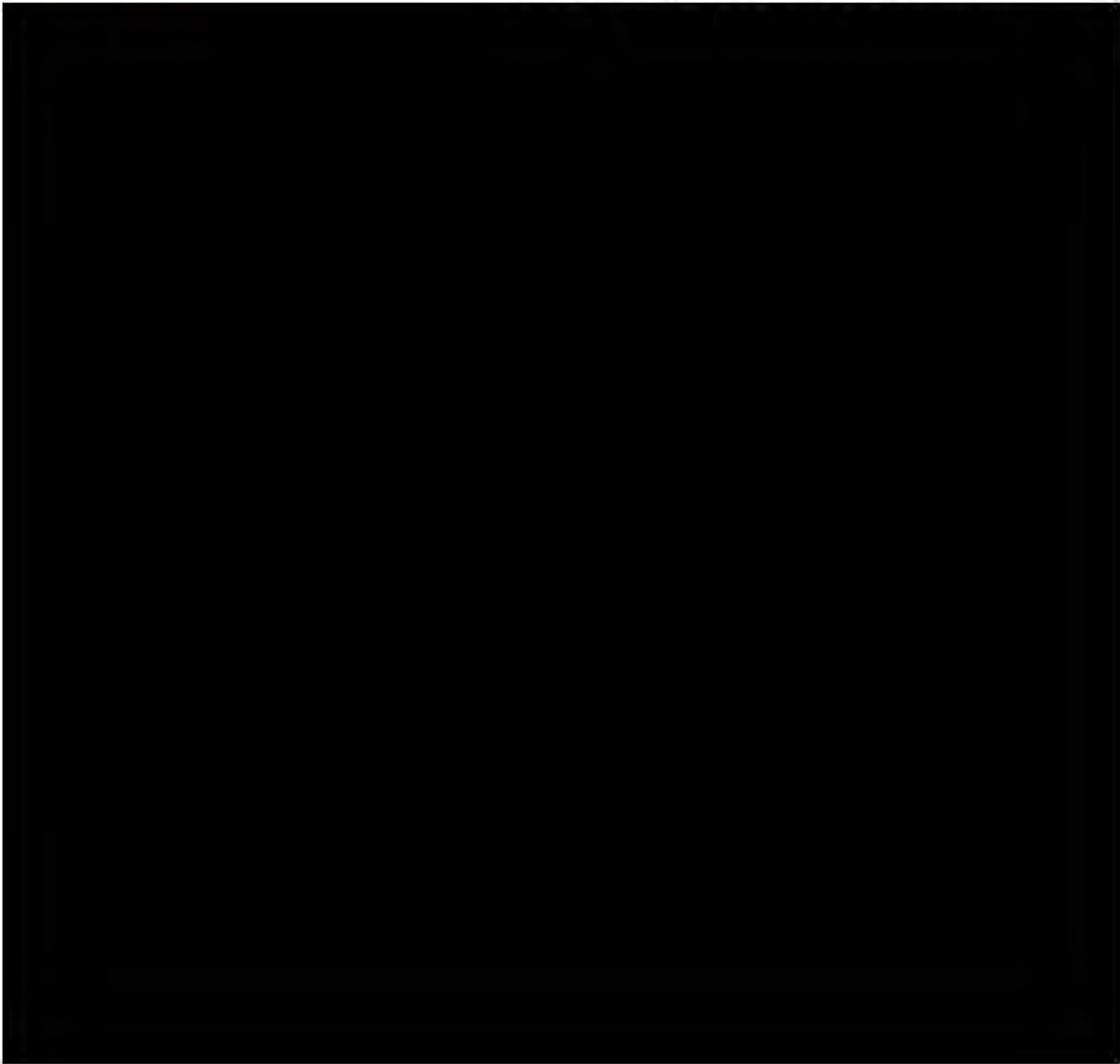
### 8.3 Acceleration Results of LSDYNA Simulated Drops: Hypothetical Accident Conditions (HAC)





**ATKINS**

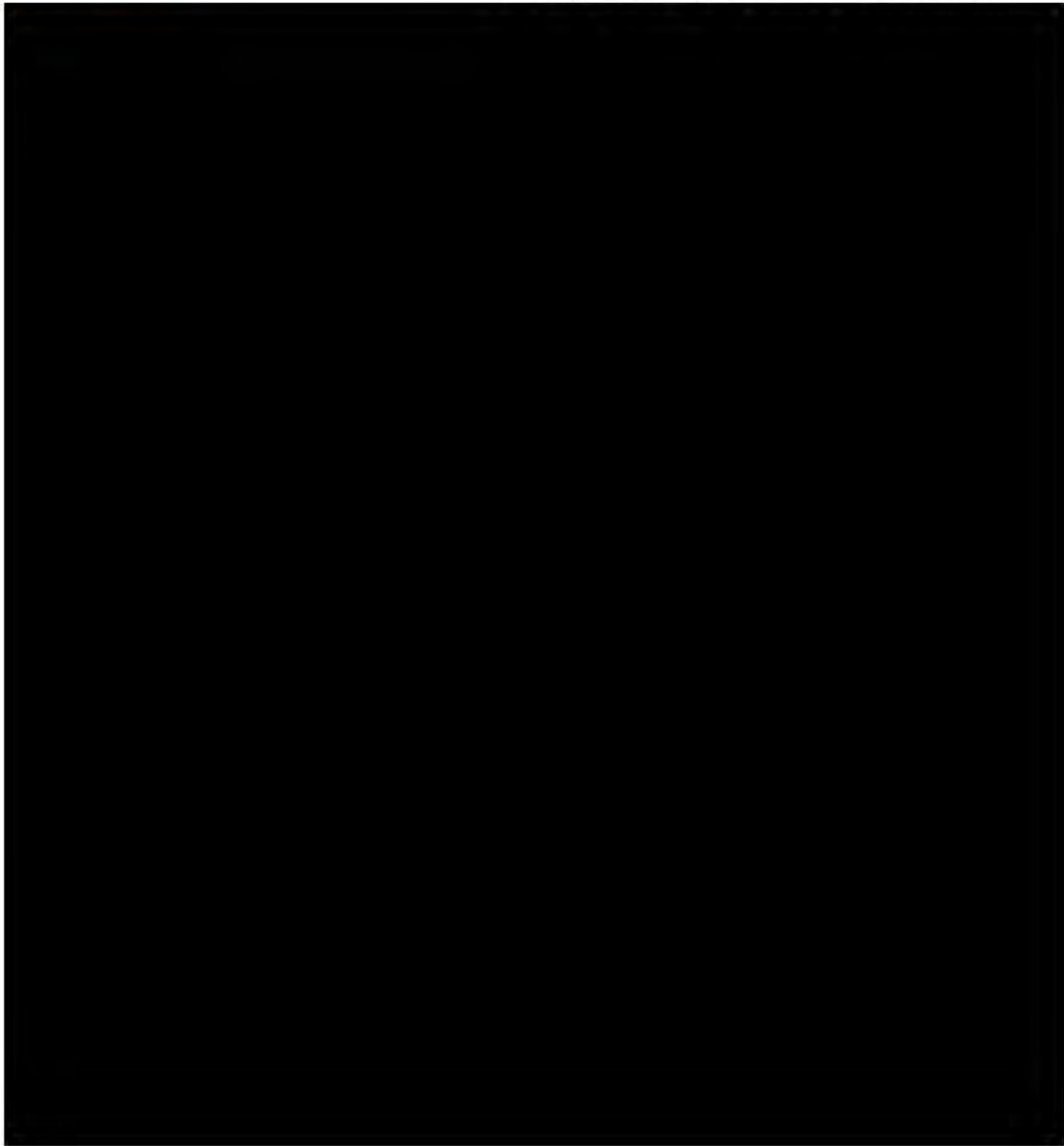
**Design Analyses and Calculation**







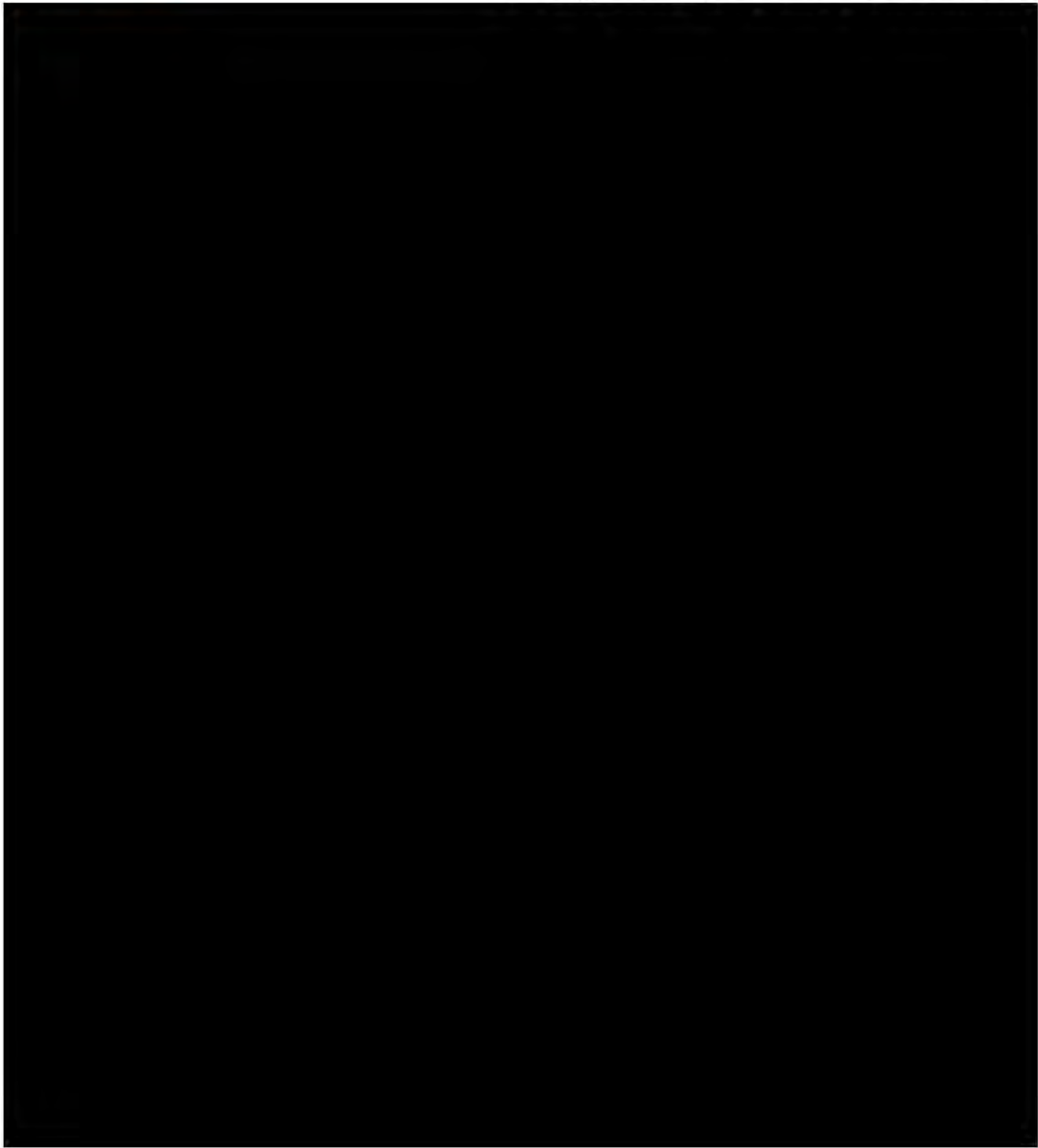
Design Analyses and Calculation





**ATKINS**

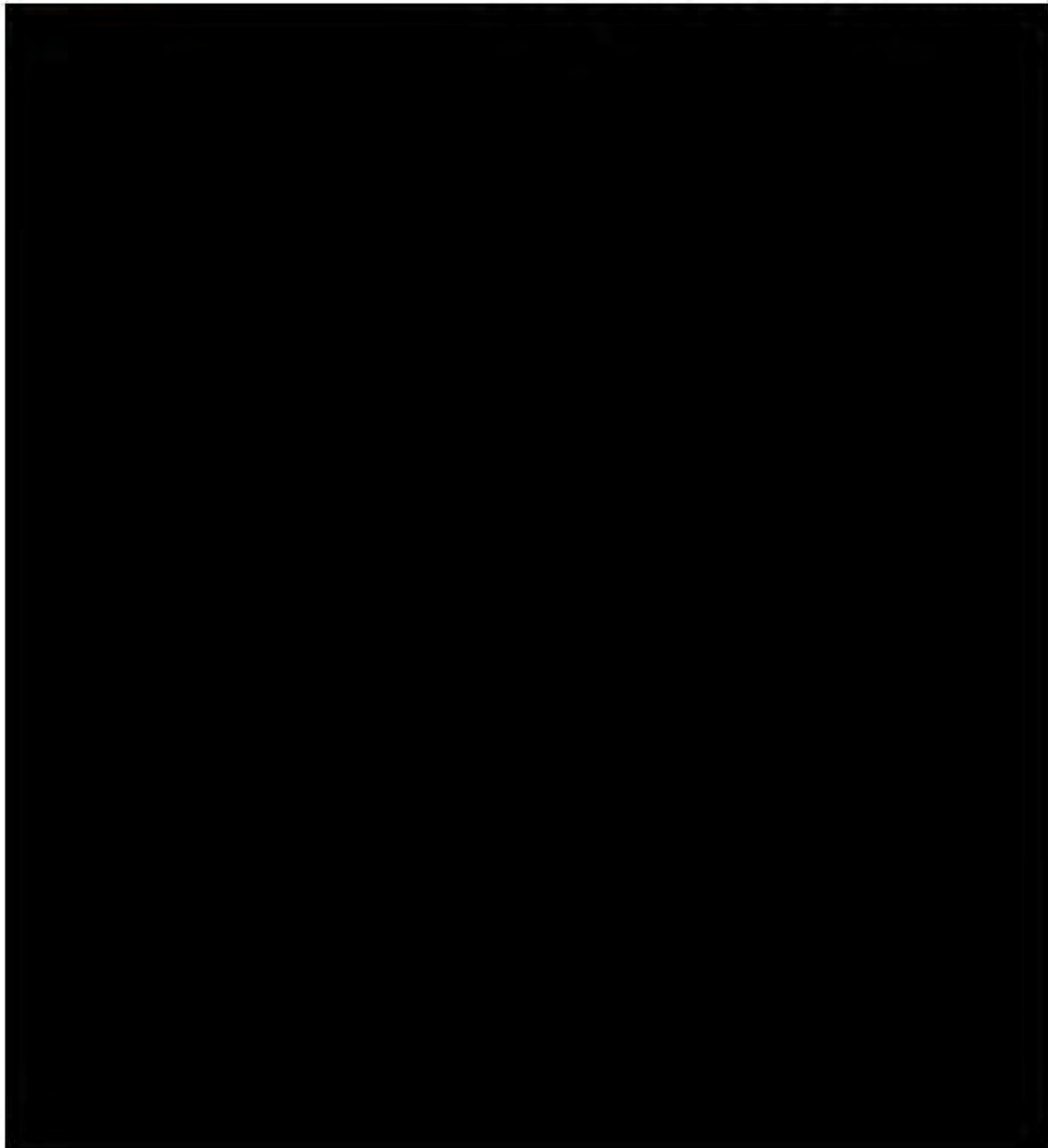
**Design Analyses and Calculation**





**ATKINS**

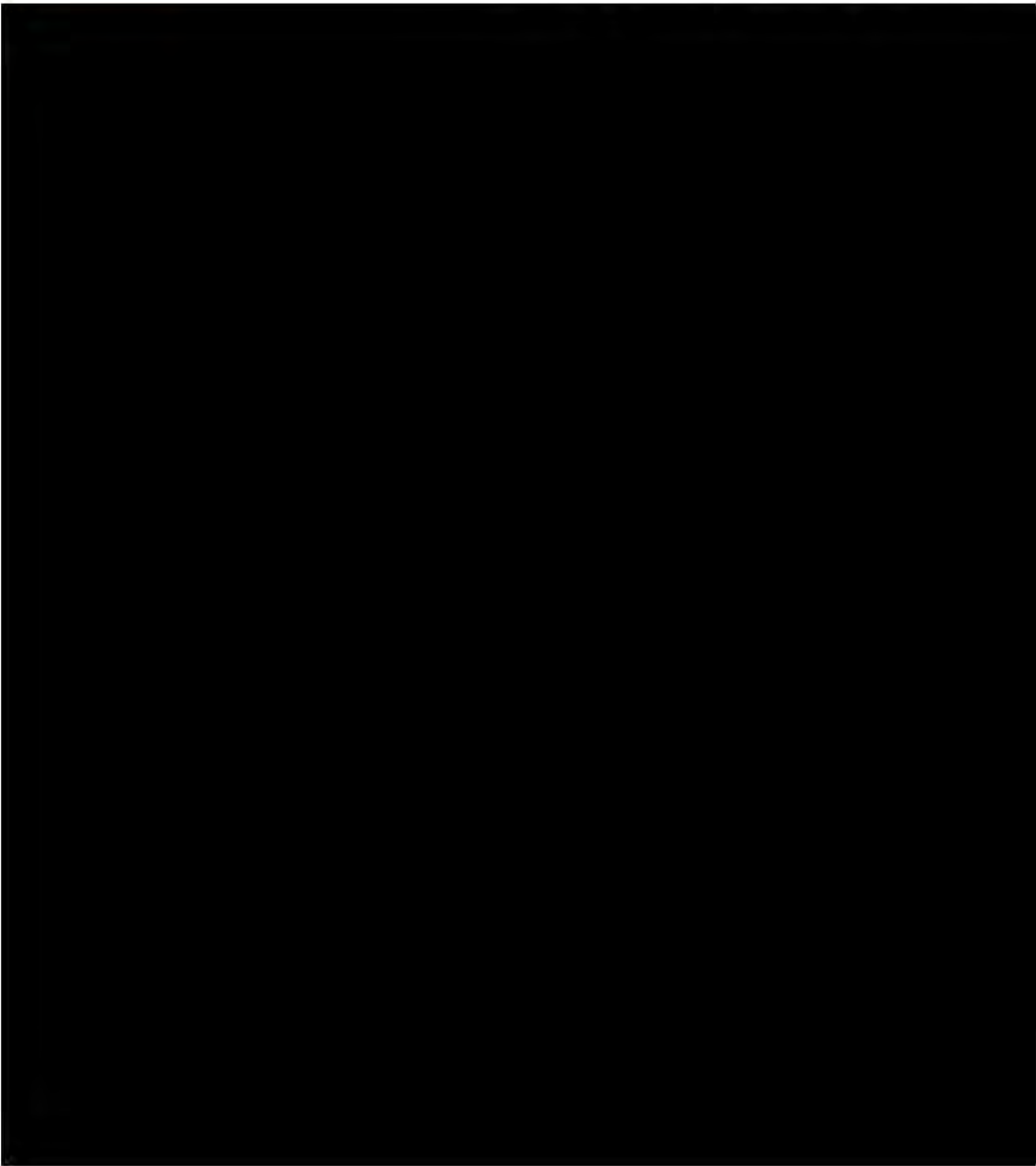
## Design Analyses and Calculation







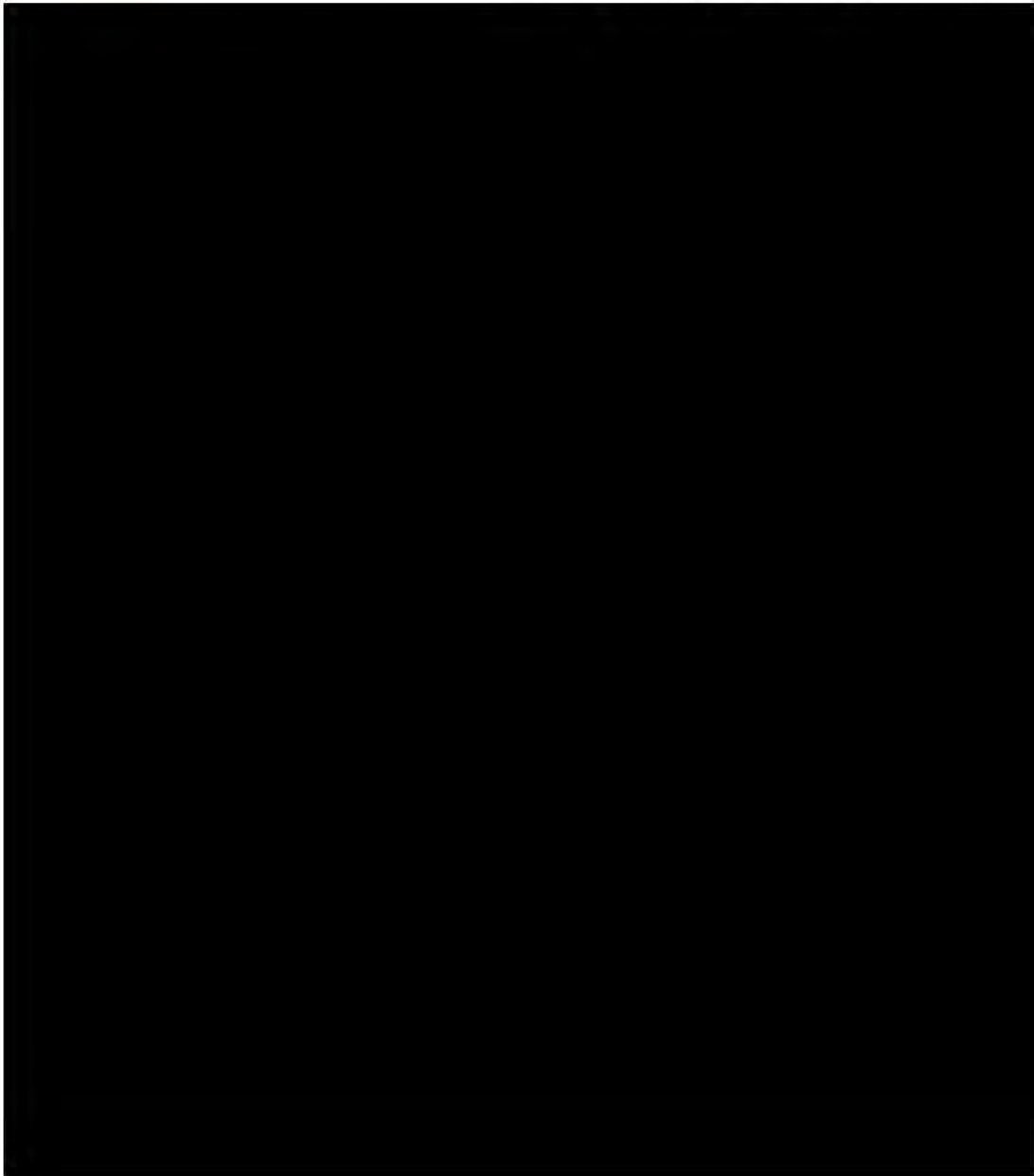
Design Analyses and Calculation







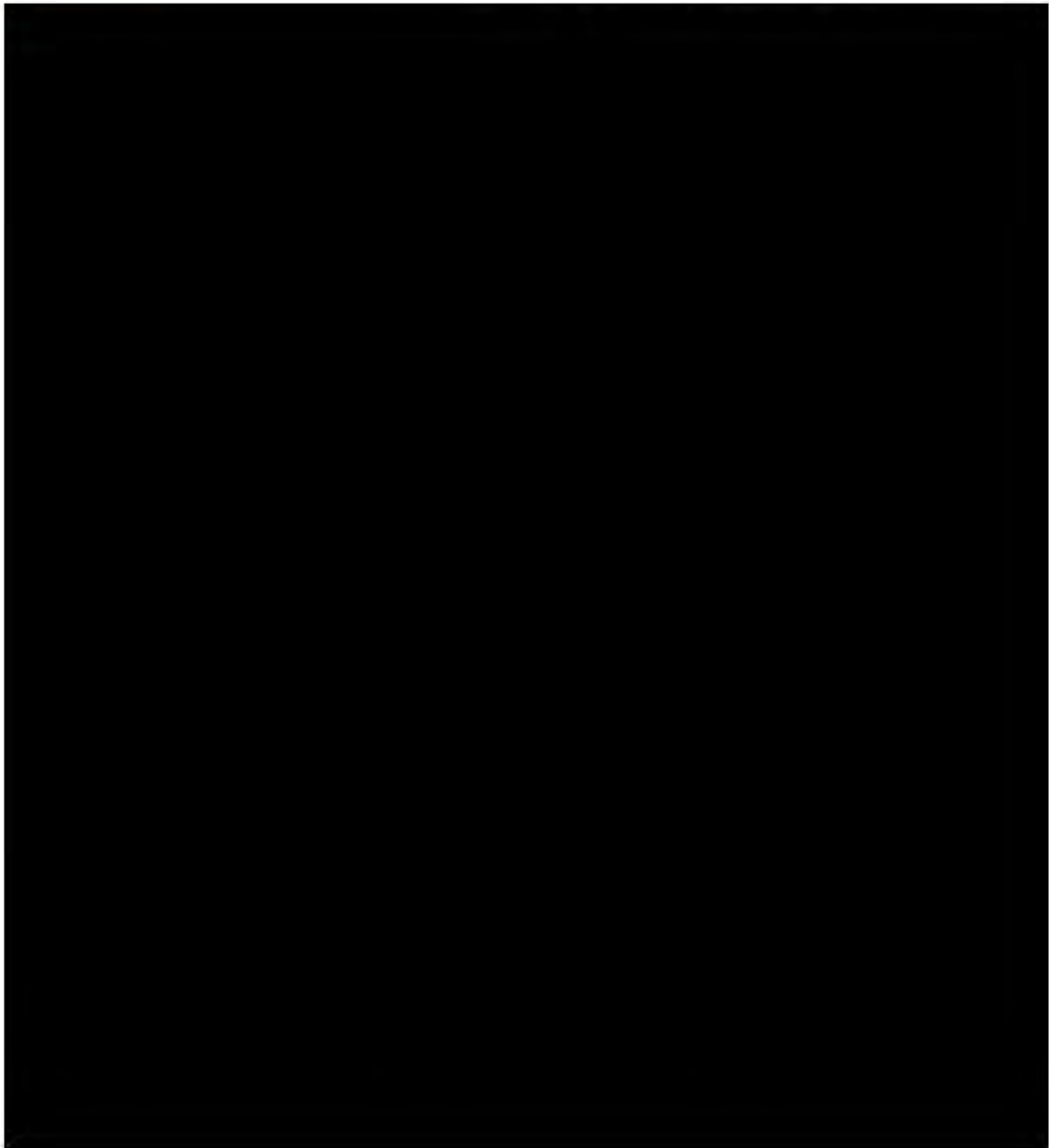
Design Analyses and Calculation







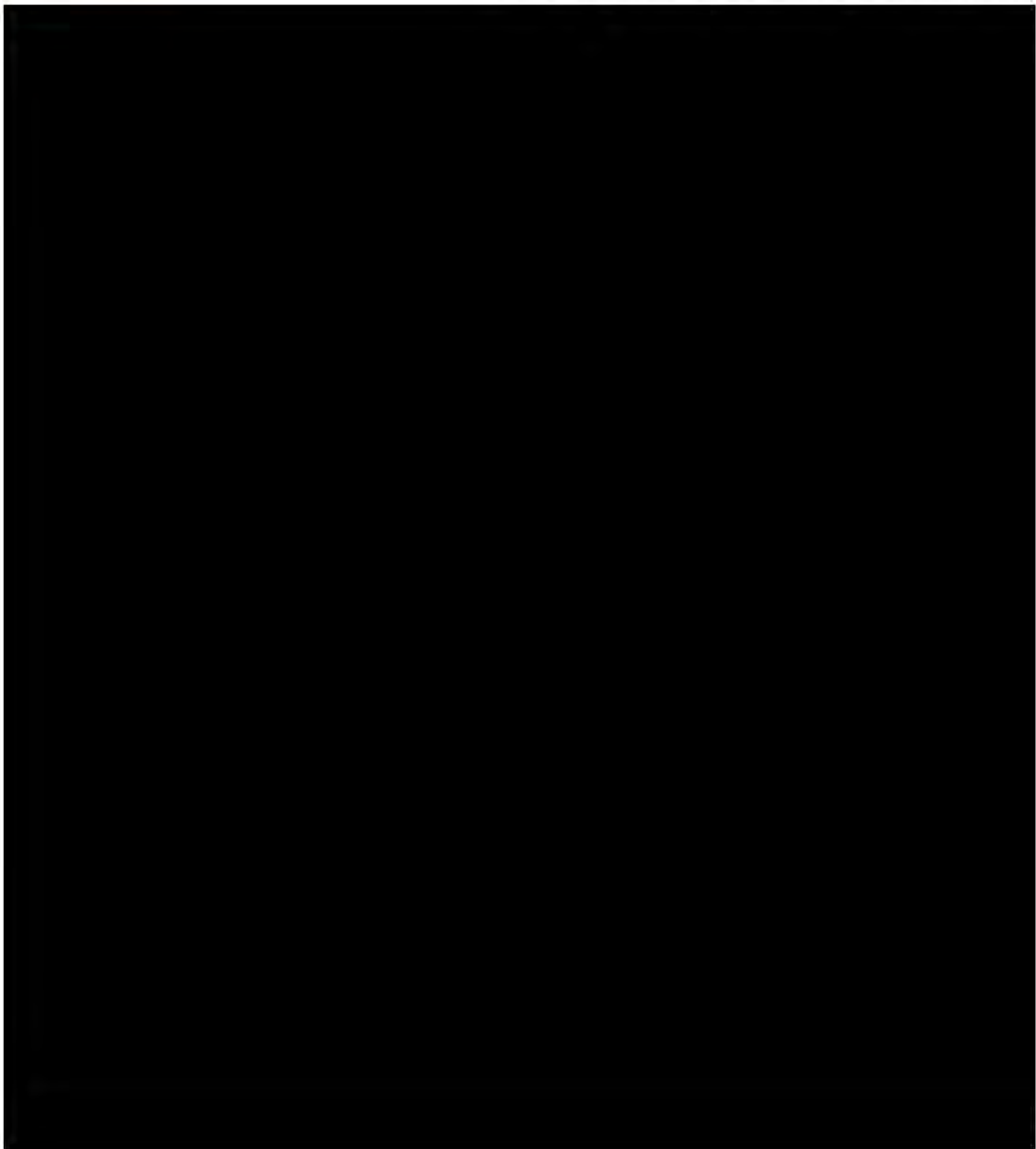
Design Analyses and Calculation







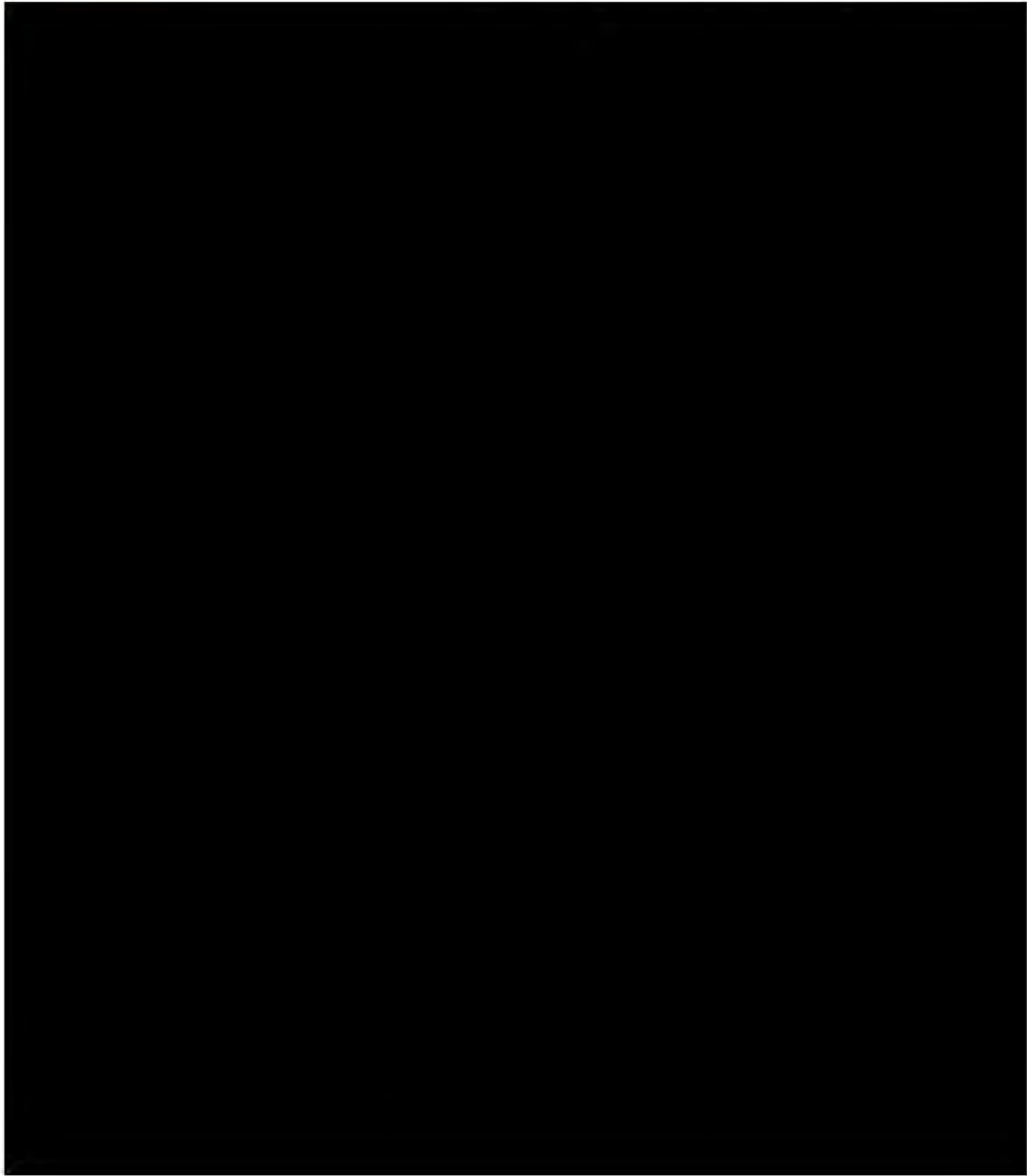
Design Analyses and Calculation







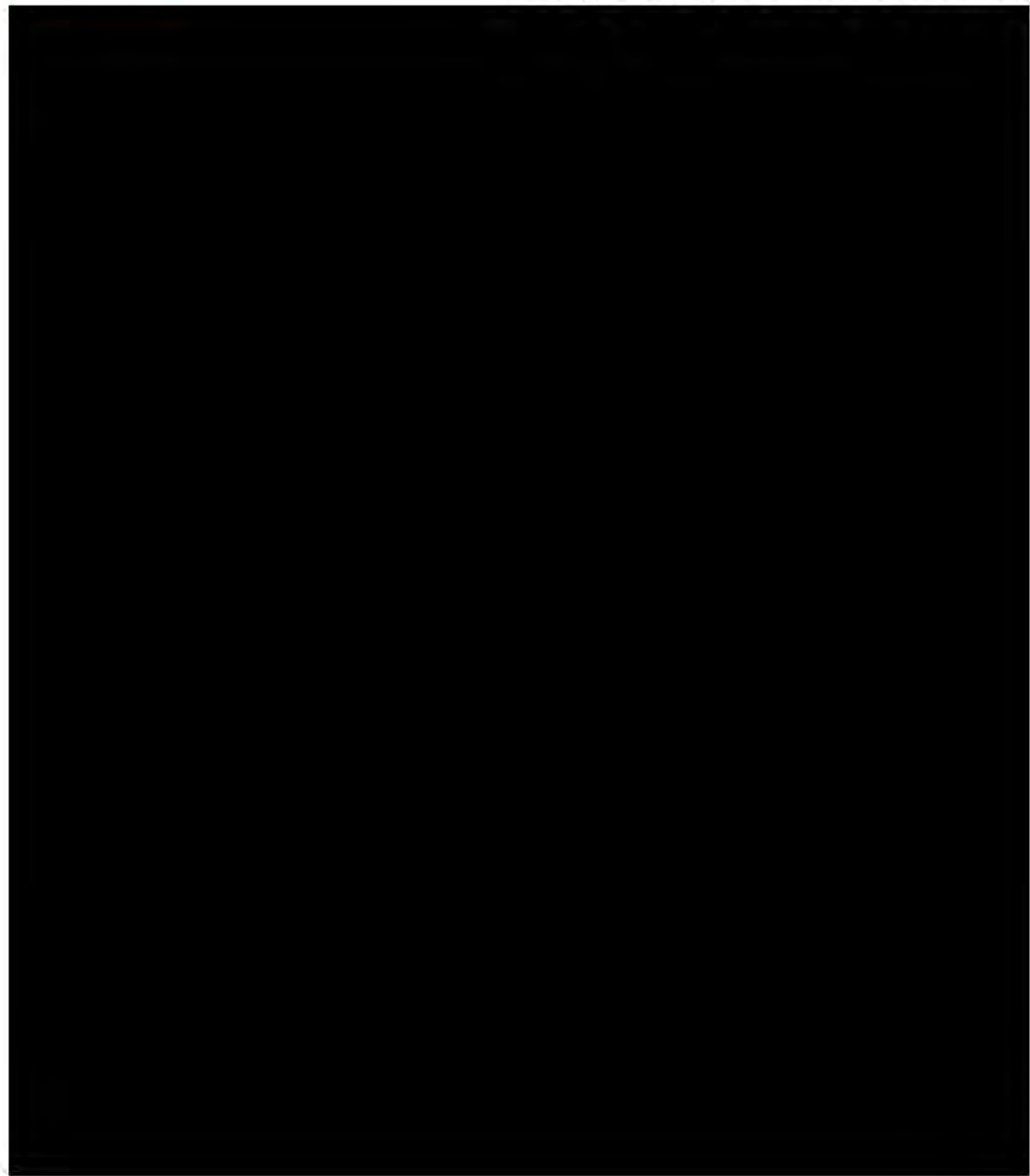
Design Analyses and Calculation







Design Analyses and Calculation







Design Analyses and Calculation

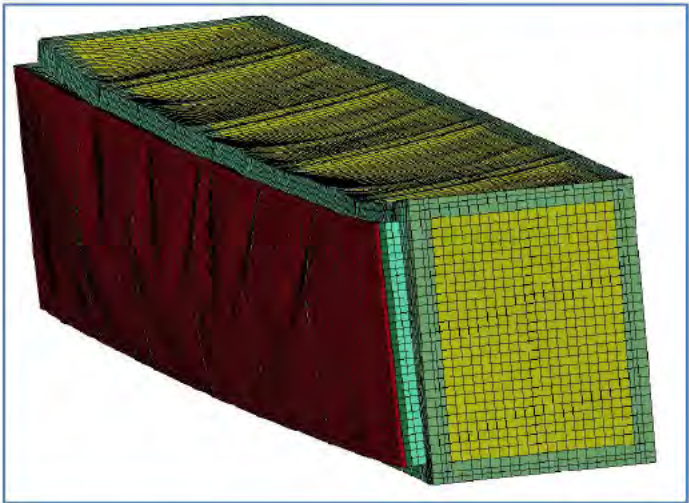
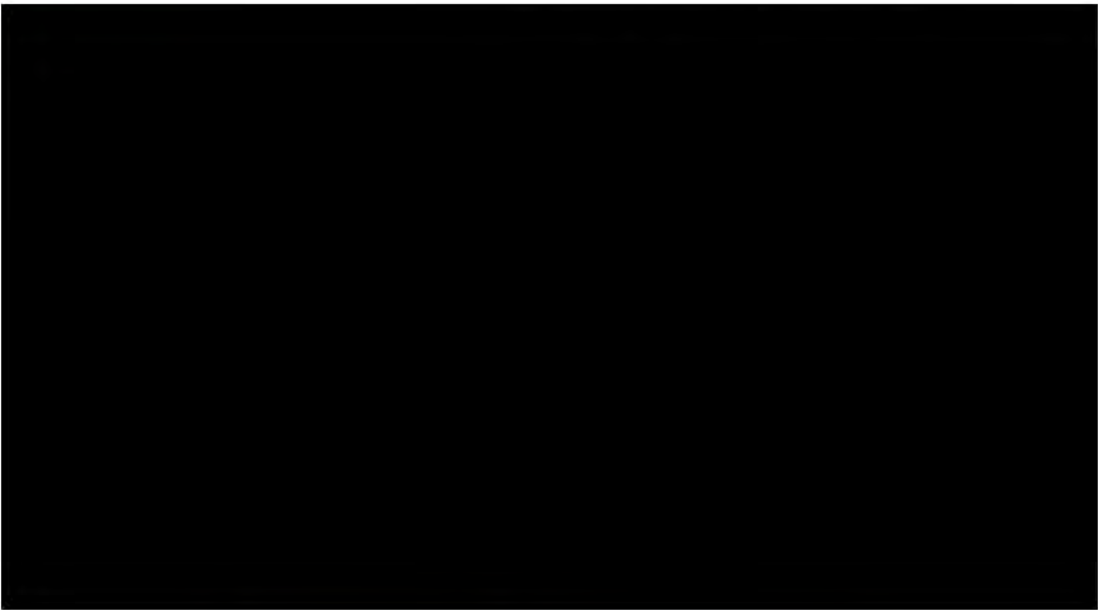


Figure 8.3-20 Container Deformation, Horizontal Drop on Side, Drop Case HAC04



**ATKINS**

# Design Analyses and Calculation

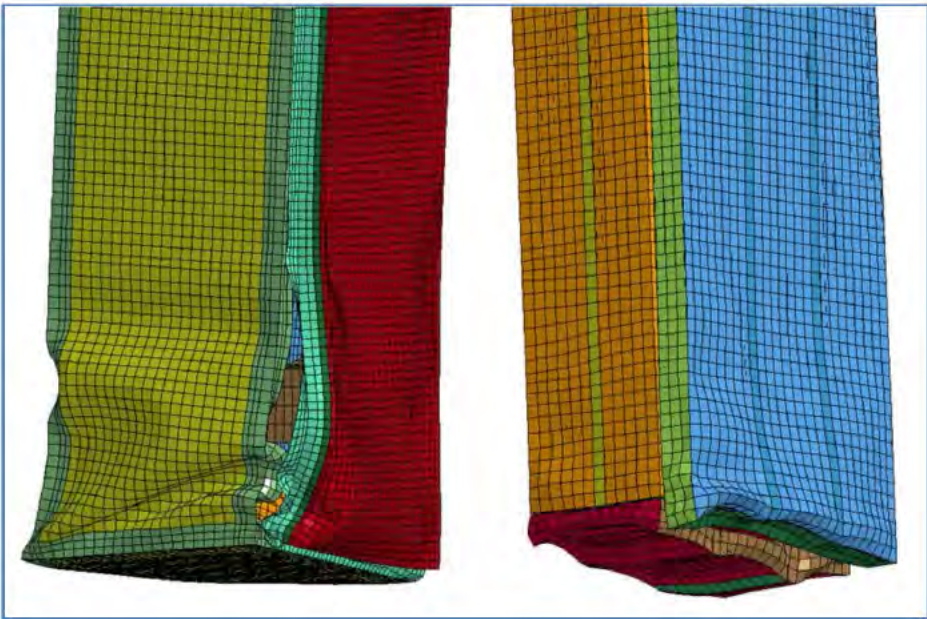


Figure 8.3-21 Deformation of Bottom of Outer Container (left) and Inner Container (right), Corner Drop on Lid, Drop Case HAC05

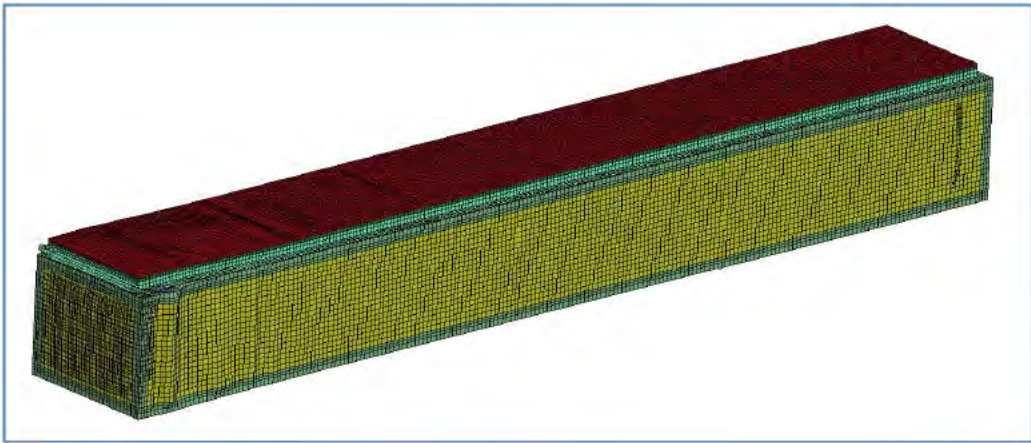


Figure 8.3-22 Container Deformation, Bottom End Drop, Light Load, Drop Case HAC14



**ATKINS**

**Design Analyses and Calculation**

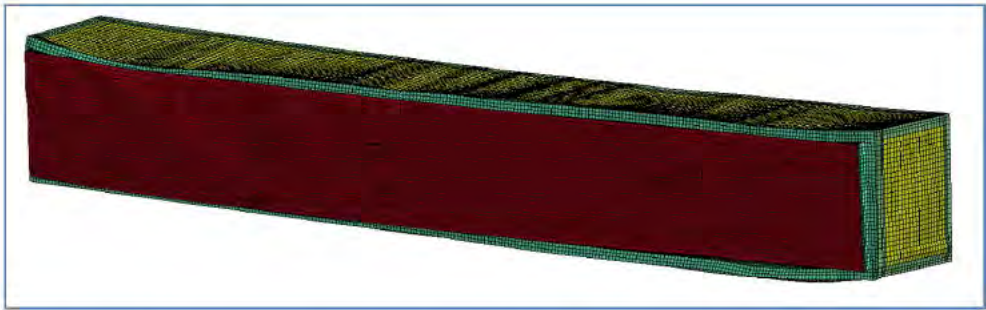


Figure 8.3-23 Container Deformation, 15° Shallow Angle Horizontal Drop, Case HAC19





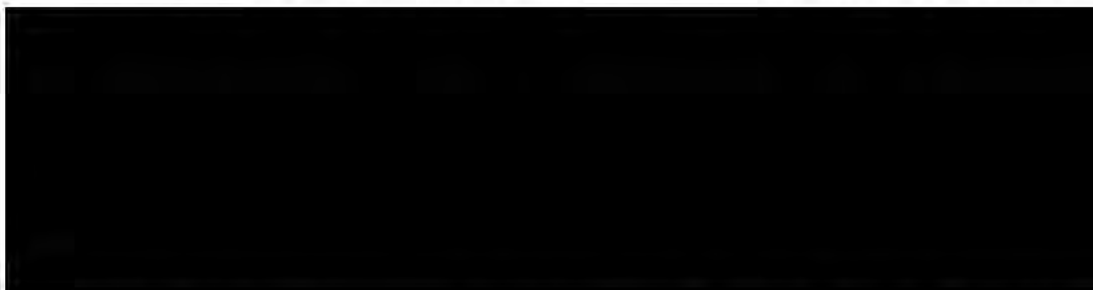
## Design Analyses and Calculation

### 8.4 Reanalysis of ATRIUM-11 Fuel Assembly Regular Shipment

The analysis of the ATRIUM-11 fuel assembly performed in Ref. 2 is based on inner container acceleration time histories from actual drop tests of the RAJ-II container at room temperature. Reanalysis of the ATRIUM-11 fuel assembly for regular fuel shipment (2 fuel assemblies) at cold temperature using the same finite element model from Ref. 2 and calculated bounding inner container acceleration time histories from the hypothetical accident condition drop Cases of HAC14 and HAC16 are performed to reconfirm that the structural integrity of the fuel assembly and a minimum factor of safety of 1.4. Details of these analyses and results are provided in Appendix B.

The calculated inner container acceleration and amplified acceleration used in these analyses are compared in Table 8.4-1 below.

**Table 8.4-1 Comparison of calculated and Amplified Peak Acceleration for Plastic Stability Assessment**



The calculated deformations showed that the fuel tubes are bent near the Lower Tie Plate (LTP), but overall the fuel bundle remains straight and aligned. The maximum plastic strain in the fuel cladding is 2.01% which is considerably lower than the ultimate strain of 16% for the Zircaloy. No cladding failure is predicted. Therefore the pressure boundary is not breached. There is no gross structural collapse of the fuel bundles. The gross structure failure is defined as the failure of the fuel assembly spacers to keep the fuel rods in proper spacing during the Horizontal Drops configuration or the buckling of the fuel rods during end drop configuration.





## Design Analyses and Calculation

### 8.5 Reanalysis of ATRIUM-11 Single Fuel Assembly Shipment

Analysis of the fuel assembly is also performed to confirm that shipping the TN-B1 container with reduced weight of a single fuel assembly can maintain the structural integrity of the fuel assembly when dropped 30-ft during HAC. Two container drop analyses using the fuel content with reduced weight are performed to prepare for the subsequent fuel assembly analyses. The drop case with vertical bottom end drop configuration at cold temperature is designated as Drop Case HAC-SF1. The drop case with horizontal drop on side configuration at cold temperature is designated as Drop Case HAC-SF2. Reanalysis of the ATRIUM-11 fuel assembly for a single fuel assembly shipment using the same finite element model from Ref. 2 and calculated fuel acceleration time histories at the location of LTP of drop Cases HAC-SF1 and HAC-SF2 are performed to reconfirm that the structural integrity of the fuel assembly and a minimum factor of safety of 1.4. Details of these analyses and results are provided in Appendix C.

The calculated LTP acceleration and amplified acceleration used in these analyses are compared in Table 8.5-1 below.

Table 8.5-1 Calculated LTP and Amplified Peak Acceleration for Plastic Stability Assessment

[REDACTED]	
------------	--

The analyses show that the LTP deformation is insignificant. The fuel rods are bent due to the deformation of the band, but overall the fuel bundle remains in-place and aligned.

No cladding failure is predicted. Therefore the pressure boundary is preserved.

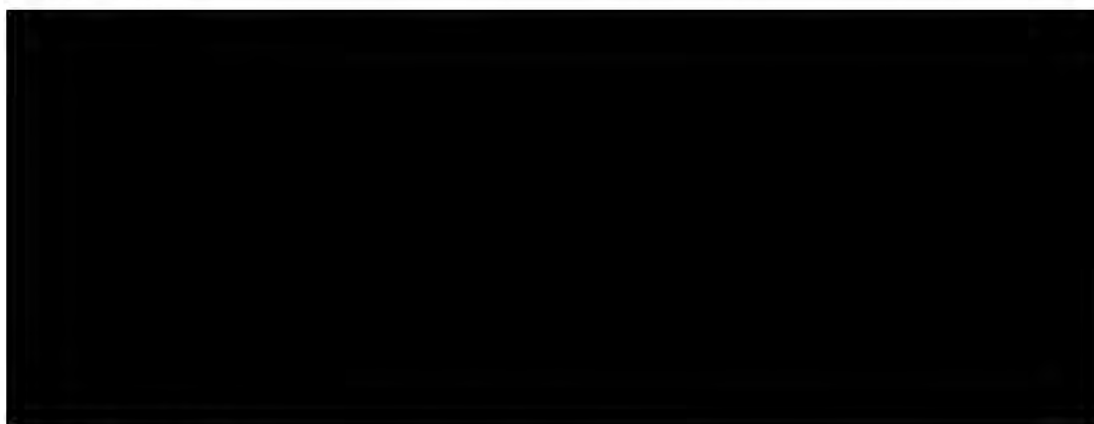




## Design Analyses and Calculation

### 8.6 Puncture Analysis

The puncture analysis is performed and presented in Appendix D. This analysis is performed to comply with the single "worst-case" 30-ft free drop as required by 10CFR 71.73(c)(1). The pin puncture is evaluated at elevated ambient temperature of 150°F, where the stiffness of the packaging material is the lowest. The container is first dropped 30-ft onto a rigid plane, rotated 25-degree from the horizontal and then dropped 40-in onto a rigid pin of 6-in diameter with 8-in long erected in the vertical direction.



### 9. Discussion and Summary

In the validation runs, the LSDYNA finite element model for evaluation of the TB-B1 container with the ARIUM-11 fuel shows reasonable agreement with the RAJ-II CTU drop tests. The inner container acceleration, both the peak g values and overall time histories, calculated for 30 ft drops on the bottom end and Horizontal Drop on lid, show reasonable agreement with test. The calculated amount of deformation is also similar to tests for these drops. Some differences are indicated, but are expected for this type of analysis when considering modeling assumptions and possible uncertainties in material properties and other factors. Figures 9-1 and 9-2 show the comparison of the acceleration time histories of the calculated value with the drop test transducer outputs. The wave forms and durations are comparable.





## Design Analyses and Calculation



Figure 9-1 Comparison of the calculated acceleration and CTU drop test result for the End Drop



Figure 9-2 Comparison of the calculated acceleration and CTU drop test result for the Horizontal Drop

The validated model is used to calculate the inner container accelerations for the NCT and HAC drop cases. The maximum peak acceleration of the inner container shell is calculated to be 335 g's for the bottom end drop with a light fuel load (HAC14) and 260 g's for the Horizontal Drop on Side with a light fuel load (HAC16). These maximum accelerations are less than those used in the structural analyses the evaluation of the ATRIUM-11 fuel assembly (Ref. 2). In addition, reanalysis of the ATRIUM-11 fuel assembly using the model from Ref. 2 and applied acceleration time histories of the inner container calculated from the bounding drop cases HAC14 and HAC16 reconfirms a minimum factor of safety





## Design Analyses and Calculation

greater than 1.4 against structural failure.

The highest peak accelerations of the inner container shell are computed for the HAC drop cases at cold temperature (-40°F) and at a bounding light fuel load (580 kg). Reanalysis of the fuel assembly model used in Ref. 2 for the case of the TN-B1 container shipped with only one fuel assembly also demonstrates a minimum factor of safety of 1.4 against structural stability. In this evaluation, inner container time histories are computed from the TN-B1 container analysis using a total fuel load of one fuel assembly and one other component (294 kg total) for the End and Horizontal Drop orientations (HAC14 and HAC16) at -40°F.

The slap down analyses, Cases HAC16, HAC17, HAC18, are performed to confirm that the peak acceleration of Horizontal Drop on side, Case HAC04, is bounding.





## Design Analyses and Calculation

### 10. REFERENCES

1. Global Nuclear Fuel – Japan (fka Japan Nuclear Fuel Co. Ltd). “Application for Approval of Packaging, Type RAJ-II.” Sto-M00-034, dated September 26, 2000
2. NSA-DAC-AREVA-14-01, “Structural Analyses of the AREVA ATRIUM-11 LTA Fuel Assembly in the RAJ-II Container during Normal and Accident Transport Conditions”, February, 2014
3. NRC Regulations 10 CFR, Part 71-“Packaging and Transportation of Radioactive Material: 71.73 Hypothetical Accident Condition.”
4. LS-DYNA Version 971 R5.1, Livermore Software Technology Corporation
5. ASME Boiler and Pressure Vessel Code, 2010 Ed.
6. Container Drawings

Drawing number	Number of sheets	Revision No.	Name
105E3737	7	1	Outer Container Assembly Licensing Drawings
105E3738	9	3	Outer Container Main Body Assembly Licensing Drawings
105E3739	5	1	Outer Container Fixture Assembly Licensing Drawings
105E3740	5	1	Outer Container Fixture Assembly Installation Licensing Drawings
105E3741	2	1	Outer Container Shock Absorber Assembly Licensing Drawings
105E3742	4	1	Outer Container Bolster Assembly Licensing Drawings
105E3743	6	1	Outer Container Lid Assembly Licensing Drawings
105E3745	9	4	Inner Container Main Body Assembly Licensing Drawings
105E3746	2	1	Inner Container Parts Assembly Licensing Drawings
105E3747	5	1	Inner Container Lid Assembly Licensing Drawings
105E3748	3	1	Inner Container End Lid Assembly Licensing Drawings
105E3773	1	1	Protective Case

7. FS1-0014159 AREVA TN-B1 SAR Rev. 3
8. NRC Certificate of Compliance for Radioactive Material Packages, No. 9309, Rev. 9, August 28, 2009
9. FS1-0021899, TN-B1 assumptions for ATRIUM 11 Reload Shipment, Rev. 1
10. LS-DYNA Version 971 R5.1, Livermore Software Technology Corporation.
11. NSA-TR-12-01-R0, “LSDYNA Verification on NSA Server”, September 10, 2012
12. NUREG/CR-6150 EGG-2750 MATPRO – A Library of Materials Properties for Light-Water-Reactor Accident Analysis





## Design Analyses and Calculation

13. "Review of Zircaloy-2 and Zircaloy-4 Properties Relevant to N.S. Savannah Reactor Design," Whitmorsh, July 9, 1962, ORNL-3281, UC-80-Reactor Technology, TID-4500, 17th Ed. C.L.
14. ASME Boiler and Pressure Code, Section II, Part D, 2010 Ed.
15. ASME Boiler and Pressure Vessel Code, Section VIII, Div 2, Annex 3.D, 2010 Edition
16. "Impact tensile testing of stainless steels at various temperatures" D.K. Morton and R. K. Blandford, March 2008, INL/EXT-08-14082
17. "Effect of Moisture and Temperature on the Mechanical Properties of Paper." D. Caulfield, Perkins, R.W.; Mark, R.E. Thorpe, J.L. eds Sold Mechanics Advanced in Paper related Industries: Proceedings of National Foundation workshop; 1986 August 13-15; Syracuse, NY. Syracuse, NY: Syracuse University, 1990; 50-62
18. Wood Handbook-Wood as an Engineering Material, Forest Products Laboratory, USDA Forest Service, Madison, Wisconsin
19. ZIRCAR Ceramics: Alumina-Silica Insulation Type AXL & AXHTM (attached in Appendix)
20. "Commercial Item Description-cushioning Material Packaging, Closed Cell Foam Plank" CID-A-A-59136, 28 October 1997. The General Services Administration.
21. ASTM D1596 Test Method for Shock Absorbing Characteristics of Package Cushioning Materials
22. Cushioning Material Testing" Herbert H. Schueneman, Westpak, Inc. San Jose, CA 95119
23. "Load-Bearing Characteristics of Polyethylene Foam: An Examination of Structural and Compression Properties.", E.J. Kuncir, R.W. Wirta and F.L. Golbranson, Journal of Rehabilitation Research and Development. Vol. 27, No. 3, 1990 Pages 229-238.
24. PolyPlank® EXT, Typical Physical Properties (attached in Appendix F)
25. AREVA Engineering Information Record No. 51-5046576-00 "RAJ-II Shipping Container Test Results" 6/28/04.
26. Docket No. 71-9309 "GNF RAJ-II Safety Analysis Report, Revision 1, 4/22/04. Sections 2.7.1, 2.7.3, 2.7.8 and Appendix 2.12
27. "full-range stress-strain curves for stainless steel alloys" Kim J.R. Rasmussen, Journal of Constructional Steel Research 59 (2003) pages 47-61
28. "Compressive Response And Failure Of Balsa Wood", Andre Da Silva, Stelios Kyriakides, International Journal of Solids and Structures, 44 (2007) pp 8685-8717, 29 June, 2007
29. "Microstructural Aspects and modeling of failure in naturally occurring porous composites" Vural and Ravichandran, Mechanics of Materials, California Institute of Technology.
30. "Investigation of the Behavior or Shock-Absorbing Structural Parts of Transport Casks Holding Radioactive Substances in Terms of Design Testing and Risk Analysis" Martin Neumann, BAM-Dissertation Series, Volume 45, Berlin, 2009





## Design Analyses and Calculation

### Appendix A Material Properties Derivation

#### A.1 Zircaloy-2

The Zircaloy Material Properties with dependency on temperature are derived based on *NUREG/CR-6150 EGG-2750 MATPRO - A Library of Materials Properties for Light-Water-Reactor Accident Analysis* [Ref. 12]. The property presented in this section corresponds to dynamic property. The equations can be shown to collapse into static properties but they are only used to compare with the conventional static material properties and are irrelevant to LSDYNA applications. The Zircaloy is modeled in LSDYNA as \*MAT\_PIECEWISE\_LINEAR\_PLASTICITY (Type 24). The cladding is modeled as shell elements.

##### A.1.1 STRESS STRAIN CURVES WITH TEMPERATURE AND STRAIN-RATE DEPENDENCY

Per Equation (4-148), the true stress and plastic strain curve is related by

$$\sigma := K \cdot \epsilon^n \cdot \left( \frac{sr}{10^{-3}} \right)^m$$

where

$\sigma$  = true effective stress, (Pa)

$\epsilon$  = true effective plastic strain

sr = rate of change of effective plastic strain

K,n,m = parameters describing the metallurgical state of the cladding

##### Defining function to convert degree F to degree Kelvin

Defining variable  $T_{\text{Kelvin}}$  as a function of  $T_F$

$$T_{\text{Kelvin}}(T_F) = (T_F - 32) \times \frac{5}{9} + 273.15$$

Where

$T_{\text{Kelvin}}$  = temperature in Kelvin

$T_F$  = temperature in Fahrenheit

Therefore, at

$T_F = -40$  in degree F

$T_{\text{Kelvin}}(T_F) = 233.15$  in degree Kelvin

At

		Page A1 of A55
--	--	----------------





## Design Analyses and Calculation

$$T_F = 70 \text{ in degree F}$$

(note: the green waggie shape under the variable is a feature imported from Mathcad program indicating the variable has been defined before)

$$T_{\text{Kelvin}}(T_F) = 294.26 \text{ in degree Kelvin}$$

At

$$T_F = 150$$

$$T_{\text{Kelvin}}(T_F) = 338.71 \text{ in degree of Kelvin}$$

### Evaluation of Parameters K, n, and m

Per equation (4-164), the values of the strain rate sensitivity exponent, m, is

For  $T < 730 \text{ K}$

$$m = 0.02$$

Per Equation (4.170), the values of the strain hardening exponent, n:

For  $T < 1,099.0772 \text{ K}$ , defining the parameter n as a function of temperature (T)

$$n(T) := -9.49010^{-2} + T \left[ \left( 1.16510^{-3} \right) + T \left( -1.99210^{-6} + T \cdot 9.58810^{-10} \right) \right]$$

$$T_F = 40 \text{ in degree F}$$

$$T = T_{\text{Kelvin}}(T_F) = 233.15 \text{ in degree of Kelvin}$$

$$n(T) = 0.081$$

At

$$T_F = 70$$

$$T = T_{\text{Kelvin}}(T_F) = 294.26 \text{ in degree Kelvin}$$

$$n(T) = 0.1$$

At

$$T_F = 150 \text{ in degree F}$$

$$T = T_{\text{Kelvin}}(T_F) = 338.71 \text{ in degree Kelvin}$$

$$n(T) = 0.108$$





## Design Analyses and Calculation

### Per Equation (4-174), Values of the strength coefficient, K:

For  $T < 750K$ , defining the parameter K as a function of temperature (T)

$$K(T) := 1.1762810^9 + T \left[ 4.5485910^5 + T \left[ -3.2818510^3 + T \cdot (1.72753) \right] \right] \times Pa$$

At  $T_F = -40$  degree F

$$T = T_{\text{kelvin}}(T_F) = 233.15 \quad \text{in degree of Kelvin}$$

$$K(T) = 1.126 \times 10^9 \text{ Pa}$$

At

$T_F = 70$  degree F

$$T = T_{\text{kelvin}}(T_F) = 294.26 \quad \text{in degree Kelvin}$$

$$K(T) = 1.07 \times 10^9 \text{ Pa}$$

At

$T_F = 150$  degree F

$$T = T_{\text{kelvin}}(T_F) = 338.71 \quad \text{in degree of Kelvin}$$

$$K(T) = 1.021 \times 10^9 \text{ Pa}$$

### Evaluation of True Effective Stress

At temperature  $T = -40$  degF

$$m = 0.02$$

$T_F = -40$  degree F

$$T = T_{\text{kelvin}}(T_F) = 233.15 \quad \text{in degree of Kelvin}$$

$$n(T) = 0.081$$

$$n := n(T) = 0.081$$

$$K(T) = 1.126 \times 10^9$$

$$K_T := K(T) = 1.126 \times 10^9 \text{ Pa}$$

For strain rate,  $sr = 0.001$

$$sr = 0.001$$





## Design Analyses and Calculation

At true effective plastic strain of

$$\varepsilon = 0.02$$

The true effective stress per equation (4-148) is

$$\sigma = K_T \varepsilon^n \left( \frac{sr}{10^{-3}} \right)^m \text{ Pa} = 1.191 \times 10^5 \text{ psi}$$

At true effective plastic strain of

$$\varepsilon = 0.04$$

The true effective stress per equation (4-148) is

$$\sigma = K_T \varepsilon^n \left( \frac{sr}{10^{-3}} \right)^m \text{ Pa} = 1.26 \times 10^5 \text{ psi}$$

At true effective plastic strain of

$$\varepsilon = 0.06$$

The true effective stress per equation (4-148) is

$$\sigma = K_T \varepsilon^n \left( \frac{sr}{10^{-3}} \right)^m \text{ Pa} = 1.302 \times 10^5 \text{ psi}$$

The same approach can be used for different strain rates.

**For strain rate=0.1**

$$sr=0.1$$

At true effective strain of

$$\varepsilon = 0.02$$

The true effective stress per equation (4-148) is

$$\sigma := K_T \cdot \varepsilon^n \cdot \left( \frac{sr}{10^{-3}} \right)^m \cdot \text{Pa} = 1.306 \times 10^5 \cdot \text{psi}$$

At true effective strain of

$$\varepsilon = 0.04$$

The true effective stress per equation (4-148) is

$$\sigma := K_T \cdot \varepsilon^n \cdot \left( \frac{sr}{10^{-3}} \right)^m \cdot \text{Pa} = 1.381 \times 10^5 \cdot \text{psi}$$

At true effective strain of

$$\varepsilon = 0.06$$

The true effective stress per equation (4-148) is

$$\sigma = K_T \varepsilon^n \left( \frac{sr}{10^{-3}} \right)^m \text{ Pa} = 1.427 \times 10^5 \text{ psi}$$





## Design Analyses and Calculation

### For strain rate=1

$$sr = 1$$

At true effective plastic strain of

$$\varepsilon = 0.02$$

The true effective stress per equation (4-148) is

$$\sigma = K_T \varepsilon^n \left( \frac{sr}{10^{-3}} \right)^m \text{ Pa} = 1.368 \times 10^5 \text{ psi}$$

At true effective plastic strain of

$$\varepsilon = 0.04$$

The true effective stress per equation (4-148) is

$$\sigma := K_T \varepsilon^n \left( \frac{sr}{10^{-3}} \right)^m \cdot \text{Pa} = 1.446 \times 10^5 \cdot \text{psi}$$

At true effective plastic strain of

$$\varepsilon = 0.06$$

The true effective stress per equation (4-148) is

$$\sigma := K_T \varepsilon^n \left( \frac{sr}{10^{-3}} \right)^m \cdot \text{Pa} = 1.494 \times 10^5 \cdot \text{psi}$$

### For strain rate=10

$$sr = 10$$

At true effective plastic strain of

$$\varepsilon = 0.02$$

The true effective stress per equation (4-148) is

$$\sigma := K_T \varepsilon^n \left( \frac{sr}{10^{-3}} \right)^m \cdot \text{Pa} = 1.432 \times 10^5 \cdot \text{psi}$$

At true effective plastic strain of

$$\varepsilon = 0.04$$

The true effective stress per equation (4-148) is

$$\sigma = K_T \varepsilon^n \left( \frac{sr}{10^{-3}} \right)^m \text{ Pa} = 1.515 \times 10^5 \text{ psi}$$

At true effective plastic strain of

$$\varepsilon = 0.06$$

The true effective stress per equation (4-148) is

$$\sigma = K_T \varepsilon^n \left( \frac{sr}{10^{-3}} \right)^m \text{ Pa} = 1.565 \times 10^5 \text{ psi}$$





## Design Analyses and Calculation

At temperature T=70 degF

$$m=0.02$$

$$T_F=70 \quad \text{in degree F}$$

$$T = T_{\text{Kelvin}}(T_F) = 294.26 \quad \text{in degree of Kelvin}$$

$$n_s := n(T) = 0.1$$

$$K(T) = 1.07 \times 10^9$$

$$K_{\text{TR}} := K(T) = 1.07 \times 10^9 \text{ Pa}$$

For strain rate=0.001

$$sr = 0.001$$

At true effective plastic strain of

$$\epsilon = 0.02$$

The true effective stress per equation (4-148) is

$$\sigma := K_{\text{TR}} \cdot \epsilon^n \cdot \left( \frac{sr}{10^{-3}} \right)^m \cdot \text{Pa} = 1.05 \times 10^5 \text{ psi}$$

At true effective plastic strain of

$$\epsilon = 0.04$$

The true effective stress per equation (4-148) is

$$\sigma := K_{\text{TR}} \cdot \epsilon^n \cdot \left( \frac{sr}{10^{-3}} \right)^m \cdot \text{Pa} = 1.125 \times 10^5 \text{ psi}$$

At true effective plastic strain of

$$\epsilon = 0.06$$

The true effective stress per equation (4-148) is

$$\sigma = K_{\text{TR}} \epsilon^n \left( \frac{sr}{10^{-3}} \right)^m \text{ Pa} = 1.172 \times 10^5 \text{ psi}$$

For strain rate=0.1

$$sr=0.1$$

At true effective plastic strain of

$$\epsilon = 0.02$$

The true effective stress per equation (4-148) is

$$\sigma = K_{\text{TR}} \epsilon^n \left( \frac{sr}{10^{-3}} \right)^m \text{ Pa} = 1.151 \times 10^5 \text{ psi}$$

At true effective plastic strain of

$$\epsilon = 0.04$$





## Design Analyses and Calculation

The true effective stress per equation (4-148) is

$$\sigma = K_T \epsilon^n \left( \frac{sr}{10^{-3}} \right)^m \text{ Pa} = 1.234 \times 10^5 \text{ psi}$$

At true effective plastic strain of

$$\epsilon = 0.06$$

The true effective stress per equation (4-148) is

$$\sigma = K_T \epsilon^n \left( \frac{sr}{10^{-3}} \right)^m \text{ Pa} = 1.285 \times 10^5 \text{ psi}$$

The same approach can be used for different strain rates

**For strain rate=1**

$$sr=1$$

At true effective plastic strain of

$$\epsilon = 0.02$$

The true effective stress per equation (4-148) is

$$\sigma = K_T \epsilon^n \left( \frac{sr}{10^{-3}} \right)^m \text{ Pa} = 1.206 \times 10^5 \text{ psi}$$

At true effective plastic strain of

$$\epsilon = 0.04$$

The true effective stress per equation (4-148) is

$$\sigma := K_T \cdot \epsilon^n \cdot \left( \frac{sr}{10^{-3}} \right)^m \cdot \text{Pa} = 1.292 \times 10^5 \text{ psi}$$

At true effective plastic strain of

$$\epsilon = 0.06$$

The true effective stress per equation (4-148) is

$$\sigma := K_T \cdot \epsilon^n \cdot \left( \frac{sr}{10^{-3}} \right)^m \cdot \text{Pa} = 1.345 \times 10^5 \text{ psi}$$

**For strain rate=10**

$$sr=10$$

At true effective plastic strain of

$$\epsilon = 0.02$$

The true effective stress per equation (4-148) is

$$\sigma := K_T \cdot \epsilon^n \cdot \left( \frac{sr}{10^{-3}} \right)^m \cdot \text{Pa} = 1.262 \times 10^5 \text{ psi}$$

At true effective plastic strain of

$$\epsilon = 0.04$$

The true effective stress per equation (4-148) is





## Design Analyses and Calculation

$$\sigma = K_T \epsilon^n \left( \frac{sr}{10^{-3}} \right)^m Pa = 1.353 \times 10^5 \text{ psi}$$

At true effective plastic strain of

$$\epsilon = 0.06$$

The true effective stress per equation (4-148) is

$$\sigma = K_T \epsilon^n \left( \frac{sr}{10^{-3}} \right)^m Pa = 1.409 \times 10^5 \text{ psi}$$

At temperature T=150 degF

$$m=0.02$$

$$T_F=150 \quad \text{in degree F}$$

$$T = T_{\text{kelvin}}(T_F) = 338.71 \quad \text{in degree of Kelvin}$$

$$n_s := n(T) = 0.108$$

$$K(T) = 1.021 \times 10^9$$

$$K_{T,T} := K(T) = 1.021 \times 10^9 \text{ Pa}$$

For strain rate=0.001

$$sr=0.001$$

At true effective plastic strain of

$$\epsilon = 0.02$$

The true effective stress per equation (4-148) is

$$\sigma = K_T \epsilon^n \left( \frac{sr}{10^{-3}} \right)^m Pa = 9.689 \times 10^4 \text{ psi}$$

At true effective plastic strain of

$$\epsilon = 0.04$$

The true effective stress per equation (4-148) is

$$\sigma := K_T \epsilon^n \left( \frac{sr}{10^{-3}} \right)^m Pa = 1.045 \times 10^5 \text{ psi}$$

At true effective plastic strain of

$$\epsilon = 0.06$$

The true effective stress per equation (4-148) is

$$\sigma := K_T \epsilon^n \left( \frac{sr}{10^{-3}} \right)^m Pa = 1.091 \times 10^5 \text{ psi}$$

For strain rate=0.1

		Page A8 of A55
--	--	----------------





## Design Analyses and Calculation

$$sr=0.1$$

At true effective plastic strain of

$$\varepsilon = 0.02$$

The true effective stress per equation (4-148) is

$$\sigma := K_T \cdot \varepsilon^n \cdot \left( \frac{sr}{10^{-3}} \right)^m \cdot Pa = 1.062 \times 10^5 \cdot \text{psi}$$

At true effective plastic strain of

$$\varepsilon = 0.04$$

The true effective stress per equation (4-148) is

$$\sigma := K_T \cdot \varepsilon^n \cdot \left( \frac{sr}{10^{-3}} \right)^m \cdot Pa = 1.145 \times 10^5 \cdot \text{psi}$$

At true effective plastic strain of

$$\varepsilon = 0.06$$

The true effective stress per equation (4-148) is

$$\sigma = K_T \cdot \varepsilon^n \cdot \left( \frac{sr}{10^{-3}} \right)^m \cdot Pa = 1.197 \times 10^5 \cdot \text{psi}$$

The same approach can be used for different strain rates

**For strain rate=1**

$$sr=1$$

At true effective plastic strain of

$$\varepsilon = 0.02$$

The true effective stress per equation (4-148) is

$$\sigma := K_T \cdot \varepsilon^n \cdot \left( \frac{sr}{10^{-3}} \right)^m \cdot Pa = 1.112 \times 10^5 \cdot \text{psi}$$

At true effective plastic strain of

$$\varepsilon = 0.04$$

The true effective stress per equation (4-148) is

$$\sigma := K_T \cdot \varepsilon^n \cdot \left( \frac{sr}{10^{-3}} \right)^m \cdot Pa = 1.199 \times 10^5 \cdot \text{psi}$$

At true effective plastic strain of

$$\varepsilon = 0.06$$

The true effective stress per equation (4-148) is





## Design Analyses and Calculation

$$\sigma := K_T \cdot \epsilon^n \cdot \left( \frac{sr}{10^{-3}} \right)^m \cdot Pa = 1.253 \times 10^5 \cdot psi$$

For strain rate=10

$$sr=10$$

At true effective plastic strain of

$$\epsilon = 0.02$$

The true effective stress per equation (4-148) is

$$\sigma = K_T \cdot \epsilon^n \cdot \left( \frac{sr}{10^{-3}} \right)^m \cdot Pa = 1.165 \times 10^5 \cdot psi$$

At true effective plastic strain of

$$\epsilon = 0.04$$

The true effective stress per equation (4-148) is

$$\sigma = K_T \cdot \epsilon^n \cdot \left( \frac{sr}{10^{-3}} \right)^m \cdot Pa = 1.256 \times 10^5 \cdot psi$$

At true effective plastic strain of

$$\epsilon = 0.06$$

The true effective stress per equation (4-148) is

$$\sigma := K_T \cdot \epsilon^n \cdot \left( \frac{sr}{10^{-3}} \right)^m \cdot Pa = 1.312 \times 10^5 \cdot psi$$

### A.1.2. MODULUS OF ELASTICITY AND POISSON'S RATIO

Per Section 4.17, the Poisson's ratio,  $\nu$ , is a constant of 0.30

$$\nu = 0.3$$

Per Section 4.17, the Young's Modulus,  $Y$ , is a function of temperature,  $T$

For  $T < 1090$  K

$$Y(T) := [1.08810^{11} - (5.4710^7) \cdot T] \cdot Pa$$

At temperature  $T = -40$  deg F

$$T_f = -40 \quad \text{in degree F}$$

$$T = T_{\text{kelvin}}(T_f) = 233.15 \quad \text{in degree Kelvin}$$

$$Y(T) = 1.393 \times 10^7 \cdot psi$$

At temperature  $T = 70$  deg F

		Page A10 of A55
--	--	-----------------





## Design Analyses and Calculation

$$T_F = 70 \quad \text{in degree F}$$

$$T = T_{\text{Kelvin}}(T_F) = 294.26 \quad \text{in degree Kelvin}$$

$$Y(T) = 1.345 \times 10^7 \cdot \text{psi}$$

In comparison with the listed Modulus of Elasticity in Ref. 7 (TN-B1 SAR, Rev. 3), page 69, Table 2-3, the modulus of elasticity is

$$E = 97.1 \text{ GPa} = 1.408 \times 10^7 \text{ psi}$$

The difference is less than 5%. The value is used by the LSDYNA material model during the restitution stage of the impact which has no effect on the permanent strain or stress of the cladding. It only affects the final deformed shape of the cladding. The calculated modulus is smaller than the value given in the SAR; therefore, it tends to over-predict the deformation, which is conservative.

At temperature  $T=150 \text{ deg F}$

$$T_F = 150 \quad \text{in degree F}$$

$$T = T_{\text{Kelvin}}(T_F) = 338.71 \quad \text{in degree Kelvin}$$

$$Y(T) = 1.309 \times 10^7 \cdot \text{psi}$$

### A.1.3. YIELD STRESS AND ULTIMATE STRESS

At temperature  $T=-40 \text{ deg F}$

$$m=0.02$$

$$T_F = -40 \quad \text{in degree F}$$

$$T = T_{\text{Kelvin}}(T_F) = 233.15 \quad \text{in degree of Kelvin}$$

$$n_-(T) = 0.081$$

$$\underline{n}_+ := n_-(T) = 0.081$$


$$K(T) = 1.126 \times 10^9 \text{ Pa}$$

$$\underline{K}_+ := K(T) = 1.126 \times 10^9 \text{ Pa}$$

The static yield strength of the Zirconium alloys as given in [Ref. 7] (TN-B1 SAR), Table 2-3 is

$$S_y = 35,000 \text{ psi}$$



N° FS1-0025122	Rev. 1.0	TEP - Technical Report	
	Page 101/177		



## Design Analyses and Calculation

This value is not used by the LSDYNA material model, the correct LSDYNA dynamic material properties are listed as follows.

For strain rate=0.001

$$sr = 0.001$$

The young's modulus is

$$E := Y(T) = 1.393 \times 10^7 \text{ psi}$$

Per Section 4.11.1, the true strain at yield is

$$\epsilon_{\text{yield\_n40}} := \left[ \frac{K_T}{\frac{E}{\text{Pa}}} \cdot \left( \frac{sr}{10^{-3}} \right)^m \right]^{\frac{1}{(1-n)}} = 7.938 \times 10^{-3}$$

Per Section 4.11.1, the true yield strength is

$$\sigma_{\text{yield\_n40\_Pa}} := \left[ \frac{K_T}{\left( \frac{E}{\text{Pa}} \right)^n} \cdot \left( \frac{sr}{10^{-3}} \right)^m \right]^{\frac{1}{(1-n)}} = 7.625 \times 10^8$$

In U.S. unit, the yield strength is

$$\sigma_{\text{yield\_n40\_us}} := \sigma_{\text{yield\_n40\_Pa}} \cdot \text{Pa} = 1.106 \times 10^5 \text{ psi}$$

Per Section 4.11.1, the true strain at maximum load is


The reference 13, ORNL-3281, TID-4500 (17TH Ed), the total elongation of Zircaloy can vary between 12 and 16%. Under dynamic impact condition, the total elongation can be greater than the static test property. Therefore, it is reasonable to use 16% as the ultimate strain at room temperature. This is consistent with the data sheet published by ATI Wah Chang-Allegheny Technologies which says at room temperature, the elongation is 28%. For cold temperature, conservatively use an ultimate elongation value that is smaller than the published data. Therefore

$$\epsilon_{\text{ult}} = 0.15$$

Per Section 4.11.1, the true ultimate stress is

		Page A12 of A55
--	--	-----------------



N° FS1-0025122	Rev. 1.0	TEP - Technical Report	
	Page 102/177		

**ATKINS**

## Design Analyses and Calculation

$$\sigma_{ult\_n40\_Pa} := K_T \left( \frac{sr}{10^{-3}} \right)^m \cdot (\epsilon_{ult})^n = 9.662 \times 10^8$$

In U.S. unit, the ultimate strength is

$$\sigma_{ult\_n40\_us} := \sigma_{ult\_n40\_Pa} \cdot Pa = 1.401 \times 10^5 \cdot psi$$

For strain rate=0.1:

$$sr=0.1$$

Per Section 4.11.1, the true strain at yield is

$$\epsilon_{yield\_n40\_Pa} := \left[ \frac{K_T}{\frac{E}{Pa}} \cdot \left( \frac{sr}{10^{-3}} \right)^m \right]^{\frac{1}{(1-n)}} = 8.775 \times 10^{-3}$$

Per Section 4.11.1, the true yield strength is

$$\sigma_{yield\_n40\_Pa} := \left[ \frac{K_T}{\left( \frac{E}{Pa} \right)^n} \cdot \left( \frac{sr}{10^{-3}} \right)^m \right]^{\frac{1}{(1-n)}} = 8.428 \times 10^8 \quad Pa$$

In U.S. unit, the yield strength is

$$\sigma_{yield\_n40\_us} := \sigma_{yield\_n40\_Pa} \cdot Pa = 1.222 \times 10^5 \cdot psi$$

As determined previously, the true strain at maximum load is

$$\epsilon_{ult} = 0.15$$

Per Section 4.11.1, the true ultimate stress is

$$\sigma_{ult\_n40\_Pa} := K_T \left( \frac{sr}{10^{-3}} \right)^m \cdot (\epsilon_{ult})^n = 1.059 \times 10^9$$

In U.S. unit, the ultimate strength is

		Page A13 of A55
--	--	-----------------





## Design Analyses and Calculation

$$\sigma_{ult\_n40\_us} := \sigma_{ult\_n40\_Pa} \cdot Pa = 1.537 \times 10^5 \cdot \text{psi}$$

For strain rate=1

$$sr = 1$$

Per Section 4.11.1, the true strain at yield is

$$\epsilon_{yield\_n40} := \left[ \frac{K_T}{\frac{E}{Pa}} \cdot \left( \frac{sr}{10^{-3}} \right)^m \right]^{\frac{1}{(1-n)}} = 9.226 \times 10^{-3}$$

Per Section 4.11.1, the true yield strength (Pa) is

$$\sigma_{yield\_n40\_Pa} := \left[ \frac{K_T}{\left( \frac{E}{Pa} \right)^n} \cdot \left( \frac{sr}{10^{-3}} \right)^m \right]^{\frac{1}{(1-n)}} = 8,861 \times 10^8$$

In U.S. unit, the yield strength is

$$\sigma_{yield\_n40\_us} := \sigma_{yield\_n40\_Pa} \cdot Pa = 1.285 \times 10^5 \cdot \text{psi}$$

As determined previously, the true strain at maximum load is

$$\epsilon_{ult} = 0.15$$

Per Section 4.11.1, the true ultimate stress is

$$\sigma_{ult\_n40\_Pa} := K_T \cdot \left( \frac{sr}{10^{-3}} \right)^m \cdot (\epsilon_{ult})^n = 1.109 \times 10^9$$

In U.S. unit, the ultimate strength is

$$\sigma_{ult\_n40\_us} := \sigma_{ult\_n40\_Pa} \cdot Pa = 1.609 \times 10^5 \cdot \text{psi}$$

For strain rate=10

$$sr = 10$$

Per Section 4.11.1, the true strain at yield is

$$\epsilon_{yield\_n40} := \left[ \frac{K_T}{\frac{E}{Pa}} \cdot \left( \frac{sr}{10^{-3}} \right)^m \right]^{\frac{1}{(1-n)}} = 9.699 \times 10^{-3}$$





## Design Analyses and Calculation

Per Section 4.11.1, the true yield strength (Pa) is

$$\sigma_{\text{yield\_n40\_Pa}} := \left[ \frac{K_T}{\left(\frac{E}{\text{Pa}}\right)^n} \cdot \left(\frac{\text{sr}}{10^{-3}}\right)^m \right]^{\frac{1}{(1-n)}} = 9.316 \times 10^8$$

In U.S. unit, the yield strength is

$$\sigma_{\text{yield\_n40\_psi}} := \sigma_{\text{yield\_n40\_Pa}} \cdot \text{Pa} = 1.351 \times 10^5 \text{ psi}$$

As determined previously, the true strain at maximum load is

$$\epsilon_{\text{ult}} = 0.15$$

Per Section 4.11.1, the true ultimate stress is (in Pa)

$$\sigma_{\text{ult\_n40\_Pa}} := K_T \cdot \left(\frac{\text{sr}}{10^{-3}}\right)^m \cdot (\epsilon_{\text{ult}})^n = 1.162 \times 10^9$$

In U.S. unit, the ultimate strength is

$$\sigma_{\text{ult\_n40\_psi}} := \sigma_{\text{ult\_n40\_Pa}} \cdot \text{Pa} = 1.685 \times 10^5 \text{ psi}$$

At temperature T=70 deg F

The static yield strength as given in Ref. 7 (TN-B1 SAR), Table 2-3 is

$$S_y = 35,000 \text{ psi}$$

This yield strength is not used by the LSDYNA material model, \*MAT\_PIECEWISE\_LINEAR\_PLASTICITY (Type 24). The LSDYNA material input is the stress-strain curve, derived previously. The dynamic material properties are derived as follows.

$$m=0.02$$

$$T_F=70 \quad \text{in degree F}$$

$$T = T_{\text{Kelvin}}(T_F) = 294.26 \quad \text{in degree of Kelvin}$$

$$n_{\text{a}}(T) = 0.1$$

$$n_{\text{b}} := n_{\text{a}}(T) = 0.1$$

$$K(T) = 1.07 \times 10^9 \text{ Pa}$$





## Design Analyses and Calculation

$$K_T := K(T) = 1.07 \times 10^9 \text{ Pa}$$

For strain rate=0.001

$$sr=0.001$$

The Young's modulus, as found earlier, is

$$E := Y(T) = 1.345 \times 10^7 \text{ psi}$$

Per Section 4.11.1, the true strain at yield is

$$\epsilon_{\text{yield}_70} := \left[ \frac{K_T}{\frac{E}{\text{Pa}}} \left( \frac{sr}{10^{-3}} \right)^m \right]^{\frac{1}{(1-n)}} = 7.036 \times 10^{-3}$$

Per Section 4.11.1, the true yield strength is

$$\sigma_{\text{yield}_70\_Pa} := \left[ \frac{K_T}{\left( \frac{E}{\text{Pa}} \right)^n} \left( \frac{sr}{10^{-3}} \right)^m \right]^{\frac{1}{(1-n)}} = 6.522 \times 10^8$$

In U.S. unit, the dynamic yield strength is

$$\sigma_{\text{yield}_70\_us} := \sigma_{\text{yield}_70\_Pa} \cdot \text{Pa} = 9.46 \times 10^4 \text{ psi}$$

The reference 11, ORNL-3281, TID-4500 (17TH Ed), the total elongation of Zircaloy can vary between 12 and 16%. Under dynamic impact condition, the total elongation can be greater than the static test property. Therefore, it is reasonable to use 16% as the ultimate strain at room temperature. This is consistent with the data sheet published by ATI Wah Chang-Allegheny Technologies which says at room temperature, the elongation is 28%. Therefore

$$\epsilon_{\text{ult}} = 0.16$$

Per Section 4.11.1, the true ultimate stress is

$$\sigma_{\text{ult}_70\_Pa} := K_T \left( \frac{sr}{10^{-3}} \right)^m \cdot (\epsilon_{\text{ult}})^n = 8.91 \times 10^8$$

In U.S. unit, the ultimate strength is

$$\sigma_{\text{ult}_70\_us} := \sigma_{\text{ult}_70\_Pa} \cdot \text{Pa} = 1.292 \times 10^5 \text{ psi}$$

For strain rate=0.1

$$sr=0.1$$





## Design Analyses and Calculation

Per Section 4.11.1, the true strain at yield is

$$\varepsilon_{\text{yield}_70} := \left[ \frac{K_T}{\frac{E}{Pa}} \cdot \left( \frac{sr}{10^{-3}} \right)^m \right]^{\frac{1}{(1-n)}} = 7.794 \times 10^{-3}$$

Per Section 4.11.1, the true yield strength is

$$\sigma_{\text{yield}_70_{Pa}} := \left[ \frac{K_T}{\left( \frac{E}{Pa} \right)^n} \cdot \left( \frac{sr}{10^{-3}} \right)^m \right]^{\frac{1}{(1-n)}} = 7.225 \times 10^8$$

In U.S. unit, the yield strength is

$$\sigma_{\text{yield}_70_{psi}} := \sigma_{\text{yield}_70_{Pa}} \cdot Pa = 1.048 \times 10^5 \cdot \text{psi}$$

As determined previously, the true strain at maximum load is

$$\varepsilon_{\text{ult}} = 0.16$$

Per Section 4.11.1, the true ultimate stress is

$$\sigma_{\text{ult}_70_{Pa}} := K_T \cdot \left( \frac{sr}{10^{-3}} \right)^m \cdot (\varepsilon_{\text{ult}})^n = 9.77 \times 10^8$$

In U.S. unit, the ultimate strength is

$$\sigma_{\text{ult}_70_{psi}} := \sigma_{\text{ult}_70_{Pa}} \cdot Pa = 1.417 \times 10^5 \cdot \text{psi}$$

The zircaloy as fuel rod claddings in the impact analysis, never reached the ultimate strength, therefore, the ultimate strength has insignificant effect on the impact analysis.

**For strain rate=1**

$$sr=1$$

Per Section 4.11.1, the true strain at yield is

$$\varepsilon_{\text{yield}_70} := \left[ \frac{K_T}{\frac{E}{Pa}} \cdot \left( \frac{sr}{10^{-3}} \right)^m \right]^{\frac{1}{(1-n)}} = 8.203 \times 10^{-3}$$

Per Section 4.11.1, the true yield strength (Pa) is



**ATKINS**

## Design Analyses and Calculation

$$\sigma_{\text{yield}_70\_Pa} := \left[ \frac{K_T}{\left(\frac{E}{Pa}\right)^n} \cdot \left(\frac{sr}{10^{-3}}\right)^m \right]^{\frac{1}{(1-n)}} = 7.604 \times 10^8$$

In U.S. unit, the yield strength is

$$\sigma_{\text{yield}_70\_psi} := \sigma_{\text{yield}_70\_Pa} \cdot Pa = 1.103 \times 10^5 \cdot \text{psi}$$

As determined previously, the true strain at maximum load is

$$\epsilon_{\text{ult}} = 0.16$$

Per Section 4.11.1, the true ultimate stress is

$$\sigma_{\text{ult}_70\_Pa} := K_T \cdot \left(\frac{sr}{10^{-3}}\right)^m \cdot (\epsilon_{\text{ult}})^n = 1.023 \times 10^9$$

In U.S. unit, the ultimate strength is

$$\sigma_{\text{ult}_70\_psi} := \sigma_{\text{ult}_70\_Pa} \cdot Pa = 1.484 \times 10^5 \cdot \text{psi}$$

For strain rate=10

$$sr=10$$

Per Section 4.11.1, the true strain at yield is

$$\epsilon_{\text{yield}_70} := \left[ \frac{K_T}{\frac{E}{Pa}} \cdot \left(\frac{sr}{10^{-3}}\right)^m \right]^{\frac{1}{(1-n)}} = 8.633 \times 10^{-3}$$

Per Section 4.11.1, the true yield strength (Pa) is

$$\sigma_{\text{yield}_70\_Pa} := \left[ \frac{K_T}{\left(\frac{E}{Pa}\right)^n} \cdot \left(\frac{sr}{10^{-3}}\right)^m \right]^{\frac{1}{(1-n)}} = 8.004 \times 10^8$$

In U.S. unit, the yield strength is

$$\sigma_{\text{yield}_70\_psi} := \sigma_{\text{yield}_70\_Pa} \cdot Pa = 1.161 \times 10^5 \cdot \text{psi}$$

As determined previously, the true strain at maximum load is

$$\epsilon_{\text{ult}} = 0.16$$





## Design Analyses and Calculation

Per Section 4.11.1, the true ultimate stress is

$$\sigma_{ult\_70\_Pa} := K_T \left( \frac{sr}{10^{-3}} \right)^m \cdot (\epsilon_{ult})^n = 1.071 \times 10^9$$

In U.S. unit, the ultimate strength is

$$\sigma_{ult\_70\_psi} := \sigma_{ult\_70\_Pa} \cdot Pa = 1.554 \times 10^5 \cdot psi$$

At temperature T=150 deg F

$$m=0.02$$

$$T_f=150 \quad \text{in degree F}$$

$$T = T_{kelvin}(T_f) = 338.71 \quad \text{in degree Kelvin}$$

$$n_-(T) = 0.108$$

$$n_+ := n_-(T) = 0.108$$

$$K(T) = 1.021 \times 10^9 \quad Pa$$

$$K_T := K(T) = 1.021 \times 10^9 \quad Pa$$

For strain rate=0.001

$$sr=0.001$$

The young's modulus is

$$E_y := Y(T) = 1.309 \times 10^7 \quad psi$$

Per Section 4.11.1, the true strain at yield is

$$\epsilon_{yield\_150} := \left[ \frac{K_T}{\frac{E}{Pa}} \cdot \left( \frac{sr}{10^{-3}} \right)^m \right]^{\frac{1}{(1-n)}} = 6.558 \times 10^{-3}$$

Per Section 4.11.1, the true yield strength is

$$\sigma_{yield\_150\_Pa} := \left[ \frac{K_T}{\left( \frac{E}{Pa} \right)^n} \cdot \left( \frac{sr}{10^{-3}} \right)^m \right]^{\frac{1}{(1-n)}} = 5.92 \times 10^8$$

In U.S. unit, the yield strength is

$$\sigma_{yield\_150\_us} := \sigma_{yield\_150\_Pa} \cdot Pa = 8.586 \times 10^4 \cdot psi$$

The reference 11, ORNL-3281, TID-4500 (17TH Ed), the total elongation of Zircaloy can vary between 12 and 16%. Under dynamic impact condition, the total elongation can be greater than the static test





## Design Analyses and Calculation

property. Therefore, it is reasonable to use 16% as the ultimate strain at room temperature. This is consistent with the data sheet published by ATI Wah Chang -Allegheny Technologies which says at room temperature, the elongation is 28%. For warm temperature, conservatively use an ultimate elongation value that is slightly larger than the published data. Therefore

$$\epsilon_{ult} = 0.17$$

Per Section 4.11.1, the true ultimate stress is

$$\sigma_{ult\_150\_Pa} := K_T \left( \frac{sr}{10^{-3}} \right)^m \cdot (\epsilon_{ult})^n = 8.425 \times 10^8$$

In U.S. unit, the ultimate strength is

$$\sigma_{ult\_150\_us} := \sigma_{ult\_150\_Pa} \text{ Pa} = 1.222 \times 10^5 \text{ psi}$$

For strain rate=0.1

$$sr=0.1$$

Per Section 4.11.1, the true strain at yield is

$$\epsilon_{yield\_150} := \left[ \frac{K_T}{\frac{E}{Pa}} \left( \frac{sr}{10^{-3}} \right)^m \right]^{\frac{1}{(1-n)}} = 7.271 \times 10^{-3}$$

Per Section 4.11.1, the true yield strength is

$$\sigma_{yield\_150\_Pa} := \left[ \frac{K_T}{\left( \frac{E}{Pa} \right)^n} \left( \frac{sr}{10^{-3}} \right)^m \right]^{\frac{1}{(1-n)}} = 6.564 \times 10^8$$

In U.S. unit, the yield strength is

$$\sigma_{yield\_150\_us} := \sigma_{yield\_150\_Pa} \text{ Pa} = 9.52 \times 10^4 \text{ psi}$$

As determined previously, the true strain at maximum load is

$$\epsilon_{ult} = 0.17$$

Per Section 4.11.1, the true ultimate stress is

$$\sigma_{ult\_150\_Pa} := K_T \left( \frac{sr}{10^{-3}} \right)^m \cdot (\epsilon_{ult})^n = 9.238 \times 10^8$$

In U.S. unit, the ultimate strength is

$$\sigma_{ult\_150\_us} := \sigma_{ult\_150\_Pa} \text{ Pa} = 1.34 \times 10^5 \text{ psi}$$





## Design Analyses and Calculation

For strain rate=1

$$sr=1$$

Per Section 4.11.1, the true strain at yield is

$$\epsilon_{yield\_150} := \left[ \frac{K_T}{\frac{E}{Pa}} \cdot \left( \frac{sr}{10^{-3}} \right)^m \right]^{\frac{1}{(1-n)}} = 7.657 \times 10^{-3}$$

Per Section 4.11.1, the true yield strength (Pa) is

$$\sigma_{yield\_150\_Pa} := \left[ \frac{K_T}{\left( \frac{E}{Pa} \right)^n} \cdot \left( \frac{sr}{10^{-3}} \right)^m \right]^{\frac{1}{(1-n)}} = 6.912 \times 10^8$$

In U.S. unit, the yield strength is

$$\sigma_{yield\_150\_psi} := \sigma_{yield\_150\_Pa} Pa = 1.002 \times 10^5 \cdot psi$$

As determined previously, the true strain at maximum load is

$$\epsilon_{ult} = 0.17$$

Per Section 4.11.1, the true ultimate stress is

$$\sigma_{ult\_150\_Pa} := K_T \cdot \left( \frac{sr}{10^{-3}} \right)^m \cdot (\epsilon_{ult})^n = 9.673 \times 10^8$$

In U.S. unit, the ultimate strength is

$$\sigma_{ult\_150\_psi} := \sigma_{ult\_150\_Pa} Pa = 1.403 \times 10^5 \cdot psi$$

For strain rate=10

$$sr=10$$


Per Section 4.11.1, the true strain at yield is

$$\epsilon_{yield\_150} := \left[ \frac{K_T}{\frac{E}{Pa}} \cdot \left( \frac{sr}{10^{-3}} \right)^m \right]^{\frac{1}{(1-n)}} = 8.063 \times 10^{-3}$$

Per Section 4.11.1, the true yield strength (Pa) is

$$\sigma_{yield\_150\_Pa} := \left[ \frac{K_T}{\left( \frac{E}{Pa} \right)^n} \cdot \left( \frac{sr}{10^{-3}} \right)^m \right]^{\frac{1}{(1-n)}} = 7.278 \times 10^8$$



N° FS1-0025122	Rev. 1.0	TEP - Technical Report	
	Page 111/177		



## Design Analyses and Calculation

In U.S. unit, the yield strength is

$$\sigma_{\text{yield\_150\_Pa}} = \sigma_{\text{yield\_150\_Pa}} \cdot \text{Pa} = 1.056 \times 10^5 \cdot \text{psi}$$

As determined previously, the true strain at maximum load is

$$\epsilon_{\text{ult}} = 0.17$$

Per Section 4.11.1, the true ultimate stress is

$$\sigma_{\text{ult\_150\_Pa}} = K_T \left( \frac{\text{sr}}{10^{-3}} \right)^m \cdot (\epsilon_{\text{ult}})^n = 1.013 \times 10^9$$

In U.S. unit, the ultimate strength is

$$\sigma_{\text{ult\_150\_Pa}} = \sigma_{\text{ult\_150\_Pa}} \cdot \text{Pa} = 1.469 \times 10^5 \cdot \text{psi}$$

		Page A22 of A55
--	--	-----------------





## Design Analyses and Calculation

### A.1.4 SUMMARY OF MATERIAL PROPERTIES FOR ZIRCALOY

Temperature = -40 degree F				
Poisson's ratio =0.3				
Strain Rate	.001	.1	1	10
Modulus of Elasticity, psi	1.393 x 10 <sup>7</sup>			
Yield Stress, psi	1.106 x 10 <sup>5</sup>	1.222 x 10 <sup>5</sup>	1.285 x 10 <sup>5</sup>	1.351 x 10 <sup>5</sup>
Yield Strain	0.0079	0.0088	0.0092	0.0097
Ultimate Stress, psi	1.401 x 10 <sup>5</sup>	1.537 x 10 <sup>5</sup>	1.609 x 10 <sup>5</sup>	1.685 x 10 <sup>5</sup>
Ultimate Strain	0.15	0.15	0.15	0.15

Temperature = 70 degree F				
Poisson's ratio =0.3				
Strain Rate	.001	.1	1	10
Modulus of Elasticity, psi	1.345 x 10 <sup>7</sup>			
Yield Stress, psi	9.46 x 10 <sup>4</sup>	1.048 x 10 <sup>5</sup>	1.103 x 10 <sup>5</sup>	1.161 x 10 <sup>5</sup>
Yield Strain	0.0070	0.0078	0.0082	0.0070
Ultimate Stress, psi	1.292 x 10 <sup>5</sup>	1.417 x 10 <sup>5</sup>	1.484 x 10 <sup>5</sup>	1.554 x 10 <sup>5</sup>
Ultimate Strain	0.16	0.16	0.16	0.16

Temperature = 150 degree F				
Poisson's ratio =0.3				
Strain Rate	.001	.1	1	10
Modulus of Elasticity, psi	1.309 x 10 <sup>7</sup>			
Yield Stress, psi	8.586 x 10 <sup>4</sup>	9.520 x 10 <sup>4</sup>	1.002 x 10 <sup>5</sup>	1.056 x 10 <sup>5</sup>
Yield Strain	0.0066	0.0073	0.0076	0.0081
Ultimate Stress, psi	1.222 x 10 <sup>5</sup>	1.340 x 10 <sup>5</sup>	1.403 x 10 <sup>5</sup>	1.469 x 10 <sup>5</sup>
Ultimate Strain	0.17	0.17	0.17	0.17





## Design Analyses and Calculation

### A.1.5 STRESS STRAIN DATA FOR ZIRCALOY

Temperature = -40 degree F				
Poisson's ratio =0.3				
Stress, psi				
Strain Rate	0.001	0.1	1	10
Strain =0.02	1.191 x 10 <sup>5</sup>	1.306 x 10 <sup>5</sup>	1.368 x 10 <sup>5</sup>	1.432 x 10 <sup>5</sup>
Strain =0.04	1.260 x 10 <sup>5</sup>	1.381 x 10 <sup>5</sup>	1.446 x 10 <sup>5</sup>	1.515 x 10 <sup>5</sup>
Strain =0.06	1.302 x 10 <sup>5</sup>	1.427 x 10 <sup>5</sup>	1.494 x 10 <sup>5</sup>	1.565x 10 <sup>5</sup>
Strain =0.079	1.331 x 10 <sup>5</sup>	1.459 x 10 <sup>5</sup>	1.528 x 10 <sup>5</sup>	1.600x 10 <sup>5</sup>
Ultimate Strain	1.331 x 10 <sup>5</sup>	1.459 x 10 <sup>5</sup>	1.528 x 10 <sup>5</sup>	1.600x 10 <sup>5</sup>

Temperature = 70 degree F				
Poisson's ratio =0.3				
Stress, psi				
Strain Rate	0.001	0.1	1	10
Strain =0.02	1.05 x 10 <sup>5</sup>	1.151 x 10 <sup>5</sup>	1.206 x 10 <sup>5</sup>	1.262 x 10 <sup>5</sup>
Strain =0.04	1.125 x 10 <sup>5</sup>	1.234 x 10 <sup>5</sup>	1.292 x 10 <sup>5</sup>	1.353 x 10 <sup>5</sup>
Strain =0.06	1.172 x 10 <sup>5</sup>	1.285 x 10 <sup>5</sup>	1.345 x 10 <sup>5</sup>	1.409x 10 <sup>5</sup>
Strain =0.098	1.23 x 10 <sup>5</sup>	1.349 x 10 <sup>5</sup>	1.412 x 10 <sup>5</sup>	1.479x 10 <sup>5</sup>
Ultimate Strain	1.23 x 10 <sup>5</sup>	1.349 x 10 <sup>5</sup>	1.412 x 10 <sup>5</sup>	1.479x 10 <sup>5</sup>

Temperature = 150 degree F				
Poisson's ratio =0.3				
Stress, psi				
Strain Rate	0.001	0.1	1	10
Strain =0.02	0.9689x 10 <sup>5</sup>	1.062 x 10 <sup>5</sup>	1.112 x 10 <sup>5</sup>	1.165 x 10 <sup>5</sup>
Strain =0.04	1.045 x 10 <sup>5</sup>	1.145 x 10 <sup>5</sup>	1.199 x 10 <sup>5</sup>	1.256 x 10 <sup>5</sup>
Strain =0.06	1.091 x 10 <sup>5</sup>	1.197 x 10 <sup>5</sup>	1.253 x 10 <sup>5</sup>	1.312 x 10 <sup>5</sup>
Strain =0.106	1.161 x 10 <sup>5</sup>	1.273 x 10 <sup>5</sup>	1.333 x 10 <sup>5</sup>	1.396x 10 <sup>5</sup>
Ultimate Strain	1.161 x 10 <sup>5</sup>	1.273 x 10 <sup>5</sup>	1.333 x 10 <sup>5</sup>	1.396x 10 <sup>5</sup>





## Design Analyses and Calculation

### A.2 AISI 304 (SUS 304) Grade Stainless Steel

#### A.2.1 MECHANICAL PROPERTIES OF SS304 AND APPLICABLE CODES

The 304 stainless steel are used in fuel cage (304L, plates) and container shells and frames (304, plates). The plates are modeled as shell elements in LSDYNA program.

The material properties for Type 304 and 304L stainless steel, taken from ASME Boiler and Pressure Code, Section II, Part D, 2010 Ed. [Ref.14], are presented in Table A.2-1 and A.2-2 below. The densities are initial values. In the LSDYNA input file, the densities are adjusted so that the total mass equal to the design weight of the fuel bundle and container. The stresses listed below are engineering stress.

**Table A.2.1-1 Mechanical Properties of 304 (SA-240) at temperature of interest**

Property	-40°F	70°F	150°F	Reference
Modulus of Elasticity, E, ksi	28,900	28,300	27,800	Ref. 14, Table TM-1
Ultimate Tensile Stress, S <sub>u</sub> , ksi	75	75	72.5	Ref. 14, Table U
Yield Stress, S <sub>y</sub> , ksi	30	30	26.7	Ref. 14, Table Y-1
Poisson's ratio	0.31			Ref. 14, Table PRD
Density, (lb/in <sup>3</sup> )	0.29			Ref. 14, Table PRD

**Table A.2.1-2 Mechanical Properties of 304L (SA-240) at temperature of interest**

Property	-40°F	70°F	150°F	Reference
Modulus of Elasticity, E, ksi	28,900	28,300	27,800	Ref. 14, Table TM-1
Ultimate Tensile Stress, S <sub>u</sub> , ksi	70	70	67.6	Ref. 14, Table U
Yield Stress, S <sub>y</sub> , ksi	25	25.0	22.7	Ref. 14, Table Y-1
Poisson's ratio	0.31			Ref. 14, Table PRD
Density, (lb/in <sup>3</sup> )	0.29			Ref. 14, Table PRD

According to TN-B1 SAR Rev. 3 [Ref. 7], Section 2.1.4, the applicable codes that would apply are the ASME Boiler and Pressure Vessel Code Section III, Subsection ND for the containment boundary which is the fuel cladding and Section III, and Subsection NG for the criticality control structure and the Section VIII for the non-containment components. This requirement is summarized in the table below.





## Design Analyses and Calculation

Table A.2.1-3 Applicable Structural Codes for the Stainless Steel 304 and 304L

Component Description	Usage	Material	Applicable Codes
Fuel Assembly Cages	criticality control	SS304L	ASME B&PV Code, Section III, Subsection NG
Container Shell	non-Containment components	SS304	ASME B&PV Code, Section VIII

### A.2.2 STRESS STRAIN CURVE FOR STAINLESS STEEL TO COMPLY WITH THE ASME B&PV CODE, SECTION III, SUBSECTION NG

The equations to generate the stress strain curves for SS alloys are given in [Ref. 27]. The equations are developed from tests performed at room temperature. In order to develop the LSDYNA input file for the material model \*MAT\_PIECEWISE\_LINEAR\_PLASTICITY (Type 24) and still complying with the mechanical strengths listed in the above two tables, the parameters in the strain-stress equations are modified so that the modulus of elasticity, yield and ultimate strengths are consistent with ASME Boiler and Pressure Codes in [Ref. 14]. . The derivation of the full-range stress-strain curve is shown in this section. The equation numbers, figure number and table number are taken directly from [Ref.27] and preserved for easy reference. The true stress-strain curve in [Ref. 27] is listed below.

$$\epsilon = \begin{cases} \frac{\sigma}{E_0} + 0.002 \left( \frac{\sigma}{\sigma_{0.2}} \right)^n & \text{for } \sigma \leq \sigma_{0.2} \\ \frac{\sigma - \sigma_{0.2}}{E_{0.2}} + \epsilon_u \left( \frac{\sigma - \sigma_{0.2}}{\sigma_u - \sigma_{0.2}} \right)^m + \epsilon_{0.2} & \text{for } \sigma > \sigma_{0.2} \end{cases} \quad (18)$$

The definitions of the parameters are taken from [Ref. Error! Reference source not found.] and shown graphically in the figure below.



ATKINS

## Design Analyses and Calculation

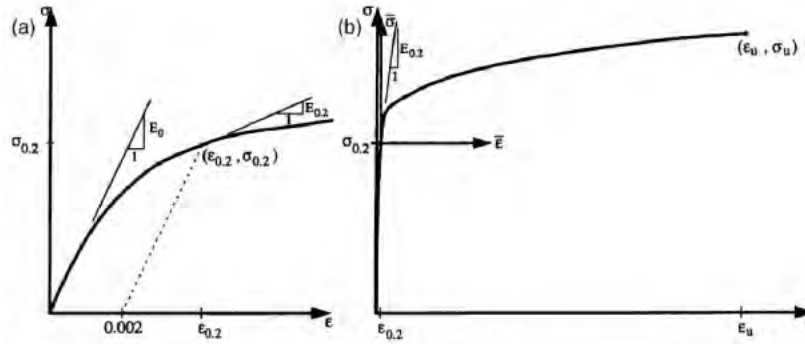


Fig. 3. Initial and full stress-strain curves. (a) Initial  $\sigma$ - $\epsilon$  curve, (b) full  $\sigma$ - $\epsilon$  curve.

The summary parameter values based on test performed on various SS alloys are shown in the table below.

Table 1  
Mechanical properties

Test	Alloy <sup>a</sup>	Reference <sup>a</sup>	Form <sup>c</sup>	$E_0$ (GPa)	$\sigma_{0.01}$ (MPa)	$\sigma_{0.2}$ (MPa)	$\sigma_u$ (MPa)	$\epsilon_u$	$e$	$n$	$m^d$
1	UNS30400	[10]	RHS	188	314	612	780	0.40	0.0032	4.49	3.7
2	UNS30400	[10]	RHS	182	297	532	731	0.45	0.0029	5.14	3.5
3	UNS30400	[10]	RHS	190	178	312	635	0.65	0.0016	5.33	2.7
4	UNS30400	[10]	RHS	197	183	286	627	0.65	0.0015	6.71	2.6
5	UNS30400	[10]	RHS	190	241	402	661	0.55	0.0021	5.85	3.1
6	UNS30400	[10]	RHS	196	203	297	638	0.61	0.0015	7.87	2.6
7	UNS30400	[8]	Ch	180	341	460	695	0.34 <sup>e</sup>	0.0026	4.66	3.3
8	UNS30400	[9]	P	190	215	327	611	0.57	0.0017	7.0	2.9
9	UNS30403	[5]	RHS	194	240	445	730 <sup>f</sup>	0.51 <sup>f</sup>	0.0023	4.85	3.1
10	UNS30403	[5]	RHS	190	240	470	730	0.51	0.0025	4.45	3.3
11	UNS30403	[5]	CHS	198	250	400	675 <sup>g</sup>	0.51 <sup>g</sup>	0.0020	6.37	3.1
12	UNS30403	[5]	CHS	198	250	400	675	0.51	0.0020	6.37	3.1
13	UNS31603	[9]	P	190	190	316	616	0.51	0.0017	5.88	2.8
14	UNS31803	[9]	P	190	526	699	878	0.32	0.0037	10.6	3.8
15	UNS31803	[11]	P	200	310	575	805	0.22	0.0029	4.85	3.5
16	UNS31803	[11]	P	215	430	635	820	0.22	0.0029	7.68	3.7
17	UNS31803	[11]	P	215	430	635	820	0.22	0.0029	7.68	3.7
18	UNS43000	[12]	P	200	200	320	622 <sup>h</sup>	0.48 <sup>h</sup>	0.0016	6.37	2.8
19	3Cr12	[12]	P	195	215	275	444 <sup>i</sup>	0.38 <sup>h</sup>	0.0014	12.2	3.2

The value of  $E_{0.2}$  used in the second formula of equation (18) is shown in the equation below.

$$E_{0.2} = \frac{E_0}{1 + 0.002n/e} \quad (13)$$

The value of  $\epsilon_{0.2}$  used in the second formula of equation (18) is derived from the first formula with  $\sigma = \sigma_{0.2}$ , that the strain value is shown below.

$$\frac{\sigma}{E_0} + 0.002$$

For ultimate stresses, the value is taken from the engineering stress listed in Table A.2.1-1 and Table A.2.1-2 and converted to true stresses using the following formula.





## Design Analyses and Calculation

$$\sigma_u = S_u \times (1 + \epsilon_u)$$

where

$\sigma_u$  = true ultimate stress used to generate the true stress-strain curve

$S_u$  = engineering ultimate stress from [Ref. 1427]

$\epsilon_u$  = ultimate strain taken from [Ref. 27], Table 1

The stress-strain values for SS304 and SS304L based on the above equations are derived and presented in the following sub-sections.





## Design Analyses and Calculation

### A.2.2.1 Stress Strain Value of SS304 at -40°F.

The parameters used in Equation (18) are tabulated below. The data for the stress-strain curve is listed in the following tables.

	$E_0$	$\sigma_{0.2}$	$\sigma_u$	$E_{0.2}$
unit, psi	2.89E+07	3.0E+04	1.18E+05	3.13E+06

$\epsilon_0$	e	n	m	$\epsilon_{0.2}$
0.57	0.0017	7.0	2.9	0.00304

Table A.2.2.1-1 Stress Strain Value of SS304 at -40°F

Strain	stress, psi
0	0
0.000173	5000
0.000347	10000
0.000535	15000
0.000809	20000
0.001423	25000
0.003038	30000
0.006132	37977.3
0.012199	45954.5
0.023853	53931.8
0.043561	61909.1
0.073707	69886.4
0.116616	77863.6
0.174564	85840.9
0.24979	93818.2
0.344503	101795
0.460881	109773
0.5700	117750.0





## Design Analyses and Calculation

### A.2.2.2 Stress Strain Value of SS304 at Room Temperature

The parameters used in Equation (18) are tabulated below. The data for the stress-strain curve is listed in the following tables.

	$E_0$	$\sigma_{0.2}$	$\sigma_u$	$E_{0.2}$
unit, psi	2.83E+07	3.00E+04	1.18E+05	3.064E+06

$\epsilon_u$	e	n	m	$\epsilon_{0.2}$
0.570	0.0017	7.000	2.900	0.00306

Table A.2.2.2-1 Stress Strain Value of SS304 at Room Temperature

Strain	stress, psi
0	0
0.000177	5000.0
0.000354	10000.0
0.000546	15000.0
0.000824	20000.0
0.001442	25000.0
0.00306	30000.0
0.006208	37977.3
0.012329	45954.5
0.024037	53931.8
0.043799	61909.1
0.073999	69886.4
0.116962	77863.6
0.174964	85840.9
0.250245	93818.2
0.345011	101795
0.461443	109773
0.5700	117750.0





## Design Analyses and Calculation

### A.2.2.3 Stress Strain Value of SS304 at 150°F.

The parameters used in Equation (18) are tabulated below. The data for the stress-strain curve is listed in the following the tables.

	$E_0$	$\sigma_{0.2}$	$\sigma_u$	$E_{0.2}$
unit, psi	2.78E+07	2.67E+04	1.14E+05	3.011E+06

$\epsilon_u$	e	n	m	$\epsilon_{0.2}$
0.57	0.0017	7.0	2.9	0.00296

Table A.2.2.3-1 Stress Strain Value of SS304 at 150°F.

Strain	stress, psi
0	0
0.00016	4450.0
0.000321	8900.0
0.000496	13350.0
0.000757	17800.0
0.001358	22250.0
0.00296	26700.0
0.006136	34625.9
0.012287	42551.9
0.024023	50477.8
0.043814	58403.8
0.074043	66329.7
0.117035	74255.7
0.175066	82181.6
0.250375	90107.6
0.345171	98033.5
0.461632	105959
0.5700	113885.4





## Design Analyses and Calculation

### A.2.2.4 Stress Strain Value of SS304L at -40°F.

The parameters used in Equation (18) are tabulated below. The data for the stress-strain curve is listed in the following tables.

	$E_0$	$\sigma_{0.2}$	$\sigma_u$	$E_{0.2}$
unit, psi	2.89E+07	2.50E+04	1.06E+05	3.921E+06

$\epsilon_u$	e	n	m	$\epsilon_{0.2}$
0.51	0.002	6.37	3.10	2.87E-03

Table A.2.2.4-1 Stress Strain Value of SS304L at -40°F

Strain	stress, psi
0	0
0.000144	4166.7
0.00029	8333.3
0.000457	12500.0
0.000728	16666.7
0.001347	20833.3
0.002865	25000.0
0.005037	32336.4
0.009192	39672.7
0.017563	47009.1
0.032512	54345.5
0.056484	61681.8
0.091988	69018.2
0.141581	76354.5
0.207866	83690.9
0.293485	91027.3
0.40111	98363.6
0.5100	105700.0





## Design Analyses and Calculation

### A.2.2.5 Stress Strain Value of SS304L at Room Temperature

The parameters used in Equation (18) are tabulated below. The data for the stress-strain curve is listed in the following tables.

	$E_0$	$\sigma_{0.2}$	$\sigma_u$	$E_{0.2}$
unit, psi	2.83E+07	2.50E+04	1.06E+05	3.840E+06

$\epsilon_u$	$e$	$n$	$m$	$\epsilon_{0.2}$
0.51	0.002	6.37	3.10	0.00288

Table A.2.2.5-1 Stress Strain Value of SS304L at Room Temperature

Strain	stress, psi
0	0
0.000147	4166.7
0.000296	8333.3
0.000466	12500.0
0.000740	16666.7
0.001362	20833.3
0.002883	25000.0
0.005095	32336.4
0.009289	39672.7
0.017700	47009.1
0.032689	54345.5
0.056701	61681.8
0.092244	69018.2
0.141877	76354.5
0.208202	83690.9
0.293860	91027.3
0.401525	98363.6
0.510000	105700.0





## Design Analyses and Calculation

### A.2.2.6 Stress Strain Value of SS304L at 150°F.

The parameters used in Equation (18) are tabulated below. The data for the stress-strain curve is listed in the following tables.

	$E_0$	$\sigma_{0.2}$	$\sigma_u$	$E_{0.2}$
unit, psi	2.78E+07	2.27E+04	1.02E+05	3.773E+06

$\varepsilon_u$	$e$	$n$	$m$	$\varepsilon_{0.2}$
0.51	0.002	6.37	3.10	0.002816

Table A.2.2.6-1 Stress Strain Value of SS304L at 150°F

Strain	stress, psi
0	0
0.00014	3783.3
0.00027	7566.7
0.00043	11350.0
0.00070	15133.3
0.00131	18916.7
0.00282	22700.0
0.00503	29916.0
0.00923	37132.0
0.01764	44348.0
0.03263	51564.0
0.05664	58780.0
0.09219	65996.0
0.14182	73212.0
0.20815	80428.0
0.29381	87644.0
0.40148	94860.0
0.51000	102076.0





## Design Analyses and Calculation

### A.2.3 STRESS STRAIN CURVE FOR STAINLESS STEEL TO COMPLY WITH THE ASME B&PV CODE, SECTION VIII

The stress strain data at temperature of interest based on the Table A.2.1-1 and the equations in ASME Boiler and Pressure Vessel Code, Section VIII, Div 2, Annex 3.D (Ref.15) are tabulated as follows.

**Table A.2.3-1 Stress-Strain Data of SS304 at -40° F**

Strain	Stress Psi
0.0	0.0
0.0015	24000.0
0.0022	27000.0
0.0034	30000.0
0.0074	34868.0
0.0182	39735.9
0.0395	44603.9
0.0625	49471.9
0.0815	54339.8
0.0997	59207.8
0.1189	64075.8
0.1397	68943.7
0.1623	73811.7
0.1869	78679.7
0.2133	83547.6
0.2417	88415.6
0.2720	93283.6
0.3044	98151.5
0.3387	103019.5
0.3751	107887.5
0.4136	112755.4
0.4541	117623.4
0.5541	117623.4





## Design Analyses and Calculation

Table A.2.3-2 Stress-Strain Data of SS304 at 70°F

Strain	Stress Psi
0.0	0.0
0.0016	24000.0
0.0023	27000.0
0.0035	30000.0
0.0075	34868.0
0.0183	39735.9
0.0396	44603.9
0.0626	49471.9
0.0817	54339.8
0.0999	59207.8
0.1191	64075.8
0.1399	68943.7
0.1626	73811.7
0.1871	78679.7
0.2136	83547.6
0.2420	88415.6
0.2723	93283.6
0.3047	98151.5
0.3391	103019.5
0.3755	107887.5
0.4139	112755.4
0.4544	117623.4
0.5544	117623.4





## Design Analyses and Calculation

Table A.2.3-3 Stress-Strain Data of SS304 at 150° F

Strain	Stress Psi
0.0	0.0
0.0015	21538.5
0.0022	24230.8
0.0033	26923.1
0.0077	31885.7
0.0205	36848.4
0.0443	41811.0
0.0670	46773.7
0.0859	51736.3
0.1048	56699.0
0.1251	61661.6
0.1473	66624.3
0.1713	71586.9
0.1972	76549.6
0.2251	81512.2
0.2550	86474.9
0.2868	91437.6
0.3206	96400.2
0.3563	101362.9
0.3941	106325.5
0.4340	111288.2
0.4758	116250.8
0.5758	116250.8





## Design Analyses and Calculation

### A.2.4 STRAIN RATE EFFECTS

At high strain rate, as in the case of dynamic impact condition, the yield stress increases and this tends to strengthen the material. The strain-rate sensitivity data of 304 and 304L, taken from "Impact tensile testing of stainless steels at various temperatures" D.K. Morton and R. K. Blandford, March 2008, INL/EXT-08-14082 [endnote 16], is listed in Table A.2.4-1 below. The strain rate sensitivity data for 304 and 304L at temperature of -40°F is the same as that at temperature -20°F.

**Table A.2.4-1 The Strain-rate Sensitivity of 304/304L**

Strain Rate	Temperature, °F				
	-20	70	150	300	600
5	1.333	1.235	1.211	1.166	1.043
10	1.361	1.278	1.254	1.210	1.094
22	1.428	1.381	1.358	1.316	1.217
25	1.445	1.407	1.384	1.342	1.247





## Design Analyses and Calculation

### A.2.9 STRESS-STRAIN CURVES OF SS304 AND SS304L

The following graphs illustrate the stress-strain curves of the data presented in the previous sections.

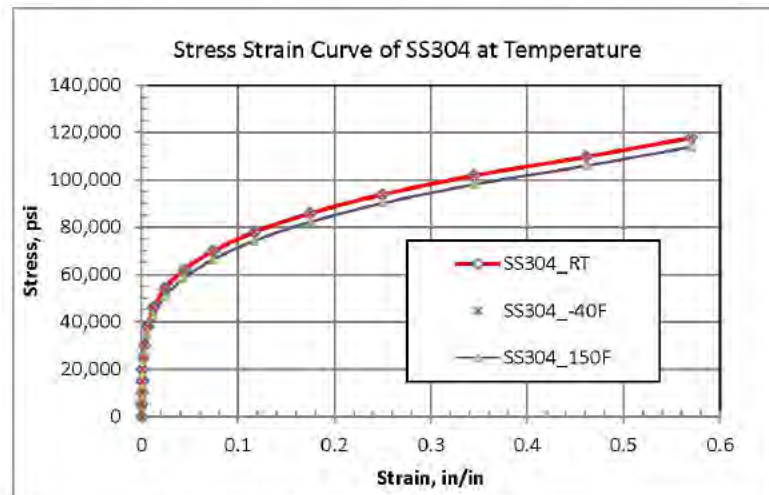


Figure A.2.9-1 Stress-Strain Curves of SS304

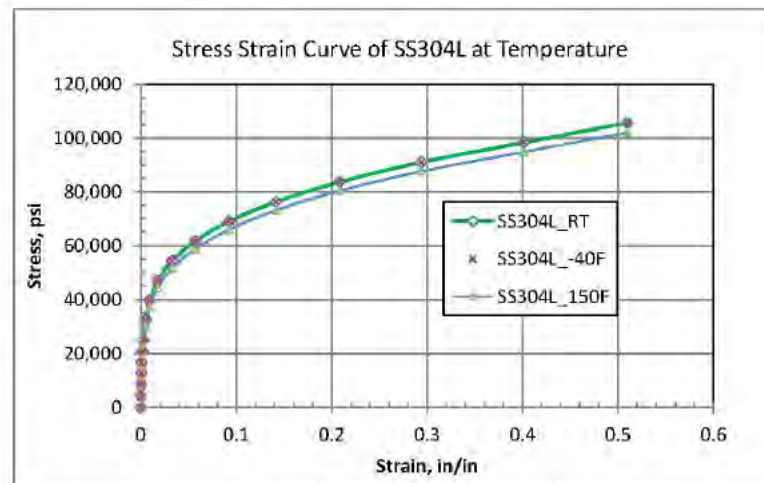


Figure A.2.9-2 Stress-Strain Curves of SS304L





## Design Analyses and Calculation

### A.3 Balsa (Shock Absorber)

This wood is used as Shock Absorber for the following applications.

Item 26 of Outer Container Main Body Assembly (Dwg 105E3738, Rev. 7)

The Balsa wood is used primarily as shock absorber in the oblique and End Drop orientation. Based on TN-B1 SAR Rev. 3 [Ref. 7] Table 2-3, the compressive strength of the Balsa wood at ambient temperature is 16 MPa. The density of the Balsa wood is 0.18 g/cm<sup>3</sup>. Therefore

The compressive strength is

$$\sigma = 16 \text{ MPa} = 2321 \text{ psi}$$

The density of the Balsa wood is

$$\rho = 0.18 \text{ g/cm}^3 = 11.24 \text{ lb/ft}^3$$

#### a. THE STRESS-STRAIN CURVE FOR COMPACTED Balsa WOOD.

The density of wood cell substance,  $\rho_s$ , is common to all woods and has been estimated to be approximately 93.6 lb/ft<sup>3</sup> (1500 kg/m<sup>3</sup>) per Ref. 28. The density of the uncompacted Balsa for the TN-B1 container,  $\rho$ , is 11.24 lb/ft<sup>3</sup> (=180 kg/m<sup>3</sup>) that  $\rho/\rho_s = 0.12$ . Figure 9a of [Ref. 28] shows the experimental measurement of the Stress and strain relationship of Balsa wood with  $\rho/\rho_s = 0.150$ . The figure is duplicated as follows.

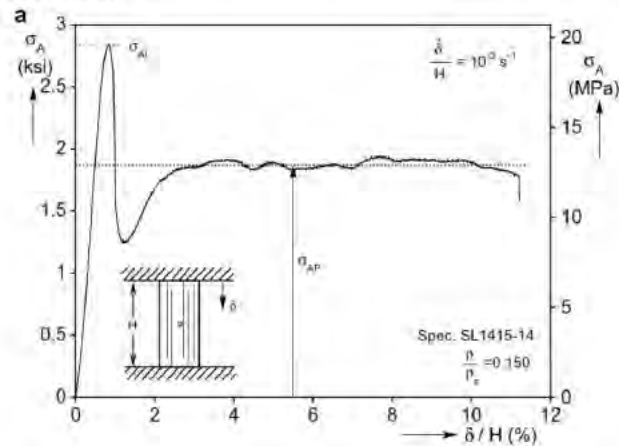


Figure A.3-1 Axial stress-displacement crushing response of balsa specimen with  $\rho/\rho_s = 0.150$   
(Cited from [Ref.28], Figure 9)

Figure 13 of Ref. 6 shows the comparison of axial crushing response of balsa wood of different

		Page A40 of A55
--	--	-----------------



densities. The figure is duplicated as follows.

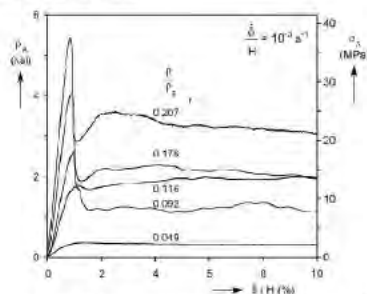


Figure A.3-2 Comparison of axial crushing response of balsa wood of different densities.  
(cited from [Ref. 28], Figure 13)

Table 3 of Ref. 6 shows the strength measured for several balsa wood densities at different wood grain orientations (the subscripts A= axial, R= Radial, T=tangential, L=limiting stress, P=plateau stress) . The table is duplicated as follows.

Table A.3-1 Strength measured for several balsa wood densities  
(cited from Ref.28, Table 3)

Strengths measured for several balsa wood densities											
$\frac{\rho}{\rho_s}$	$\sigma_{AL}$ ksi (MPa)	$\sigma_{AP}$ ksi (MPa)	$\frac{\rho}{\rho_s}$	$\sigma_{LR}$ psi (MPa)	$\frac{\rho}{\rho_s}$	$\sigma_{LT}$ psi (MPa)	$\frac{\rho}{\rho_s}$	$\tau_{LR}$ psi (MPa)	$\frac{\rho}{\rho_s}$	$\tau_{LT}$ psi (MPa)	
0.065	0.92 (6.4)	0.70 (4.8)	0.044	63 (0.43)	0.047	48 (0.33)	0.044	132 (0.91)	0.050	96 (0.66)	
0.096	1.78 (12.3)	1.37 (9.45)	0.086	103 (0.710)	0.077	81 (0.56)	0.100	298 (2.05)	0.100	212 (1.46)	
0.137	3.06 (21.1)	2.19 (15.1)	0.118	171 (1.18)	0.111	109 (0.752)	0.141	449 (3.10)	0.140	312 (2.15)	
0.165	4.07 (28.1)	2.79 (19.2)	0.135	198 (1.37)	0.150	124 (0.855)	0.163	526 (3.63)	0.188	421 (2.90)	
0.215	5.70 (39.3)	3.59 (24.8)	0.160	236 (1.63)	0.169	180 (1.24)	0.207	736 (5.07)	0.242	541 (3.73)	

For the current balsa wood density with  $\rho/\rho_s = 0.12$ , the compressive strength of 16 MPa is similar to the plateau stress of 15.1 MPa with  $\rho/\rho_s = 0.137$ .

Figure 4 of [Ref. 29] shows the effect of density on the stress-strain curves for confined specimens. The figure is duplicated as follows.

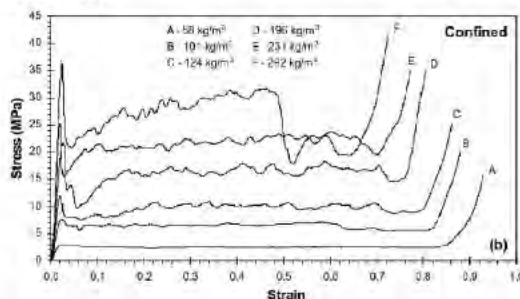


Figure A.3-3 Effect of density on the stress-strain curves for confined specimens of balsa wood.  
(cited from [Ref.29], Figure 4b)





## Design Analyses and Calculation

It is noted in the above figure that at wood density of  $196 \text{ kg/m}^3$  (curve D), the average compressive stress of 16 MPa is very close to the current strength specification of Balsa wood. Therefore, the stress strain curve of balsa wood at ambient temperature can be developed with a curve similar to Curve D of above figure that the plateau stress is 16 MPa and the lock-up condition approaches 75% of the volumetric strain level. At the lock-up condition of the wood, the stress increases asymptotically with increasing strain. The stress-strain curve for the balsa wood developed for this calculation is shown in the table below. The slope of the stress strain curve is made positive to minimize the run problems often encountered in LSDYNA. The curve is for impact with direction parallel to the axial grain direction which is the direction the balsa wood is installed as shock absorber.

Table A.3-2 Stress Strain Data Developed for Balsa Wood ( $\rho=180\text{kg/m}^3$ )

Volumetric Strain	Stress, psi
0.000	0
0.020	1,500
0.040	2,000
0.100	2,250
0.150	2,300
0.600	2,400
0.700	2,600
0.770	4,000
0.800	6,000

The stress-strain curve for the data in the above table is presented as follows.

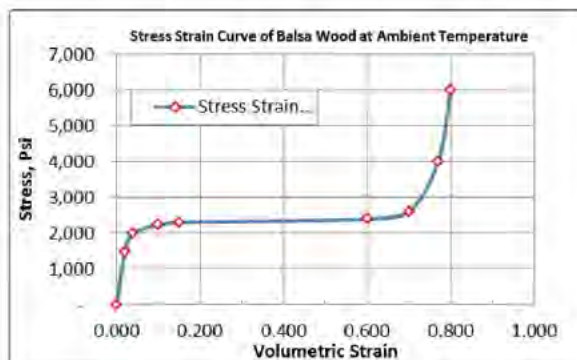


Figure A.3-4 Stress Strain Curve Developed for Balsa Wood ( $\rho=180\text{kg/m}^3$ )





## Design Analyses and Calculation

### b. EFFECTS OF TEMPERATURE ON THE STRENGTH OF Balsa Wood.

Basically, declining strengths can be expected in case of rising temperatures according to cited papers of [Ref. 30, Section 3.3.3]. The magnitude of the influence exerted by the temperature on the elasticity module amounts to as much as 40% between -20°C (-4°F) and 60°C (140°F). The drop in the pressure strength amounts to about 55% between -20°C (-4°F) and +150°C (302°F). Assuming the temperature effect varies linearly with respect to temperature, using the compressive stress at ambient temperature as the base line, the resulted compressive stress increase is 14% (=1.14-1) more for temperature at -40°F and 10% less (=1-0.899) for temperature at 150°F. The derivation of the temperature effect correction factors is presented in the following Table.

Table A.3-3 Correction Factors for Compressive Strength of Balsa Wood at extreme Temperatures

at degree C (Ref. 30Error! Bookmark not defined.)		-20			150
at degree F	-40	-4	70	150	302
interpolated and extrapolated					
Scale from research, [Ref. 30]	1.61	1.55	1.42	1.27	1.00
New scale to be used in LSDYNA input	1.140	1.09	1.00	0.899	

### c. POISSON'S RATIO

The Balsa Wood is modeled using the LSDYNA material model crushable\_foam (Material 63 and 163). After the initial limiting stress (the threshold of plastic deformation), the material model generally is uncoupled between the axial direction and the radial or tangential directions. Therefore, the use of a plastic Poisson's ratio of  $\nu=0.0$  is recommended. In this calculation, a small value of  $\nu=0.01$  is used to represent the marginal effect.

### d. DYNAMIC EFFECTS ON STRESS-STRAIN CURVE OF Balsa Wood

Since there is no readily available published data on dynamic effects of balsa wood under impact, this calculation relies on the benchmark drop test performed on the RAI-II container to make material property adjustment to reflect the dynamic effect on the compressive strength of the Balsa Wood. The strength correction factor will be developed from the benchmark runs at ambient temperature then applied to the LSDYNA runs for cold and hot temperature.

The Balsa Wood is modeled using the LSDYNA material model of Crushable\_Foam.





## Design Analyses and Calculation

### A.4 Paper Honeycomb

This is used as shock absorber for the following applications.

- Items 1, 2, 3, 4, 5 of Outer Container Shock Absorber Assembly (Dwg 105E3741, Rev. 1)
- Item 4 of Protective Case (Dwg 105e3773, Rev. 1)

This material is used as shock absorber primarily during the two Horizontal Drop orientations. Based on TN-B1 SAR Rev. 3 [Ref. 7] Table 2-3, the static initial peak stress of the Paper Honeycomb at ambient temperature is 2.35 MPa. The density of the Paper Honeycomb is 0.06 g/cm<sup>3</sup>. Therefore

The initial peak stress is

$$\sigma = 2.35 \text{ MPa} = 342.3 \text{ psi}$$

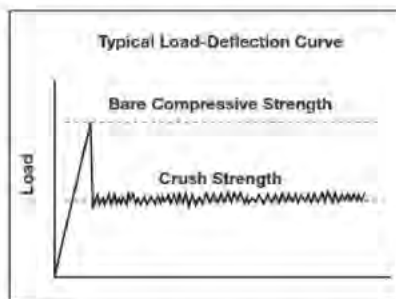
The density of the Paper Honeycomb is

$$\rho = 0.06 \text{ g/cm}^3 = 3.746 \text{ lb/ft}^3$$

$$\text{or } \rho = 60 \text{ kg/m}^3$$

#### a. LOAD-DEFLECTION CURVE OF HONEYCOMB MATERIAL

The initial peak stress is the stabilized compressive strength, which represents the ultimate compressive strength of the honey comb in pounds per square inch. After honeycomb has exceeded its ultimate compressive strength, it will continue to deform plastically and crush uniformly. The load deflection curve below shows such a typical response.



The average crush load per unit cross-sectional area is defined as the crush strength, expressed in pounds per square inch. Honey comb will crush at virtually a constant stress level; hence its energy absorption capacity is predictable, making it ideal for energy absorption applications. When used in this manner, the core is often pre-crushed slightly to remove the compressive peak in the load-deflection curve. There is no test report on the honeycomb material used in the current analysis, therefore it is assumed that the compressive peak is removed and a preliminary load-deflection curve is developed as shown in the table below. The graphical representation of the load-deflection curve is

		Page A44 of A55
--	--	-----------------





## Design Analyses and Calculation

presented following the load-deflection data table. The actual value of the crush strength will be corrected by benchmarking the predicted acceleration (G) values against the drop test result. Because the load-deflection curve behaves so much like orthotropic crushable foam, and the other material properties of a true honeycomb are not known or relevant, the honey comb in the container is therefore modeled using the LSDYNA material model of Crushable\_Foam.

**Table A.4-1 Load Deflection Data Developed for Paper Honeycomb**

Volumetric Strain	Stress, psi
0.000	0
0.020	390
0.040	350
0.100	343
0.200	343
0.300	343
0.500	343
0.700	343





## Design Analyses and Calculation

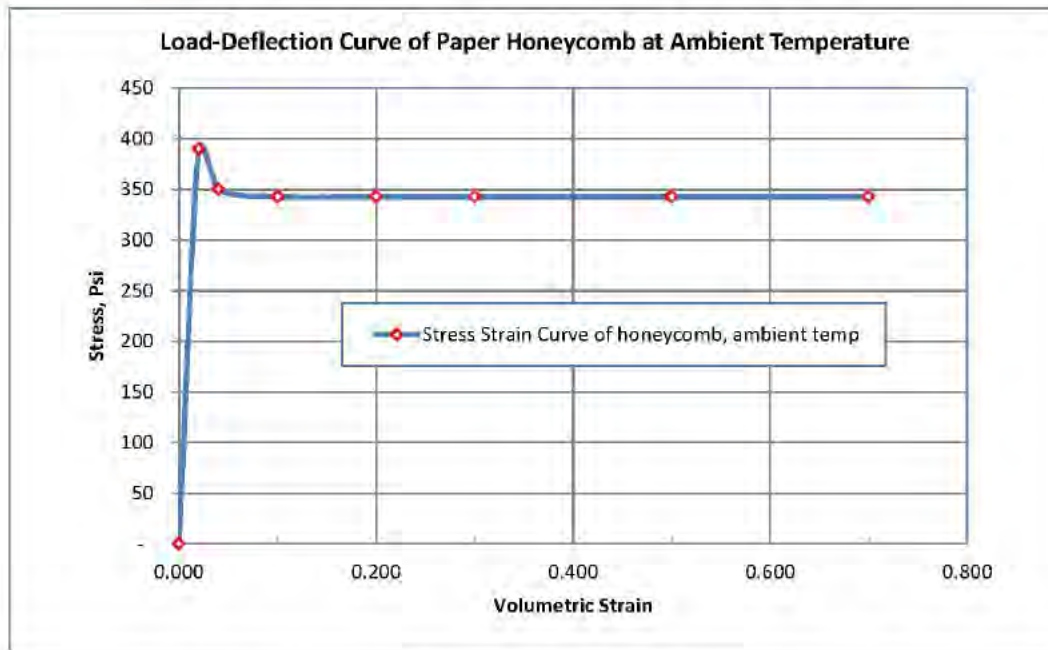


Figure A.4-1 Load-Deflection Curve Developed for Paper Honeycomb

**b. POISSON'S RATIO**

The deformation of the honeycomb material generally is uncoupled between the axial direction and the lateral directions. A small value of  $PR=0.01$  is used to represent the marginal effect of Poisson's ratio.

**c. EFFECTS OF TEMPERATURE ON THE STRENGTH OF PAPER HONEYCOMB.**

Several studies on the effects of temperature on the strength of paper were reported in [Ref. 17]. Between  $-25^{\circ}\text{C}$  and  $175^{\circ}\text{C}$ , the elastic modulus of paper decreases at an average rate of 0.3% per degree C. The ultimate strength of paper decreases at a rate comparable to the tensile modulus. Therefore, it is reasonable to assume that between  $-40^{\circ}\text{F}$  and  $150^{\circ}\text{F}$ , the change in paper honeycomb strength is comparable; recognizing that the test for temperature below  $-25^{\circ}\text{C}$  ( $-13^{\circ}\text{F}$ ) is lacking. In the case of metals, where the test data are abundant, material properties between  $-20^{\circ}\text{F}$  and  $-40^{\circ}\text{F}$ , the changes in elastic modulus are very small. At cold temperature ( $-40^{\circ}\text{F}$ ), the stiffness correction factor (CF) applied to the honeycomb material property of room temperature is





## Design Analyses and Calculation

$$CF = 1 + 0.003 \times (70+40) \times 5/9 = 1.18$$

Where

0.003 = rate of change for the elastic modulus per degree C (=0.3%)

(70+40) = temperature span between -40°F to room temperature (70°F) = 110 °F

5/9 = conversation factor between °F to °C

At hot temperature (150°F), the stiffness correction factor (CF) applied to the honeycomb material property of room temperature is

$$CF = 1 - 0.003 \times (150-70) \times 5/9 = 0.86$$

Where

0.003 = rate of change for the elastic modulus per degree C (=0.3%)

(150-70) = temperature span between 150°F to room temperature (70°F) = 80 °F

5/9 = conversation factor between °F to °C

Therefore, the correction factors for the honeycomb strength for cold and hot temperature are 1.18 and 0.86, respectively.

### d. DYNAMIC STRENGTH OF THE HONEYCOMB MATERIAL

Since there is no readily available published data on dynamic effects of paper honeycomb under impact, this calculation relies on the benchmark drop test performed on the RAJ-II container to make material property adjustment to reflect the dynamic effect on the compressive strength of the paper honeycomb. The strength correction factor will be developed from the benchmark runs at ambient temperature and then applied to the LSDYNA runs for cold and hot temperature.

### A.5 Lumber (Hemlock)

This wood is used as thermal insulator for the following applications.

- Items 24, 25, 26, 27 of Inner Container Main Body Assembly (Dwg 105E3745, Rev. 8)
- Item 13 of Inner Container Lid (Dwg 105E3747, Rev. 4).
- Item 7 of Inner Container End Lid (Dwg 105E3748, Rev. 2)

### a. THE ELASTIC MODULUS AND DENSITY FOR COMPACTED HEMLOCK.

The Hemlock is used as thermal insulator; therefore there is no structural value intended for the





## Design Analyses and Calculation

Hemlock. During the end drop orientation, the Hemlock is not in the load path of the fuel bundle except its own weight. During the Horizontal Drop orientation, the Hemlock plates provide support for the fuel rod bundle. Therefore the hemlock is treated as elastic material. The loading on the Hemlock is compression perpendicular to grain direction. The properties of the Hemlock are taken from Ref. 18, Table 4-3b. There are 3 species of Hemlock wood published in [Ref. 18]. For this calculation, the Hemlock wood (Western Hemlock) with the strongest modulus is conservatively selected (that could produce the greatest acceleration during impact).

Specific gravity = 0.45 from [Ref. 18], Table 4-3a, 12% moisture content

Density =  $0.45 \text{ gm/cm}^3 = 0.016 \text{ lb/in}^3$

The compressive stress parallel to grain = 7200 psi

The compressive stress perpendicular to grain = 550 psi

The modulus of elasticity in the parallel to grain direction =  $1.63 \times 10^6 \text{ lbf/in}^2$ .

Normally, the modulus of elasticity in the perpendicular to grain direction takes the same reduction as the compressive stress; therefore the modulus of elasticity in the perpendicular to grain direction is:

$$E = 1.63 \times 10^6 \text{ lbf/in}^2 \times 550/7200 = 125 \times 10^3 \text{ lbf/in}^2$$

### b. POISSON'S RATIO

Per [Ref. 18], Table 4-2, the Poisson's ratio in the perpendicular to grain direction (Radial to Tangential direction) is

$$\mu_{RL} = 0.442$$

### c. EFFECT OF TEMPERATURE ON THE ELASTIC MODULUS

The same temperature effect applied to the Balsa Wood in Section A.3 is applicable to Hemlock wood. Similarly, the resulted compressive stress increase is 14% (=1.14-1) more for temperature at -40°F and 10% less (=1-0.899) for temperature at 150°F. The same temperature correction factors for the modulus of elasticity (compression perpendicular to grain) are presented in the following Table.





## Design Analyses and Calculation

Table A.5-1 Correction Factors for Compressive Strength of Hemlock Wood at extreme Temperatures

at degree C [endnote 17]		-20			150
at degree F interpolated and extrapolated	-40	-4	70	150	302
Scale from research, Ref. 8	1.61	1.55	1.42	1.27	1.00
New scale to be used in LSDYNA input	1.140	1.09	1.00	0.899	

**d. DYNAMIC EFFECT ON ELASTIC MODULUS.**

There is no published literature of experiment data on the dynamic effect on elastic modulus of Hemlock wood. The dynamic effect of Hemlock is not considered.

The Hemlock wood is modeled using \*Mat\_crushable\_foam. The strips are modeled as brick elements.

### A.6 Alumina Silicate

This is used as thermal insulator for the following applications.

Items 28, 29, 30, 31, 32, 33, 34, 35 of Inner Container Main Body Assembly (Dwg 105E3745, Rev. 8)

Items 14, 15 of inner container Lid (Dwg 105E3747, Rev 4)

Items 8, 9 of Inner Container End Lid (Dwg 105E3748, Rev 2)

**a. THE ELASTIC MODULUS AND DENSITY OF ALUMINA SILICATE**

The Alumina Silicate is used as thermal insulator; therefore there is no structural value intended for the Alumina Silicate. During the end drop orientation, the Alumina Silicate is not in the load path of the fuel bundle except its own weight. During the Horizontal Drop orientation, the Alumina Silicate blocks provide support for the fuel rod bundle and the Hemlock plates. The loading on the Alumina Silicate is compression. The density and compressive strength of the material are given in Table 2-3 of TN-B1 SAR Rev. 3.

Density = 0.25 gm/cc

Density = 0.009 lb/in<sup>3</sup>

The compressive strength = 294 kPa = 42.6 psi. A search on the internet found a commercial product provided by Zircar [Ref. 19] closely matches the density and strength of the Alumina Silicate. The product data sheet is attached in Appendix F. According to the Zircar data sheet, the compressive



N° FS1-0025122	Rev. 1.0	TEP - Technical Report	
	Page 139/177		



## Design Analyses and Calculation

strength is expressed parallel to thickness at 10% compression. Therefore the modulus of elasticity is  
 $E = 42.6 \text{ psi}/0.1 = 426 \text{ psi}$ .

### **b. POISSON'S RATIO**

There is no data available on the Poisson's ratio. Since this is a ceramic fiber material with porous interior (as demonstrated by very low density), the deformation of the ceramic material generally is uncoupled between the axial direction and the radial or tangential directions. Therefore, the use of a Poisson's ratio of  $\nu=0$  is recommended.

### **c. EFFECT OF TEMPERATURE ON THE ELASTIC MODULUS**

The ceramic material is suitable for extreme high temperature service up to 2600°F. The mechanical strength is not expected to change significantly between -40°F and 150°F. Therefore, the material property remains constant for this calculation.

### **d. DYNAMIC EFFECT ON ELASTIC MODULUS.**

There is no published literature of experiment data on the dynamic effect on elastic modulus of alumina silicate. Therefore, the dynamic effect of alumina silicate is not considered.

The alumina silicate is a ceramic fiber with a rigid outer surface and unbound interior space. It is modeled in LSDYNA using material model Crushable\_Foam. Since the material is loaded to less than 10% strain, it behaves elastically in this container application.

## **A.7. Polyethylene Foam**

This is used as shock absorber for the following applications.

- Items 36, 37, 38, 39, 40, 41 of Inner Container Main Body Assembly (Dwg 105E3745, Rev. 8)
- Item 16 of Inner Container Lid (Dwg 105E3747, Rev 4)

### **a. THE LOAD-DEFLECTION CURVE AND DENSITY OF POLYETHYLENE FOAM**

The density and compressive strength of the material are given in AREVA FS1-0014159 TN-B1 Rev. 3 [Ref. 7], Table 2-3.

Specific gravity = 0.144


Density =  $0.068 \text{ gm/cm}^3 = 0.00246 \text{ lb/in}^3 = 4.3 \text{ PCF}$

This is the Type III material specified in [Ref. 20].

Per AREVA FS1-0021899 Rev. 1, Section 3.5, the compressive strength is 0.2MPa at 50% strain.

		Page A50 of A55
--	--	-----------------



N° FS1-0025122	Rev. 1.0	TEP - Technical Report	
	Page 140/177		



## Design Analyses and Calculation

$$\sigma_{50\%}=0.2\text{MPa}=29\text{ psi}$$

Per Ref. 13, for the Type III foam (4 PCF), the average compressive strength at 25% strain is 16 psi.

$$\sigma_{25\%}=16\text{ psi}$$

This material is modeled using LSDYNA material model crushable\_foam in the calculation.

### b. POISSON'S RATIO

There is no data available on the Poisson's ratio. Since this is a foam material with porous interior (as demonstrated by very low density), the material deformation is generally uncoupled between the axial direction and the radial or tangential directions. Therefore, the use of a Poisson's ratio of  $\nu=0$  is recommended.

### c. EFFECT OF TEMPERATURE ON THE ELASTIC MODULUS

The mechanical strength is not expected to change significantly between -40°F and 150°F. Therefore, the material property remains constant for this calculation.

### d. DYNAMIC EFFECT ON ELASTIC MODULUS

Based on a test sample of 50 mm thick x 125 mm x 125mm to ASTM D1596 standard [Ref. 21], the Load-Deflection curve of the dynamic cushioning properties for the Type III foam taken from Figure 2 of [Ref. 20] is shown in the figure below.

		Page A51 of A55
--	--	-----------------





Design Analyses and Calculation

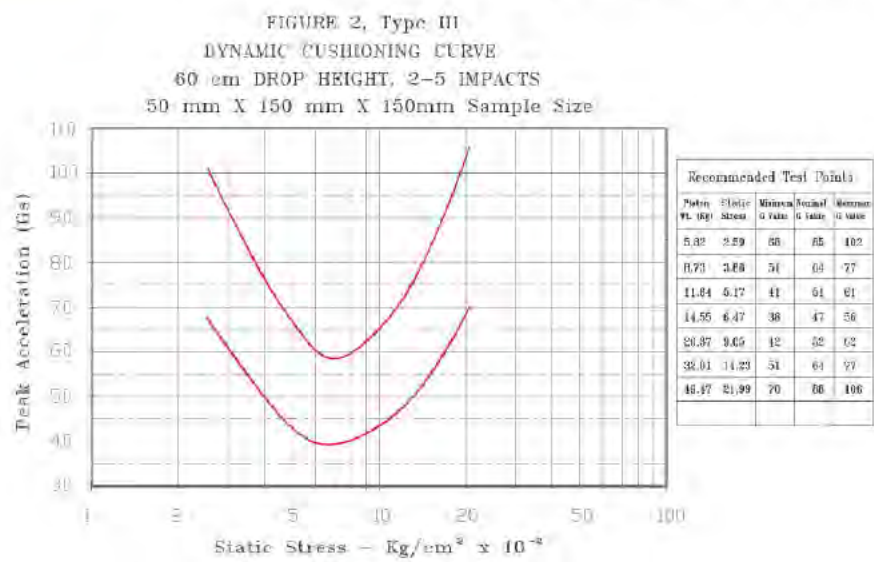


Figure A.7-1 Dynamic Cushioning Curve for Polyethylene, Type III

According to the test procedure described in [Ref. 22], the shock performance of cushion materials is measured using instrumented impacts resulting in a cushion curve such as that shown in Figure A.7-1. The cushion curve describes the level of deceleration transmitted through a given thickness of material as a function of static stress (loading) on the cushion and the drop height.

Procedures for running a cushion curve are covered by ASTM D1596, D4168, and similar MIL Specs. They are basically a matter of dropping a guided platen of predetermined mass onto a cushion of known thickness and area from a given drop height. The amount of deceleration transmitted through the cushion is measured by an accelerometer mounted on the platen or test block. The results are displayed on an oscilloscope or similar readout device.

The procedure results in cushion curves, such as those in Figure 7.3.7-1, with peak deceleration on the vertical axis and static stress on the horizontal axis (static stress = weight/bearing area). Each curve should be drawn from a minimum of 5 test points (static stress levels) and each test point is the average of the last 4 of 5 (the first impact data point is discarded. The average of No 2 to No 5 impacts as indicated on the above figure) deceleration readings from the cushion material. Most cushion curves have the general shape of those in Figure 7.3.7-1 above. The left-hand portion of the curve shows a relatively high deceleration transmitted through the cushion. In this area the static stress is relatively low because of the light weight on the cushion; the object (the platen in the cushion test) does not have sufficient force to deflect the cushion and the result is a rigid or "stiff" impact. The effect resembles dropping a product onto a rigid surface. In the center portion of the curve (where the cushion is being used effectively), the falling object has sufficient force to deflect the cushion and





## Design Analyses and Calculation

cause the deceleration to be spread over a longer period of time. The result is a lower deceleration level. On the right-hand portion of the curve, the cushion material is being overloaded and the falling object continues right through the cushion (it bottoms out) and impacts with the surface on which the cushion is resting. Thus, it approaches using no cushion at all resulting in, once again, high deceleration levels. It is desirable to use the cushion in the lower portion of the curve where its performance is optimum. When the product limiting acceleration, weight and design drop height are known, the usable range of cushion area can be determined for a given cushion material and thickness.

Assuming the Load-deflection curve of the cushion is linear; using the formula in Page 10 of [Ref. 22], the deflection of the cushion can be calculated as follows.

$$X = 2 \times H / (G - 2) \quad \text{Equation (a)}$$

Where:

X = cushion dynamic deflection in cm (or inches)

H = drop height in cm (or inches) = 60 cm

G = the require deceleration level (G's)

Remember that this exercise gives the theoretical dynamic deflection necessary, not the overall cushion thickness. In general, cushion materials such as expanded polystyrene and polyethylene foam will compress approximately 40 to 70% of their total thickness before "bottoming out" starts to occur. More flexible materials such as polyurethane foam will compress up to 80% of total thickness before beginning to bottom out.

A typical compressive Load-Deflection curve for the polyethylene foam taken from [Ref. 23] is shown in the figure below.

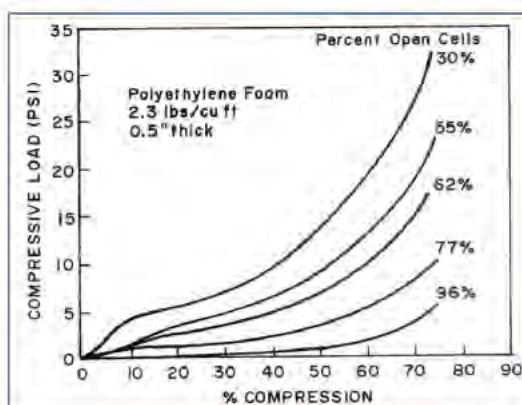


Figure A.7-2 Compressive Load Versus Compression of Different Fraction Open Cells.





## Design Analyses and Calculation

The data table in Figure A.7-1 is processed into the table below.

**Table A.7-1 Dynamic Drop Test Data Processed**

1	2			3			4			5		
	g value			Stress from g value, psi			Deflection, cm Based on Equation (a)			Volumetric Strain based on Deflection		
Platen Wt (kg)	Min	average	Max	Min	average	Max	Min	average	Max	min	average	max
5.82	68.0	85.0	102.0	36.03	45.03	54.04	1.8	1.4	1.2	0.364	0.289	0.240
8.73	51.0	64.0	77.0	40.53	50.86	61.19	2.4	1.9	1.6	0.490	0.387	0.320
11.64	41.0	51.0	61.0	43.44	54.04	64.63	3.1	2.4	2.0	0.615	0.490	0.407
14.55	38.0	47.0	56.0	50.33	62.25	74.17	3.3	2.7	2.2	0.667	0.533	0.444
20.37	42.0	52.0	62.0	77.88	96.42	114.96	3.0	2.4	2.0	0.600	0.480	0.400
32.01	51.0	64.0	77.0	148.61	186.49	224.37	2.4	1.9	1.6	0.490	0.387	0.320
49.47	70.0	88.0	106.0	315.23	396.28	477.34	1.8	1.4	1.2	0.353	0.279	0.231

In the above table, data in column No. 1 and 2 are taken directly from the data table in Figure A.7-1.

The stress in column No. 3 is calculated based on the formula below.

$$\sigma = \text{Force/area}$$

Where

$$\text{Force} = m \times G$$

m = mass of platen, given in data table of Figure A.7-1

G = acceleration given in data table of Figure A.7-1

$$\text{Area} = \text{surface area of polyethylene foam} = (12.5 \text{ cm} \times 12.5 \text{ cm} = 24.2 \text{ in}^2)$$

The data in column No. 4 are derived from equation (a), where the height is H=60 cm.

Note that It is desirable to design with the cushion in the lower portion (where the stresses are lower) of the curve in Figure A.7-1 where its performance is optimum. Based on the average stresses in the above table (rows No. 2, 3, 4) and the PolyPlank [Ref. 24] specification at 25% strain, the load-deflection curve is tabulated below. The stress value beyond strain level of 0.522 is the best-guess value from the drop test data. According to the material description provided by vendor, Polyethylene foam is a resilient material that has very little degradation with repeated impacts.





## Design Analyses and Calculation

**Table A.7-2 Load Deflection Data for LSDYNA Analyses**

Strain	Stress, psi
0.000	0.0
0.250	23.0
0.387	50.9
0.490	54.0
0.533	62.3
0.600	90.0
0.75	200.0

The Load-Deflection data in the above table is plotted as follows; which is similar to the Figure A.7-2.

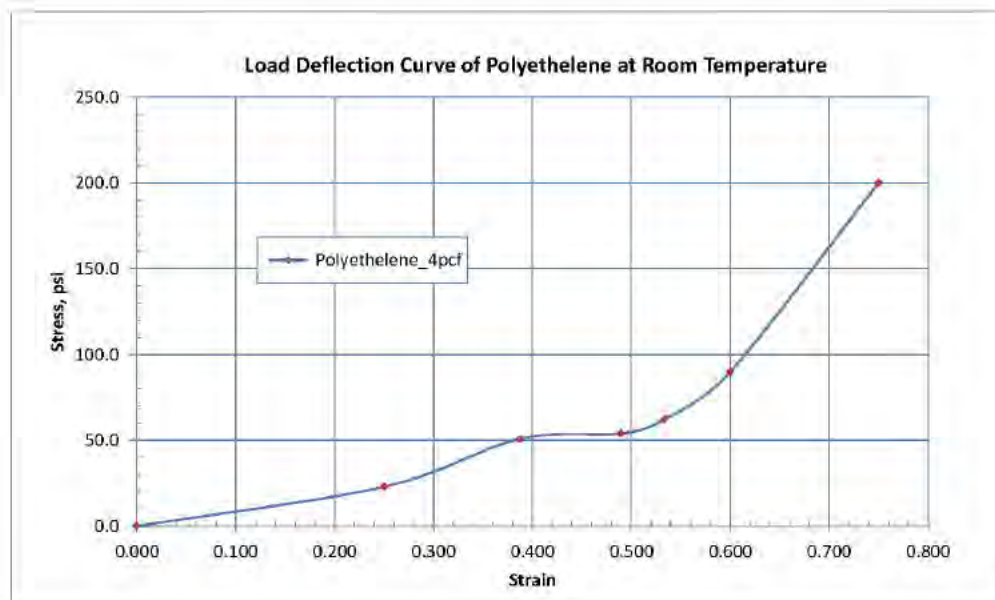


**Figure A.7-3 Load-Deflection Curve used for the LSDYNA input.**



N° FS1-0025122	Rev. 1.0	TEP - Technical Report	
	Page 145/177		



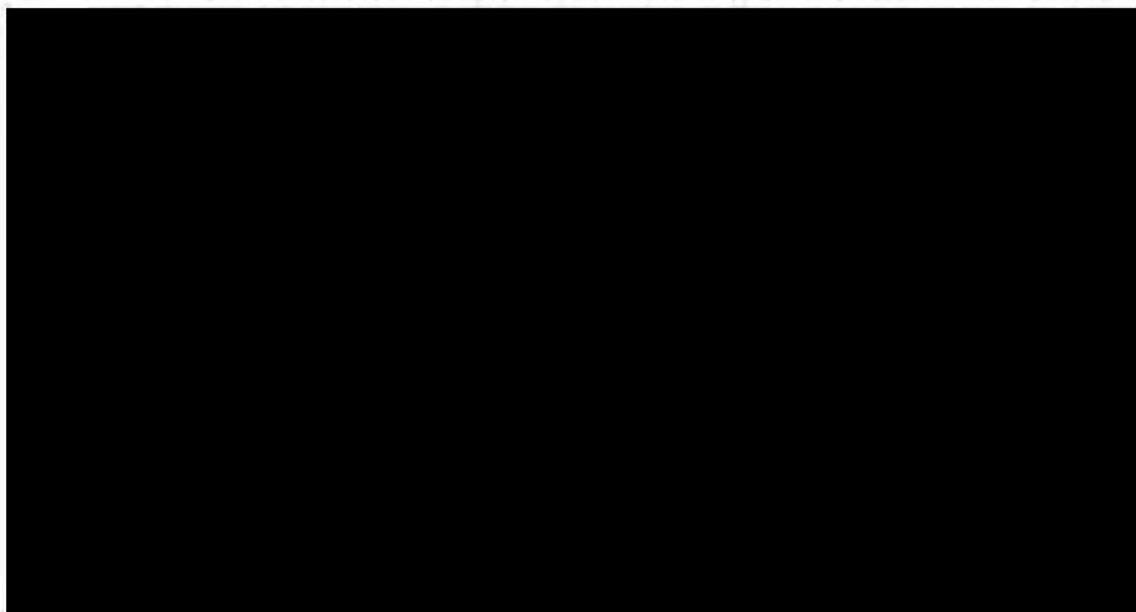
## Design Analyses and Calculation

### Appendix B Reconfirmation of ATRIUM-11 Fuel Assembly Structural Integrity

#### B.1 Introduction

As reported in [Ref. 2], the ATRIUM-11 fuel assembly can withstand the 30ft-drop impact using the accelerations measured at the inner container shell of the CTU taken from the drop test [Ref. 1] which was performed at room temperature condition. The structural integrity and plastic stability of the fuel assembly is confirmed by subjecting the fuel assembly to amplified, factored (140%) peak accelerations of the actual drop test. This procedure established that the minimum factor of safety for the fuel assembly is greater than 1.4.

When the ambient temperature drops below room temperature, the stiffness of the impact-absorbing material in the TN-B1 container become greater. The change in stiffness at lower temperature for the stainless steel in the container shell is insignificant. Under the cold temperature condition, when the container is dropped from the 30-ft height during the transportation accident, the acceleration experienced by the inner container and the fuel bundle become greater than that occurred during a room temperature drop condition. With lighter payload, the inner container acceleration becomes even greater. As reported in the main text of this report, the bounding accelerations of the drops occur at cold temperature are tabulated below and compared with the measured acceleration for drops performed at room temperature. The acceleration for corner drop is not included because it is bound by that of the end drop and Horizontal Drop configuration. The accelerations for hot temperature drops are not considered because they are bound by that of the cold temperature drops.



		Page B1 of B9
--	--	---------------



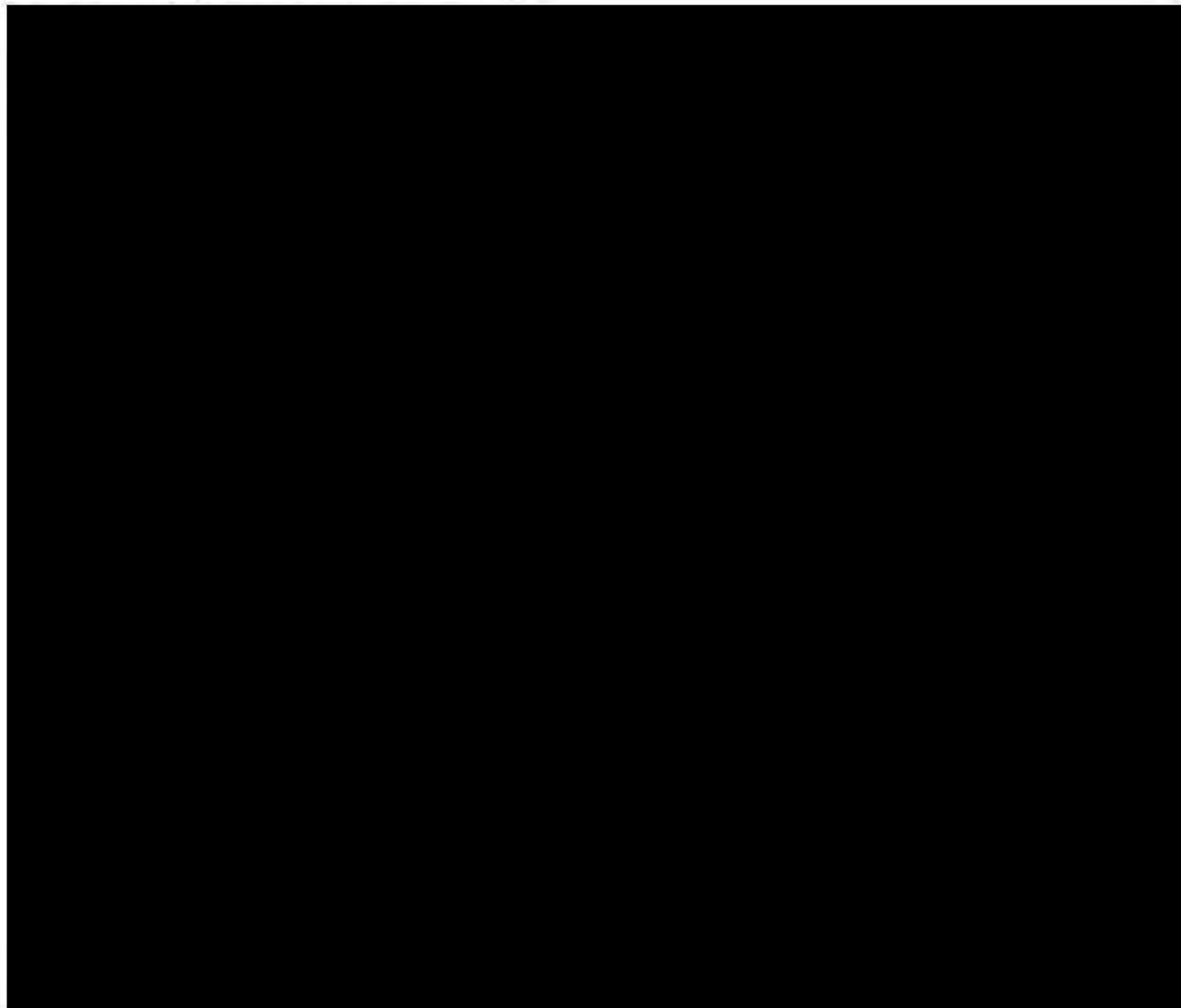


## Design Analyses and Calculation

Table B.1-2 Designation of Analysis Drop Cases for Fuel Assembly Evaluation

Case ID	Corresponding Drop Case	Drop Orientation
HAC-FA1	HAC14	HAC free drop, Vertical Bottom End
HAC-FA2	HAC16	HAC free drop, 15° shallow angle off Horizontal Drop on Lid

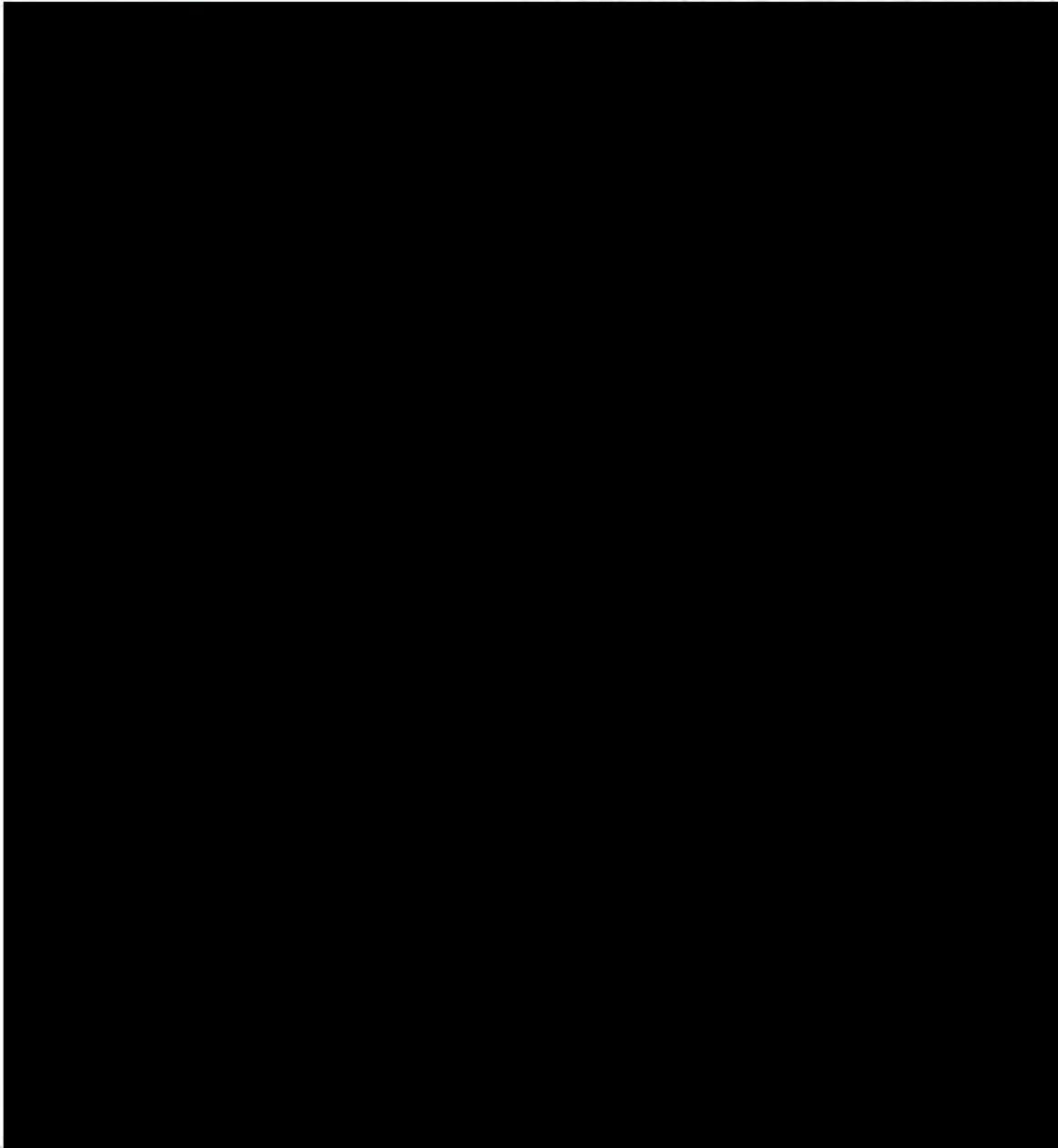
### B-2 Amplified Acceleration Time Histories





**ATKINS**

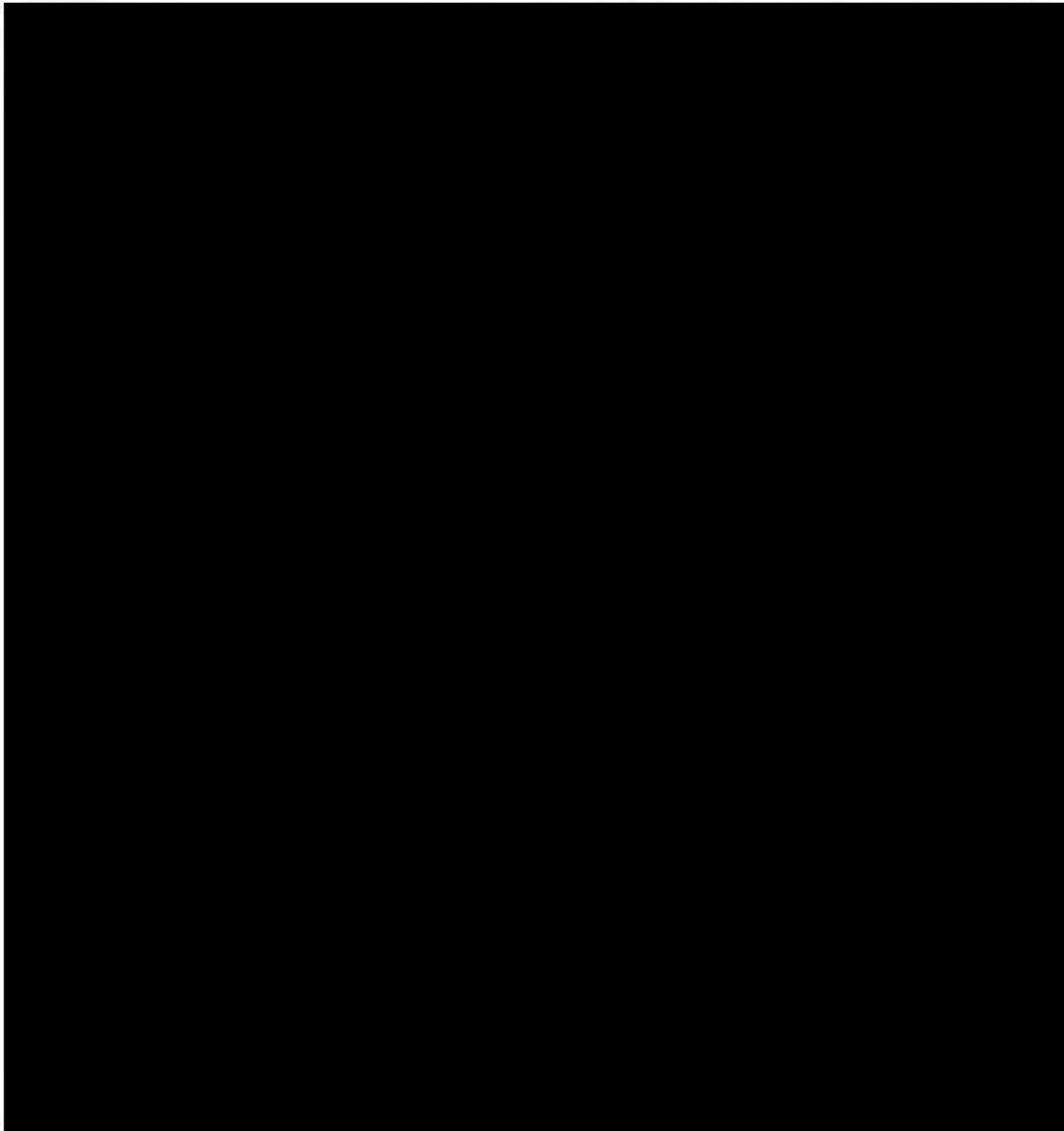
## Design Analyses and Calculation





**ATKINS**

## Design Analyses and Calculation





### ***B.3 Acceptance Criteria***

The fuel cladding is the containment boundary. The ultimate strain of the cladding material Zircaloy is 16% as listed in Section 7.3.1. Therefore, the criteria for plastic stability are described below.

- (1) The plastic strain of the cladding material does not exceed the ultimate strain to prevent breach of the containment boundary.
- (2) There is neither gross deformation of the fuel rods nor localized structural collapse of the fuel bundle array.

### ***B.4 Finite Element Models***

The finite element models of the fuel assembly to resist end drop is shown in Figure B.4-1 below. The fuel assembly model is the same model as described in [Ref. 2]. Below the (Lower Tie Plate) LTP of the fuel assembly are the hemlock wood and the Alumina Silicate plates that are inside the inner container. The rigid plane represents the inner container end shell where the acceleration is measured from the container drop analyses.

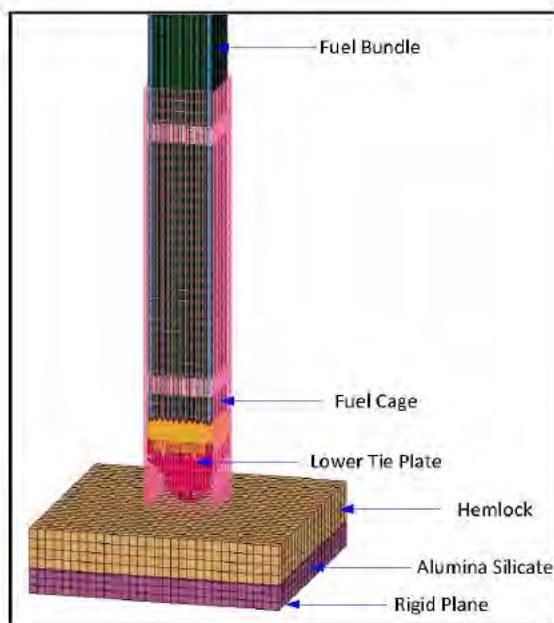


**Figure B.4-1 FEM Model of the Fuel Assembly for the Plastic Stability Evaluation against End Drop Impact**





## Design Analyses and Calculation

For the Horizontal Drop analysis, partial view of the finite element model is shown in Figure B.4-2 below. This is the same FEM model described in [Ref. 2]. The cushioning material of hemlock wood and the Alumina Silicate plates are conservatively ignored in the model.

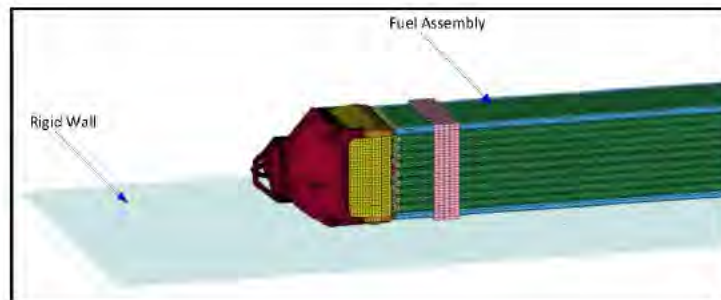
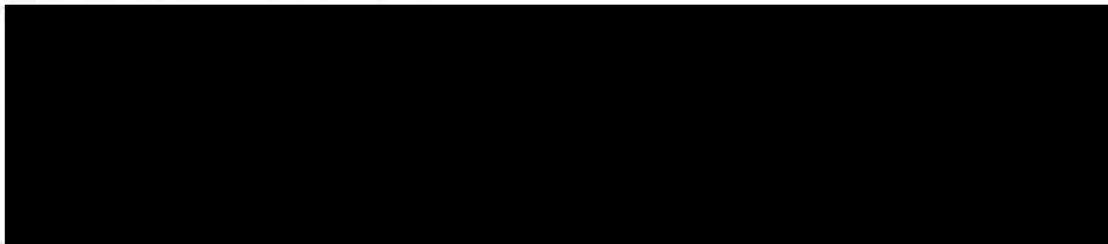


Figure B.4-2 FEM Model of the Fuel Assembly Plastic Stability Evaluation against the Horizontal Drop impact.

### B.5 Plastic Stability Evaluation Results





**ATKINS**

**Design Analyses and Calculation**

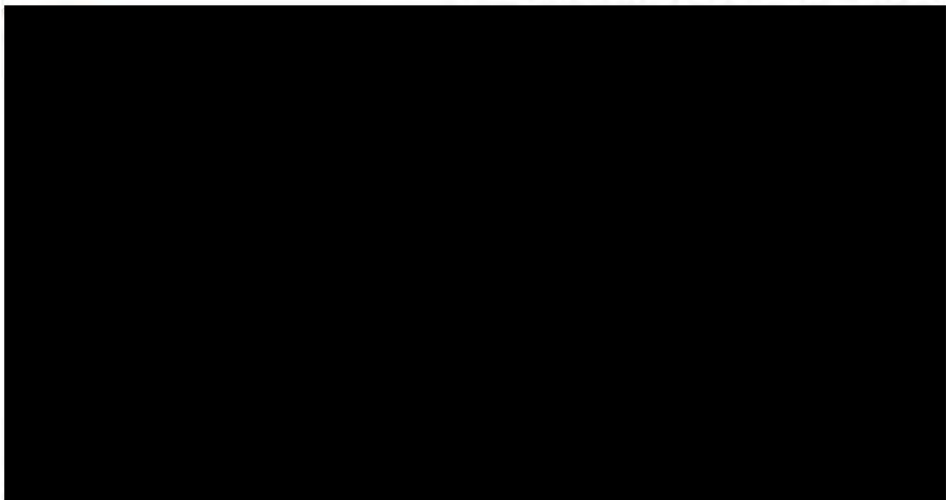


Figure B.5.1-1 Plastic Strain of the Fuel Assembly after 30-ft End Drop Accident, Case HAC-FA1

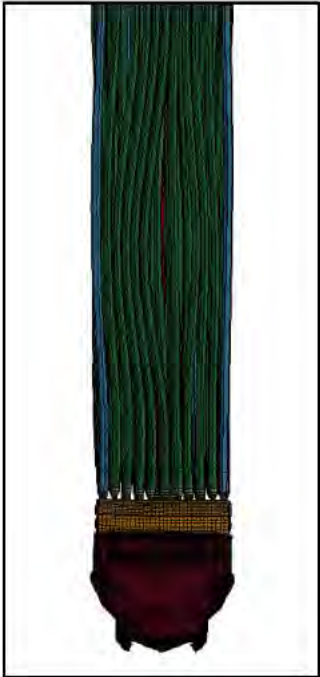
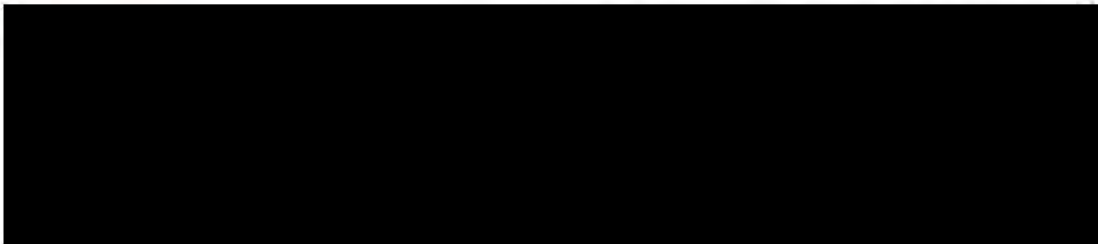


Figure B.5.1-2 Deformation of the Fuel Assembly and LTP after 30-ft End Drop Accident, Case HAC-FA1





Design Analyses and Calculation





**ATKINS**

## Design Analyses and Calculation

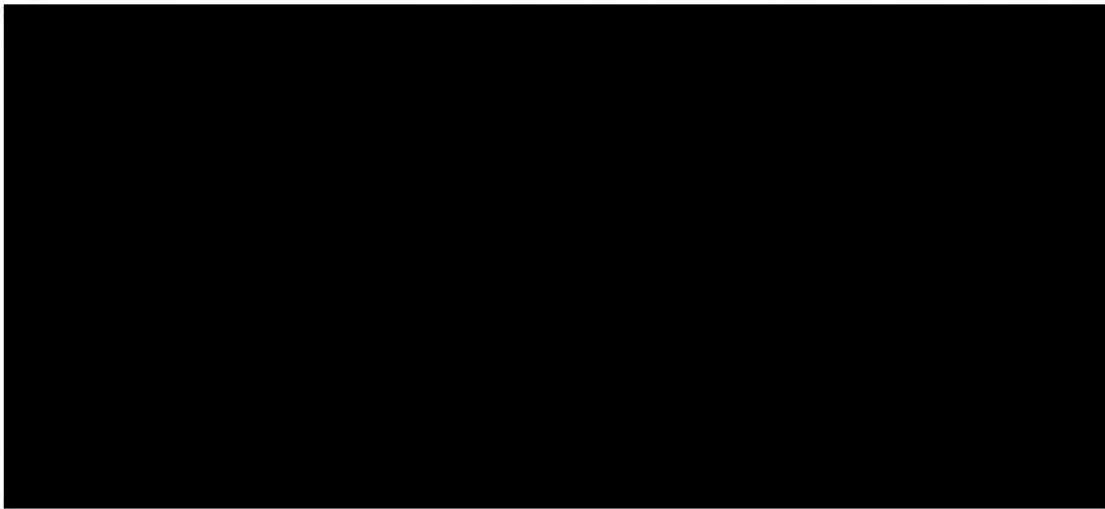


Figure B.5.2-2 Deformation of the Fuel Assembly near the Handle, 30-ft Horizontal Drop Accident, Case HAC-FA2

### ***B.6 Fuel Assembly Structural Stability Conclusion***

From the above observation, it can be concluded that under the cold temperature condition, with the greater impact accelerations and lighter fuel load, the fuel assembly maintains a factor of safety of 1.4 against plastic instability.



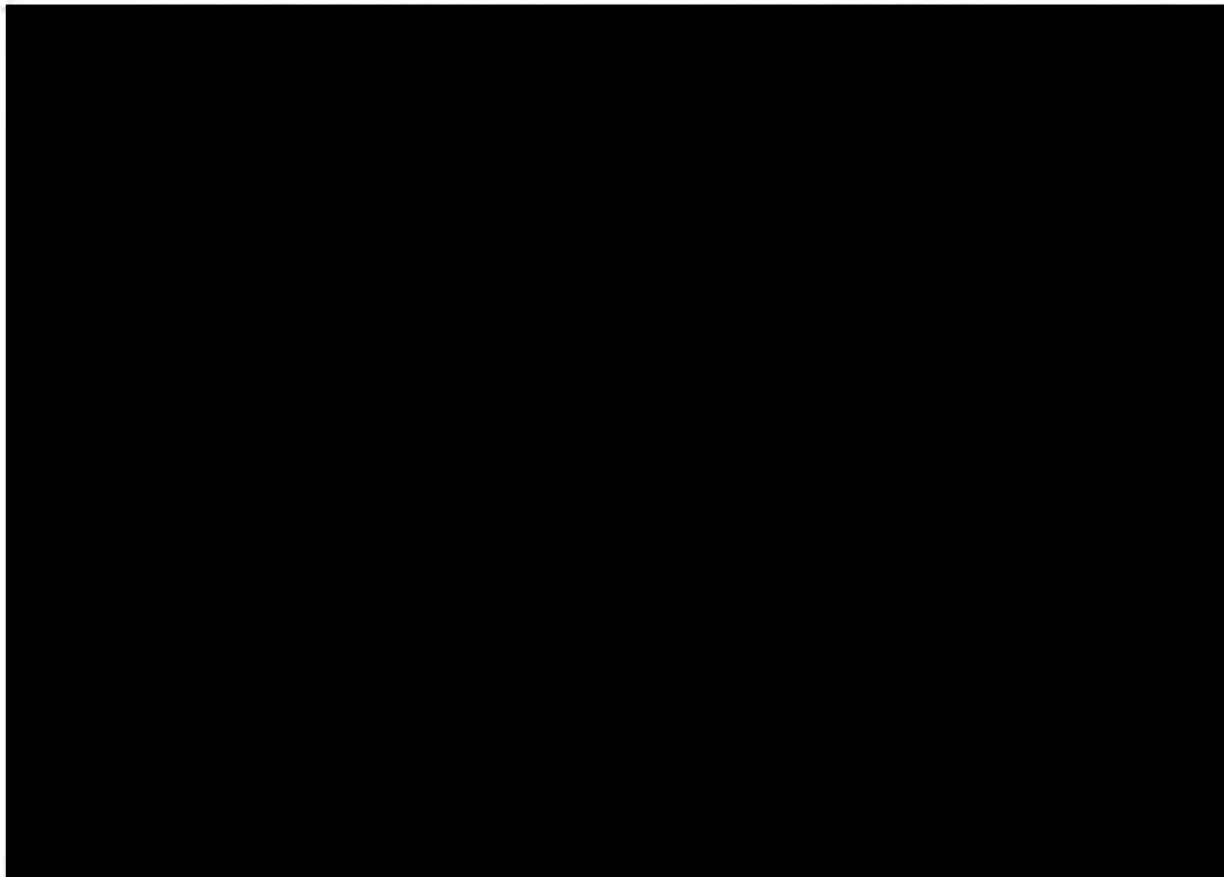


## Design Analyses and Calculation

### APPENDIX C. Shipping with A Single Fuel Assembly in the TN-B1 Container

#### C.1. Introduction

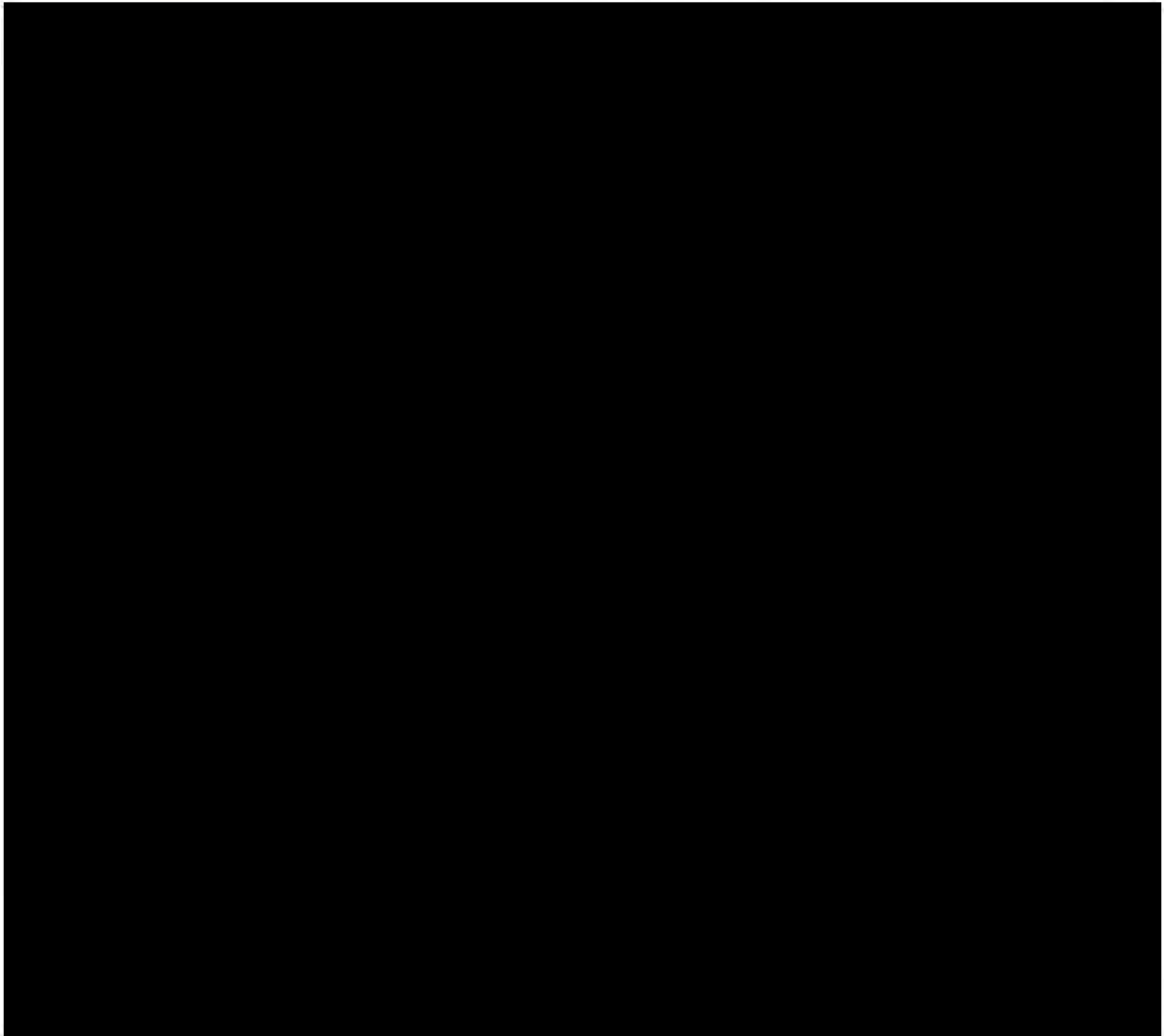
The total weight of the TN-B1 container with payload in the drop simulation [main report] is 1614 kg. The weight of the ballast simulating the two fuel bundle is 684 kg. The weight of the TN-B1 container is 930 kg. It is based on the assumption that the TN-B1 container is fully loaded that the LSDYNA simulation of the accident drops of the fuel bundle is performed as reported in the main report. According to Appendix B of Ref. 2, the TN-B1 container (2050 pounds) may be shipped with one fuel assembly (584 pounds) and one other component with a minimum weight of 65 pounds. When the TN-B1 container holds the reduced weight, the dynamic behavior of the shipping container is altered and the effects on the peak acceleration is determined and reported in this appendix.





**ATKINS**

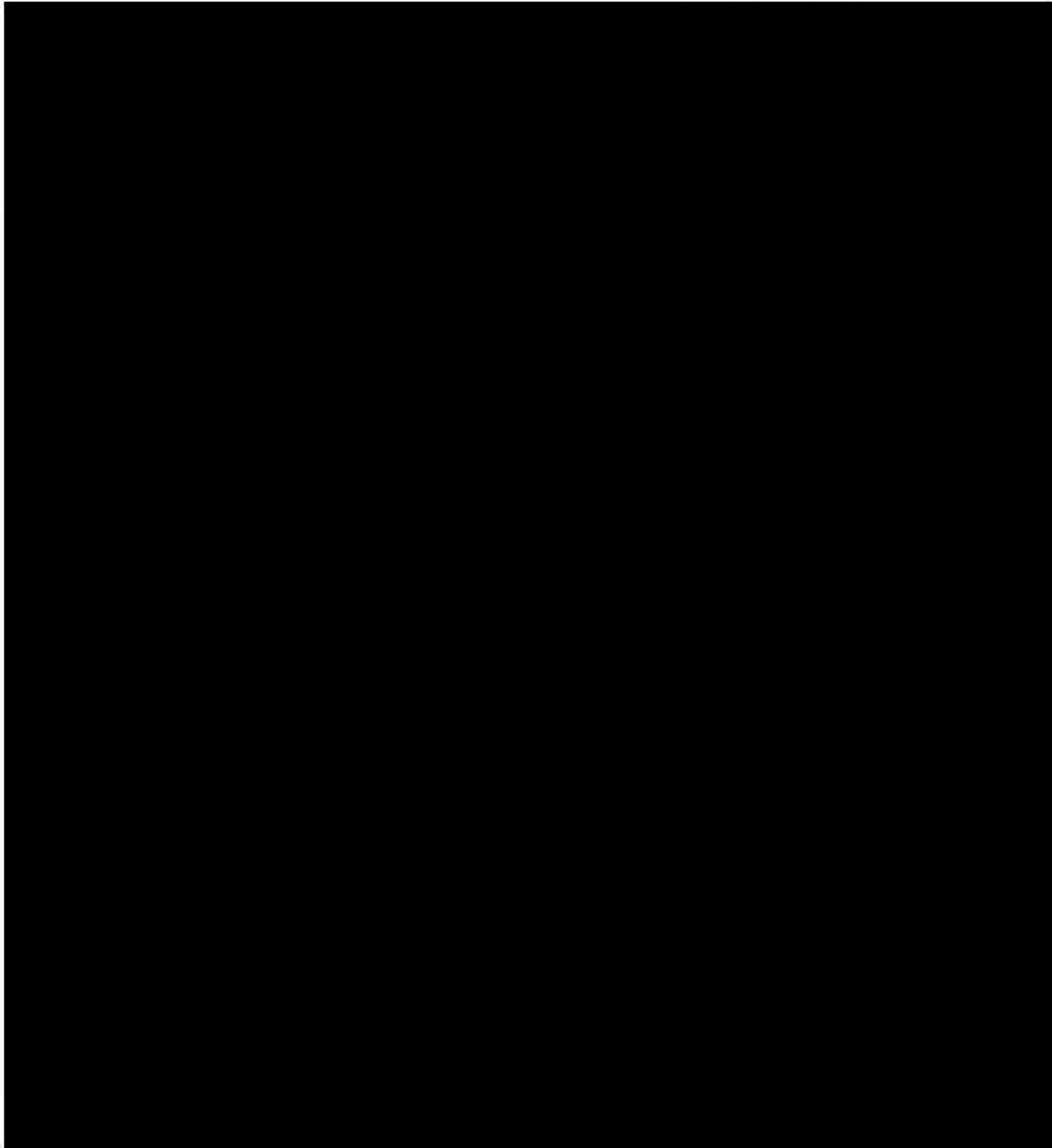
## Design Analyses and Calculation





**ATKINS**

## Design Analyses and Calculation

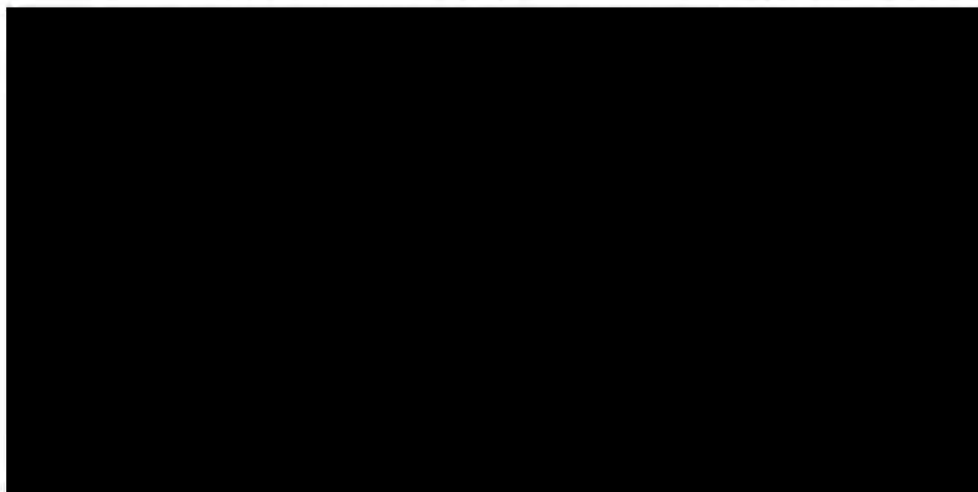






## Design Analyses and Calculation

Figure C.2-1 Acceleration Time History Input to the Bottom End Drop Case HAC-SFA1



### **C.3 Acceptance Criteria**

The fuel cladding is the containment boundary. The ultimate strain of the cladding material Zircaloy is 16% as listed in Section 7.3.1. Therefore, the criteria for plastic stability are the same as described in Appendix B.

### **C.4 Finite Element Models**

The finite element models for this plastic stability evaluation for single fuel bundle consist of the fuel assembly impacting on a rigid plane. The model for the fuel assembly is the same model described in [Ref. 2]. There is no cushioning material in the model. For the end drop analysis, the finite element is shown in Figure C.4-1 below.



**ATKINS**

## Design Analyses and Calculation

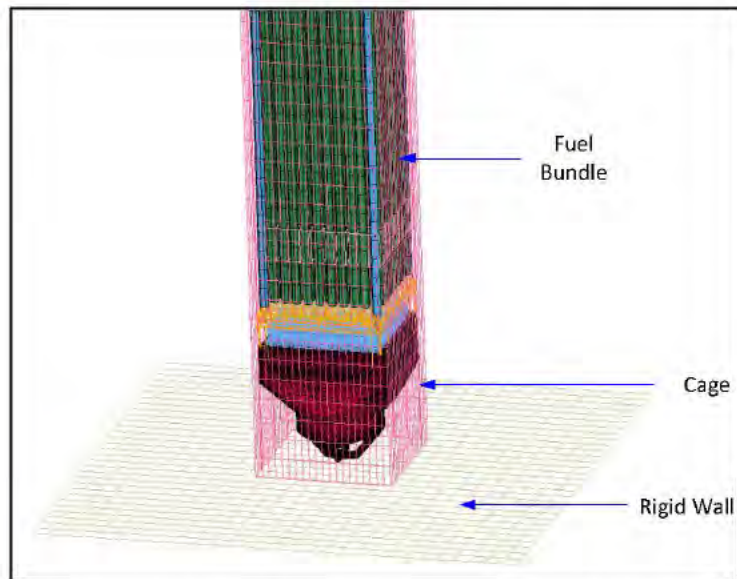


Figure C.4-1 Finite element model for the 30-ft end drop impact of a single fuel bundle, Case HAC-SFA1.

For the Horizontal Drop analysis, the finite element is shown in Figure C.4-2 below.

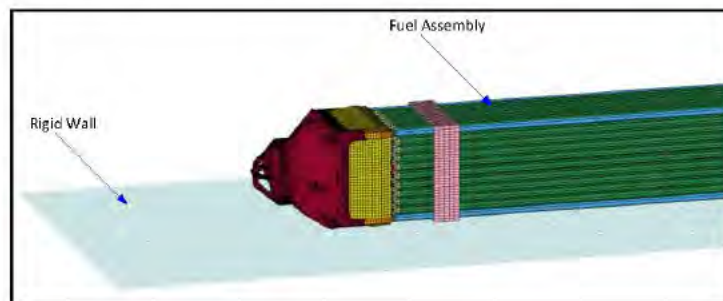


Figure C.4-2 Finite element model for the 30-ft Horizontal Drop impact of a single fuel bundle, Case HAC-SFA2.

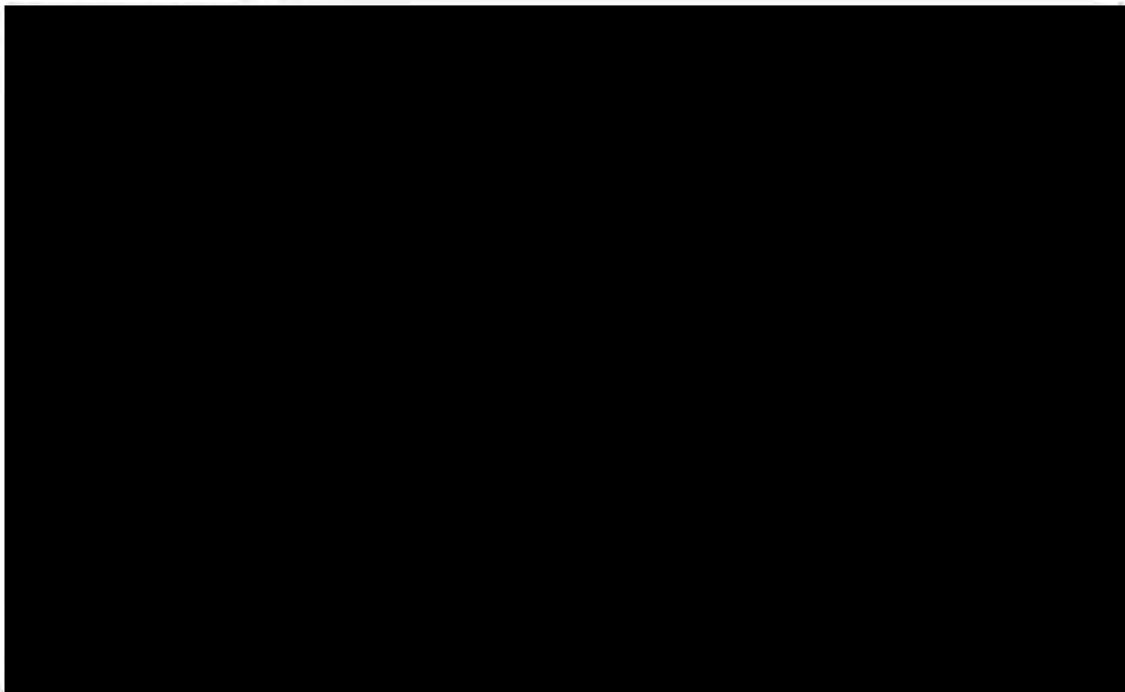




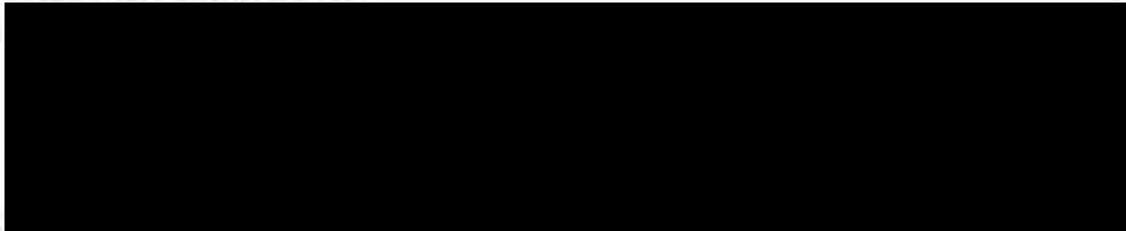
Design Analyses and Calculation

C.5 Plastic Stability Evaluation Results

C.5.1 End Drop Evaluation



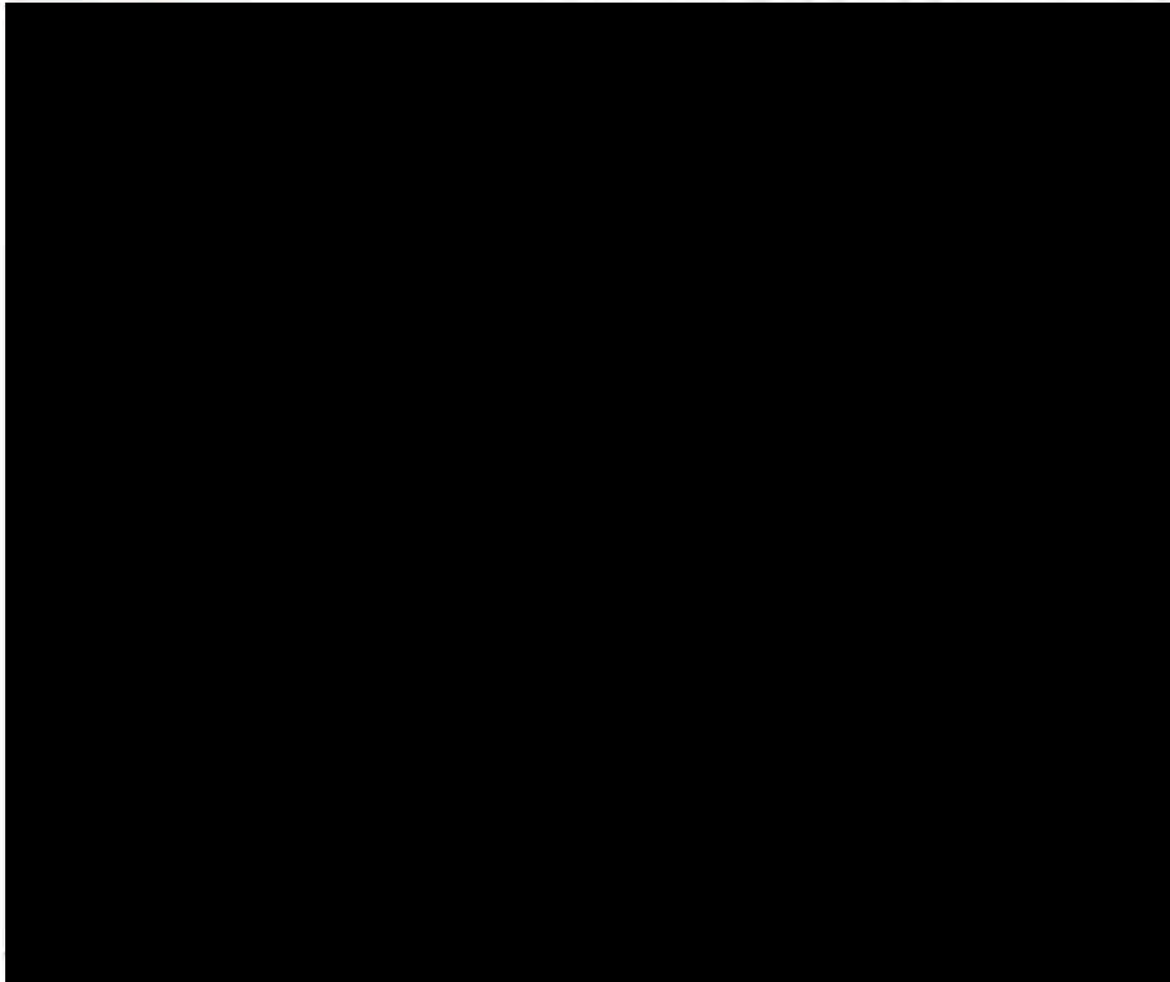
C.5.1 Horizontal Drop Evaluation







## Design Analyses and Calculation



### ***C.6 Fuel Assembly Structural Stability Conclusion***

From the above observation, it can be concluded that under the cold temperature condition, with the greater impact accelerations due to the very light weight of a single fuel bundle, the fuel assembly still maintains a factor of safety of 1.4 against plastic stability.





## Design Analyses and Calculation

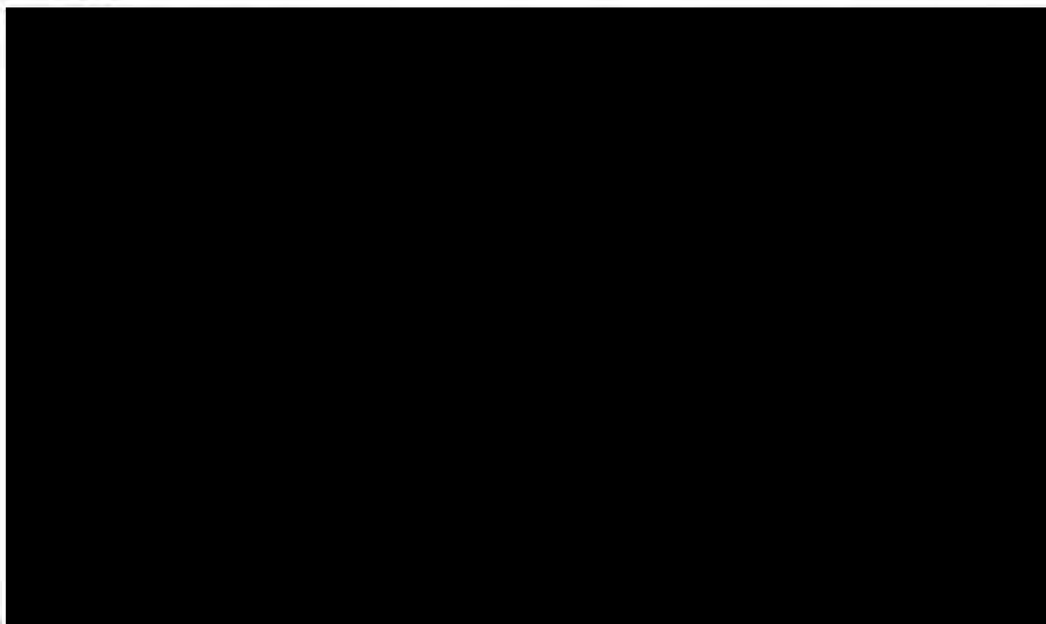
### APPENDIX D Pin Puncture Evaluation

#### D.1 Code Requirements

10 CFR Part 71.73 (3) requires that a free drop of the specimen through a distance of 1 m (40 in) in a position for which maximum damage is expected, onto the upper end of a solid, vertical, cylindrical, mild steel bar mounted on an essentially unyielding, horizontal surface. The bar must be 15 cm (6 in) in diameter, with the top horizontal and its edge rounded to a radius of not more than 6 mm (0.25 in), and of a length as to cause maximum damage to the package, but not less than 20 cm (8 in) long. The long axis of the bar must be vertical. The drop case is designated as Case HAC-PIN1.

#### D.2 Pin Puncture Analysis Methodology

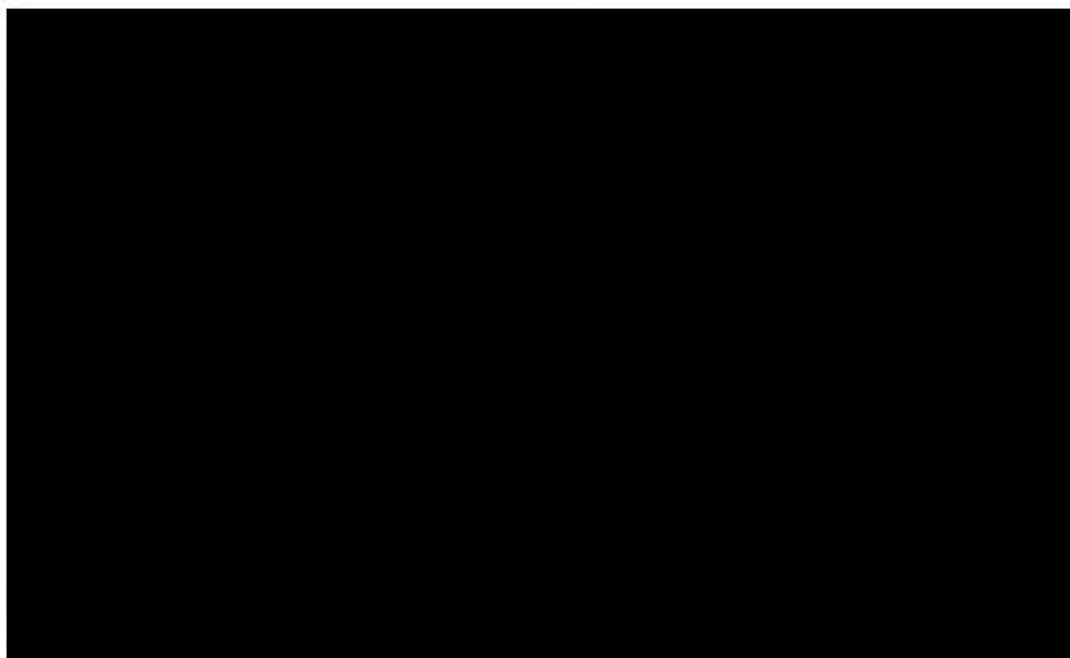
A single "worst-case" 30-ft free drop is required by 10CFR 71.73(c)(1). The pin puncture is evaluated at elevated ambient temperature of 150°F, where the stiffness of the packaging material is the lowest. As shown in Figure D2-1 below, a rigid plane with 25-degree from the horizontal and a rigid pin of 6-in diameter with 8-in long erected in the vertical direction are created for the sequential drops of (a) 30-ft drop of the package with the lid down followed by (b) a 40-in vertical drop on the pin with the lid at 25-degree from horizontal. The orientation of the lid after first impact is the drop orientation with the maximum damage [Ref. 7, Section 2.7.3]. The finite element model is shown with a cross-sectional view.







## Design Analyses and Calculation



### ***D.3 Puncture and Penetration Results.***

Figure D.3-1 and D.3-2 below show the package before and after the impact respectively. The pictures demonstrate that the absence of the rigid plane at the beginning of the secondary impact (pin puncture).

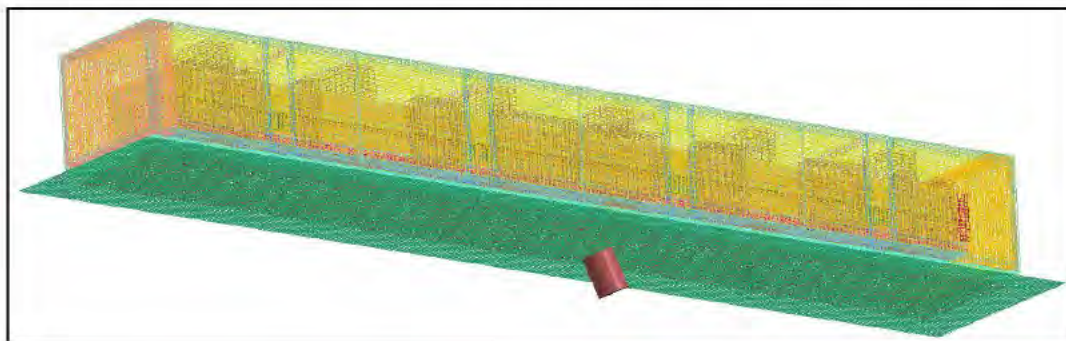


**Figure D.3-1 Package Before the 30-ft impact**



**ATKINS**

**Design Analyses and Calculation**

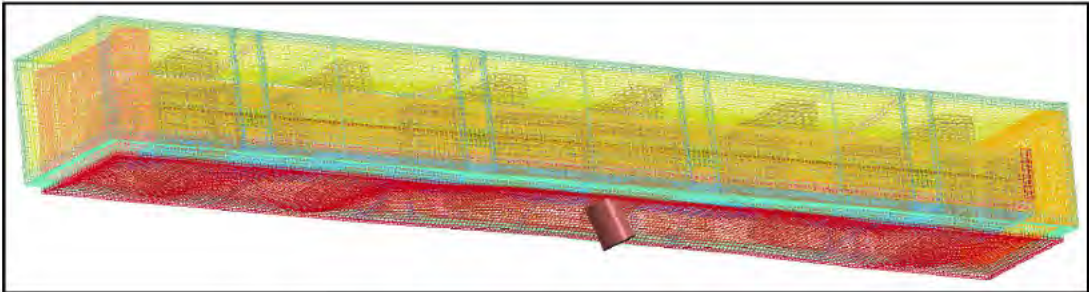


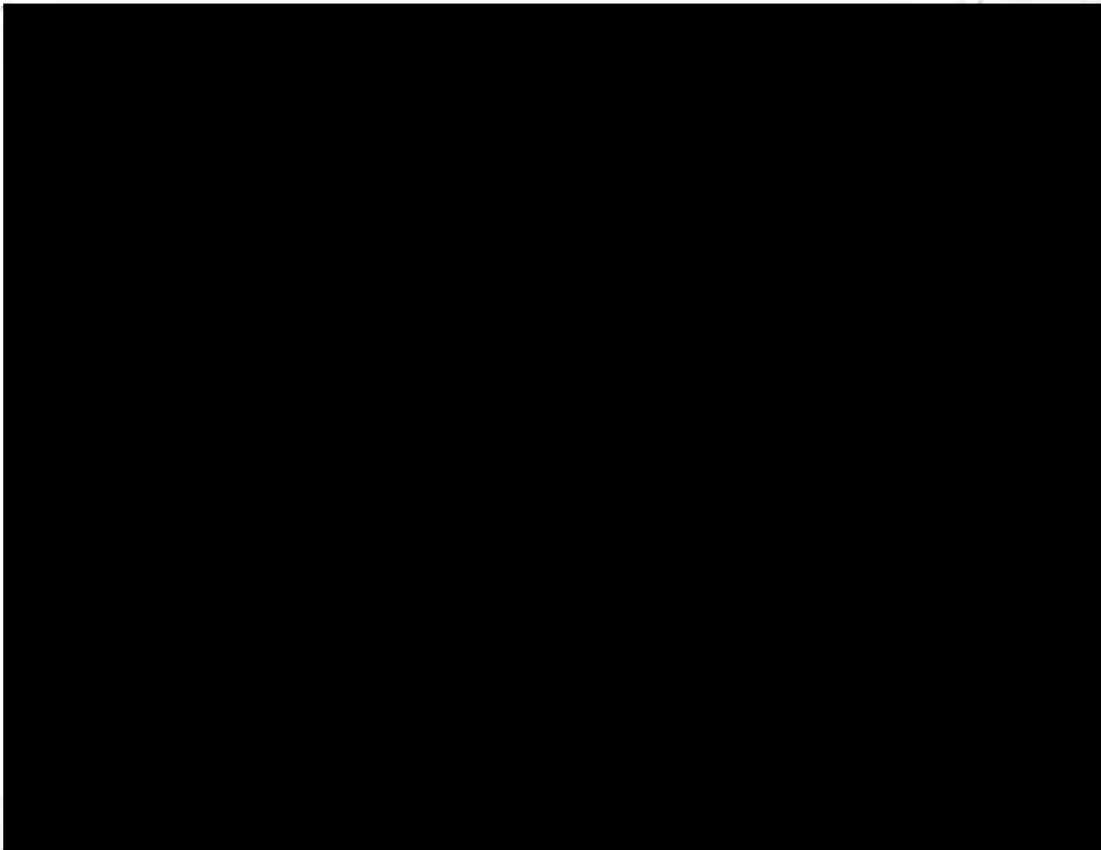
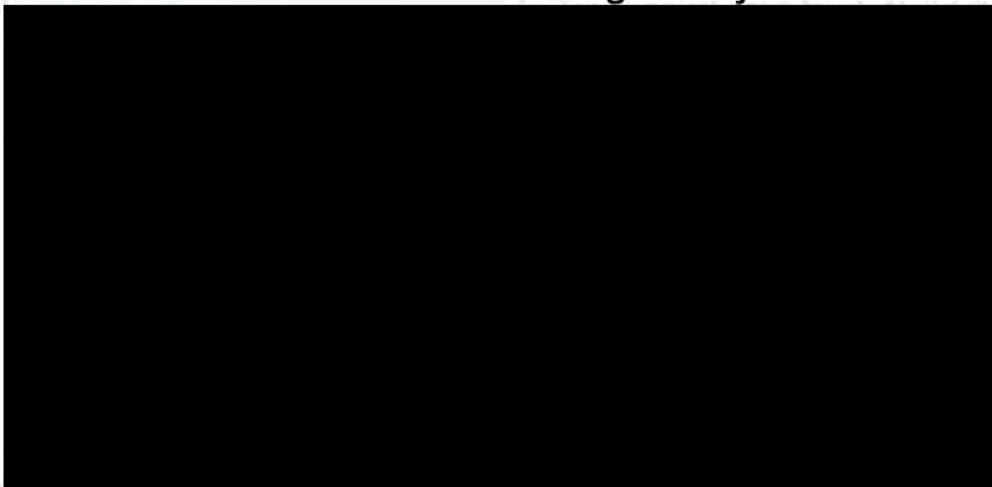
Figure D.3-2 Package After the 30-ft Impact and Pin Puncture







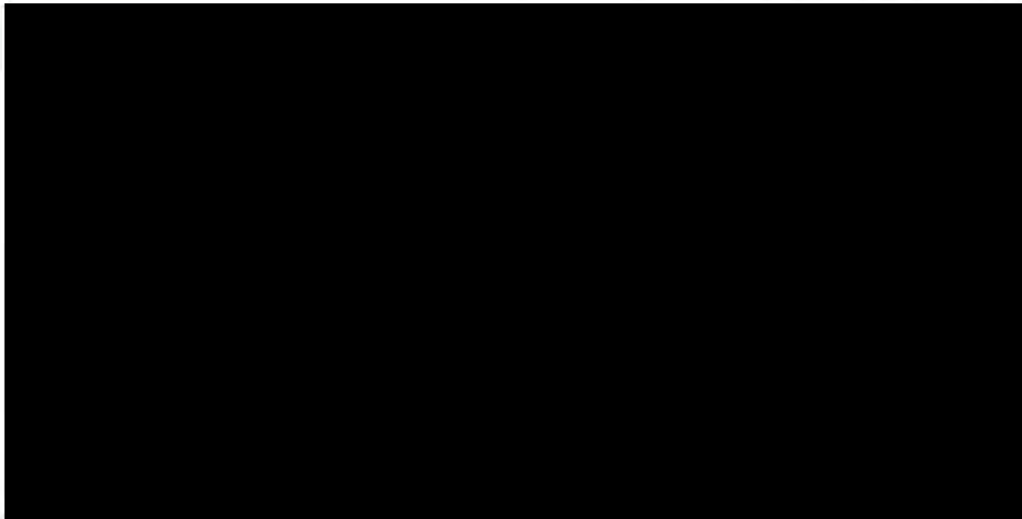
Design Analyses and Calculation







## Design Analyses and Calculation



### ***D.4 Conclusion of Pin Puncture***

The puncture pin did not penetrate the outer container. It deformed the lid inward and it contacted the inner container lid and deformed it a small amount. The outer lid total deformation was less than 4.7 inches and the inner container lid deformed less than 0.6 inches.





## Design Analyses and Calculation

### APPENDIX E Listing of Input Files

The input files for the analysis are listed in this section and stored on the DVD. For each of the drop case, the folder name, file name, and the simple description of the file are listed.

**Table E-1. LSDYNA Input Files, Normal Conditions of Transport**

NCT01 Top End Drop -40°F		
\end2\normal_n40	Run file	Run_end_2_m13a_n40_normal.dyn
	Geometry file	Top_end_drop2_geom13.dyn
	Material file	Matprop-40a_1614_m13.dyn
	Node constraint file	Constrainlid.dyn
NCT02 Bottom End Drop -40°F		
\end1\normal_n40	Run file	Run_end_1_m13a_n40_normal.dyn
	Geometry file	Bot_end_drop1_geom13.dyn
	Material file	Matprop-40a_1614_m13.dyn
	Node constraint file	Constrainlid.dyn
NCT03 Horizontal Drop on Lid -40°F		
\side3\normal_n40	Run file	Run_side_3_m13a_n40_normal.dyn
	Geometry file	Side_drop3_geom13.dyn
	Material file	Matprop-40a_1614_m13.dyn
	Node constraint file	Constrainlid.dyn
NCT04 Horizontal Drop on Side -40°F		
\side2\normal_n40	Run file	Run_side_2_m13b_n40_normal.dyn
	Geometry file	Side_drop2_geom13.dyn
	Material file	Matprop-40a_1614_m13.dyn
	Node constraint file	Constrainlid.dyn

**Table E-2. LSDYNA Input Files, Hypothetical Accident Conditions**

HAC01 Top End Drop -40°F		
\end2\neg40deg	Run file	Run_end_2_m13a_n40.dyn
	Geometry file	Top_end_drop2_geom13.dyn
	Material file	Matprop-40a_1614_m13.dyn
	Node constraint file	Constrainlid.dyn
HAC02 Bottom End Drop -40°F		
\end1\neg40deg	Run file	Run_end_1_m13a_n40.dyn
	Geometry file	Bot_end_drop1_geom13.dyn
	Material file	Matprop-40a_1614_m13.dyn
	Node constraint file	Constrainlid.dyn





## Design Analyses and Calculation

HAC03 Horizontal Drop on Lid -40°F		
\side3\neg40deg	Run file	Run_side_3_m13a_n40.dyn
	Geometry file	Side_drop3_geom13.dyn
	Material file	Matprop-40a_1614_m13.dyn
	Node constraint file	Constrainlid.dyn
HAC04 Horizontal Drop on Side -40°F		
\side2\neg40deg	Run file	Run_side_2_m13b_n40.dyn
	Geometry file	Side_drop2_geom13.dyn
	Material file	Matprop-40b_1614_m13.dyn
	Node constraint file	Constrainlid.dyn
HAC05 Corner Drop on Lid -40°F		
\corner2\neg40deg	Run file	Run_corner_2_m13a_n40.dyn
	Geometry file	Bot_corner_drop2_geom13.dyn
	Material file	Matprop-40a_1614_m13.dyn
	Node constraint file	Constrainlid.dyn
HAC06 Corner Drop on Side -40°F		
\corner1\neg40deg	Run file	Run_corner_1_m13_n40a.dyn
	Geometry file	Bot_corner_drop1_geom13.dyn
	Material file	Matprop-40a_1614_m13.dyn
	Node constraint file	Constrainlid.dyn
HAC07 Top End Drop 150°F		
\end2\150deg	Run file	Run_end_2_m13a_150.dyn
	Geometry file	Top_end_drop2_geom13.dyn
	Material file	Matprop150a_1614_m13.dyn
	Node constraint file	Constrainlid.dyn
HAC08 Bottom End Drop 150°F		
\end1\150deg	Run file	Run_end_1_m13a_150.dyn
	Geometry file	Bot_end_drop1_geom13.dyn
	Material file	Matprop150a_1614_m13.dyn
	Node constraint file	Constrainlid.dyn
HAC09 Horizontal Drop on Lid 150°F		
\side3\150deg	Run file	Run_side_3_m13a_150.dyn
	Geometry file	Side_drop3_geom13.dyn
	Material file	Matprop150a_1614_m13.dyn
	Node constraint file	Constrainlid.dyn
HAC10 Horizontal Drop on Side 150°F		
\side2\150deg	Run file	Run_side_2_m13b_150.dyn
	Geometry file	Side_drop2_geom13.dyn
	Material file	Matprop150b_1614_m13.dyn





## Design Analyses and Calculation

	Node constraint file	Constrainlid.dyn
HAC11 Corner Drop on Lid 150°F		
\corner2\150deg	Run file	Run_corner_2_m13a_150.dyn
	Geometry file	Bot_corner_drop2_geom13.dyn
	Material file	Matprop150a_1614_m13.dyn
	Node constraint file	Constrainlid.dyn
HAC12 Corner Drop on Side 150°F		
\corner1\150deg	Run file	Run_corner_1_m13_150.dyn
	Geometry file	Bot_corner_drop1_geom13.dyn
	Material file	Matprop150a_1614_m13.dyn
	Node constraint file	Constrainlid.dyn
HAC13 Bottom End Drop, Heavy Load -40°F		
\end1\neg40_heavy	Run file	Run_end_1_m13a_n40_heavy.dyn
	Geometry file	Bot_end_drop1_geom13.dyn
	Material file	Matprop-40a_1650_m13.dyn
	Node constraint file	Constrainlid.dyn
HAC14 Bottom End Drop, Light Load -40°F		
\end1\neg40_light	Run file	Run_end_1_m13a_n40_light.dyn
	Geometry file	Bot_end_drop1_geom13.dyn
	Material file	Matprop-40a_1510_m13.dyn
	Node constraint file	Constrainlid.dyn
HAC15 Horizontal Drop on Side, Heavy Load -40°F		
\side2\neg40_heavy	Run file	Run_side_2_m13b_n40_heavy.dyn
	Geometry file	Side_drop2_geom13.dyn
	Material file	Matprop-40a_1650_m13.dyn
	Node constraint file	Constrainlid.dyn
HAC16 Horizontal Drop on Side, Light Load -40°F		
\side2\neg40_light	Run file	Run_side_2_m13b_n40_light.dyn
	Geometry file	Side_drop2_geom13.dyn
	Material file	Matprop-40b_1510_m13.dyn
	Node constraint file	Constrainlid.dyn
HAC17 5° Shallow Angle Horizontal Drop on Side -40°F		
\slap2-5\neg40deg	Run file	Run_slap_2_5deg_m13b_n40.dyn
	Geometry file	Slap2_5deg_geom13.dyn
	Material file	Matprop-40b_1614_m13.dyn
	Node constraint file	Constrainlid.dyn
HAC18 10° Shallow Angle Horizontal Drop on Side -40°F		
\slap2-10\neg40deg	Run file	Run_slap_2_10deg_m13b_n40.dyn
	Geometry file	Slap2_10deg_geom13.dyn





## Design Analyses and Calculation

	Material file	Matprop-40b_1614_m13.dyn
	Node constraint file	Constrainlid.dyn
HAC19 15° Shallow Angle Horizontal Drop on Side -40°F		
\slap2-15\neg40deg	Run file	Run_slap_2_15deg_m13b_n40.dyn
	Geometry file	Slap2_15deg_geom13.dyn
	Material file	Matprop-40b_1614_m13.dyn
	Node constraint file	Constrainlid.dyn

Table E-3. LSDYNA Input Files, Validation Runs

HAC-V1, HAC Bottom End Drop, 1490 Kg Package Weight, 70°F, GNF-Japan		
\end1\test70	Run file	Run_end_1_m13a_70.dyn
	Geometry file	Bot_end_drop1_geom13.dyn
	Material file	Matprop70a_1490_m13.dyn
	Node constraint file	Constrainlid.dyn
HAC-V2, HAC Horizontal Drop on Lid, 1490 Kg Package Weight, 70°F, GNF-Japan		
\side3\test70	Run file	Run_side_3_m13a_70.dyn
	Geometry file	Side_drop3_geom13.dyn
	Material file	Matprop70a_1490_m13.dyn
	Node constraint file	Constrainlid.dyn
HAC-V3, HAC Bottom End Drop, 1614 Kg Package Weight, 70°F, NTRC CTU-2		
\end1\test70_1614	Run file	Run_end_1_m13a_70.dyn
	Geometry file	Bot_end_drop1_geom13.dyn
	Material file	Matprop70a_1614_m13.dyn
	Node constraint file	Constrainlid.dyn
HAC-V4, HAC 15° Shallow Angle Horizontal Drop on Lid, 1614 Kg Package Weight, 70°F, NTRC CTU-1		
\slap3-15\test70_1614	Run file	Run_slap_3_15deg_m13a_70.dyn
	Geometry file	Slap_3_15deg_geom13.dyn
	Material file	Matprop70a_1614_m13.dyn
	Node constraint file	Constrainlid.dyn





## Design Analyses and Calculation

Table E-4. LSDYNA Input Files, Appendix B Runs

HAC-FA1, Fuel Assembly Evaluation for End Drop Case HAC14		
\Appendix B Fuel Analyses\HAC-FA1_BtmEnd_InCon_480G_HemBalsa	Run file	HAC014_Incon_wood_480G_run.k
HAC-FA2, Fuel Assembly Evaluation for Horizontal Drop Case HAC16		
\Appendix B Fuel Analyses\HAC-FA2_SideDrop_ZV_Incon_380G_RW	Run file	HAC016_Side_Cold_380G_ZV.dyn

Table E-5. LSDYNA Input Files, Appendix C Runs

HAC-SF1, HAC Bottom End Drop, 294 Kg Single Fuel Assembly weight, -40°F		
\end1\neg40_294	Run file	Run_end_1_m13a_n40_294.dyn
	Geometry file	Bot_end_drop1_geom13.dyn
	Material file	Matprop-40a_1224_m13.dyn
	Node constraint file	Constrainlid.dyn
HAC-SF2, HAC Horizontal Drop on Side, 294 Kg Single Fuel Assembly weight, -40°F		
\side2\neg40_294	Run file	Run_side_2_m13b_n40_294.dyn
	Geometry file	Side_drop2_geom13.dyn
	Material file	Matprop-40b_1224_m13.dyn
	Node constraint file	Constrainlid.dyn
HAC-SFA1 Single Fuel Assembly Evaluation for End Drop Case HAC-SF1		
Appendix C SingleFuel Analysis\HAC-SFA1_EndDrop	Run file	HAC014_Fuel_RW_650G_RUN.K
HAC-SFA2, Single Fuel Assembly Evaluation for Horizontal Drop Case HAC-SF2		
\Appendix C SingleFuel Analysis\HAC-SFA2_SideDrop	Run file	HAC016_Side_Cold_533G_ZV.dyn





## Design Analyses and Calculation

Table E-6 Fuel Assembly Reevaluations and Pin Puncture Analysis

HAC-PIN1 Pin Puncture Evaluation For Horizontal Drop		
Appendix D Puncture	Run file	Run_pin3_m13a_n40_TF5.dyn
	Material file	matprop-40a_1614_m13.dyn
	Geometry file	side_pin3_geom13.dyn
	Node constraint file	constrainlid.dyn





## Design Analyses and Calculation

### Appendix F Vendor Data Sheets

#### F.1 Product Data Sheet of Alumina Silicate

8/18/2015

ZIRCAR Ceramics: Alumina-Silica Insulation Type AXL & AXHTM

You are here: [Home](#) > [Products](#) > [Rigid Materials](#) > [Alumina-Silica Products](#) > [AXL & AXHTM](#)

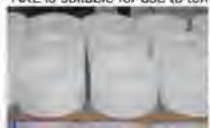


#### Alumina-Silica Insulation Type AXL & AXHTM

##### GENERAL INFORMATION

ZIRCAR Alumina-Silica Insulation Types AXL & AXHTM are strong, rigid refractory structures of high temperature ceramic fibers and high purity inorganic binders. Utilizing an inorganic silica binder system Type AXL and Type AXHTM offer low thermal conductivity, excellent thermal shock resistance and are an effective thermal insulator in numerous thermal process systems.

AXL is suitable for use to temperatures of 1260°C (2300°F). AXHTM is suitable for 1427°C (2600°F). They are noted for their rigid outer surfaces and unbound interiors. In applications where it is necessary to custom cut these materials their original exterior hardness can be easily restored with the use of ZIRCAR Silica Rigidizer Type [SL-RIG](#).



AXL & AXHTM contain no organic binders and produce no smoke or odor when heated.

##### CHARACTERISTICS & PROPERTIES

	AXL	AXHTM
Color	White to tan with light brown areas	
Typical Composition, %		
Al <sub>2</sub> O <sub>3</sub>	38	59
SiO <sub>2</sub>	62	41
Organics	0	0
Bulk Density, gm/cc (pcf)	0.28 (18)	0.26 (16)
Maximum Use Temperature*, °C (°F)	1260 (2300)	1427 (2600)
Linear Shrinkage†, %		
24 hrs. at 1000°C (1832°F)	1.8	-
24 hrs. At 1200°C (2192°F)	2.5	0.75
Thermal Conductivity, W/m²K (BTU/hr ft² °F/in)		
400°C (752°F)	0.10 (0.8)	0.08 (0.6)
800°C (1472°F)	0.17 (1.2)	0.14 (1.0)
1100°C (2012°F)	0.22 (1.5)	0.26 (1.7)
Flexural Strength**, Mpa (psi)	0.17 (26)	0.14 (21)
Compressive Strength**, Mpa (psi) at 10% Compression	0.05 (8.1)	0.03 (4.8)
Durometer**, ASTM 02240, (PTC Type A, Model 306L)	≥20	≥15

\*Maximum use temperature is dependent on variables such as stresses, both thermal and mechanical, and the chemical environment that the material experiences.

\*\* Properties expressed parallel to thickness.

‡ Properties expressed perpendicular to thickness.

##### SUGGESTED APPLICATIONS

Primary thermal insulation in low mass furnaces and thermal process systems operating to 1260°C (2300°F) for AXL and 1480°C (2696°F) for AXHTM.

Backup thermal insulation in furnaces and thermal process systems operating to high temperatures.

<http://www.zircoceramics.com/pages/rigidmaterials/specs/axl.htm>

1/4





## Design Analyses and Calculation

### F.2 PolyPlank EXT Data Sheet



#### PolyPlank® EXT Typical Physical Properties


Property	Test Method	1.7 PCF	2.2 PCF	4 PCF	6 PCF	9 PCF
Type		Type I	Type I	Type III	Type IV	Type V
Density (lb/ft <sup>3</sup> )	ASTM D-3575 SUFFIX W	NLT 1.6	NLT 2.1	NLT 4.3	NLT 5.7	NLT 8.8
Cell Count (cells/inch)	ASTM D-3576	20	24	30	30	30
Compressive Strength <sup>1</sup> (lb/in <sup>2</sup> )	ASTM D-3575 SUFFIX D	6 - 8 14	7 - 9 13 - 16	13 - 20 16 - 24	26 - 30 36 - 43	46 62 - 70
Compressive Set <sup>1</sup> (%)	ASTM D-3575 SUFFIX B	21 16	22 16	9 6	10 7	20 11
Compressive Creep <sup>1</sup> (%)	ASTM D-3575, SUFFIX BB	6	6	0.8	0.8	0.8
Water Absorption <sup>1</sup> (lb/ft <sup>3</sup> )	ASTM D-3575 SUFFIX L	0.06	0.04	0.02	0.02	0.05
Thermal Stability <sup>1</sup> (%)	ASTM D-3575	<2	<2	<2	<2	<2
Service Temperature °F		-30 to +180	-30 to +180	-30 to +180	-30 to +180	-30 to +180

<b>For Anti-Static Product Only</b>			
Electrostatic Decay <sup>1</sup>	EIA 541	seconds	Less Than 2.0
Surface Resistivity <sup>1</sup>	EIA 541	Ohms	>1.00 x 10 <sup>12</sup> <1.00 x 10 <sup>14</sup>
<b>For Fire Retardant Only</b>			
UL Listed	UL 94		Classified HF-2
<b>For Fire Retardant A/S Product Only</b>			
Flame Spread Index <sup>1</sup>	ASTM E-162		<25
Specific Optical Density <sup>1</sup>	ASTM E-662		<100

1. Denotes properties specified in CID-AA-59136, (formerly Federal Specification PPP-C-1752D).

www.Pregis.com  
1-888-828-2850  
Rev. 10.26.05



N° FS1-0025122	Rev. 1.0	TEP - Technical Report	
	Page 174/177		

**ATKINS**

## Design Analyses and Calculation

### F.3 Data Sheet for Zircaloy



TECHNICAL DATA SHEET

### Reactor Grade Zirconium Alloys for Nuclear Waste Disposal

#### ZIRCONIUM ALLOYS

Zirconium is a commercially available refractory metal with excellent corrosion resistance, good mechanical properties, very low thermal neutron cross section, and can be manufactured using standard fabrication techniques. The unique properties of zirconium made ideal cladding material for the U.S. Navy nuclear propulsion program in the 1950's. The initial commercial nuclear power reactors used stainless steel to clad the uranium dioxide fuel due to cost. But by mid-1960 zirconium alloys were the principle cladding material due to the superior neutron economy and corrosion resistance. These same zirconium alloys are available to designers of high level nuclear waste disposal containers as internal components or external cladding. Additional advantages of zirconium alloys for long term nuclear waste disposal include excellent radiation stability and 100% compatibility with existing Zircaloy fuel cladding to alleviate any concerns of galvanic corrosion.

The various zirconium alloy grades used in water-cooled nuclear reactors are also available for nuclear waste disposal components. Reactor grade designates that the material has low hafnium content suitable for nuclear service. The hafnium is typically 0.010% maximum. The American Society for Testing and Materials (ASTM) offers widely recognized grades of zirconium alloys. Zircaloy-2 (Grade R60802) is composed of Zr-1.5%Sn-0.15%Fe-0.1%Cr-0.05%Ni and has been predominantly used as fuel cladding in Boiling Water Reactors (BWR) and as calandria tubing in CANadian Deuterium Uranium (CANDU) reactor types. Zircaloy-4 (Grade R60804) has removed the nickel and increased the iron content for less hydrogen uptake in certain reactor conditions. The alloy is typically used as fuel cladding in Pressurized Water Reactors (PWR) and CANDU reactors. The nominal Zircaloy-4 composition is Zr-1.5%Sn-0.2%Fe-0.1%Cr. Refinements in the ingot homogeneity have allowed tighter control of the alloy elements within the ASTM specification. Controlled Composition Zircaloy offers optimized in-reactor corrosion resistance by adjusting the alloy aim point within the ASTM specification ranges. Controlled Composition Zircaloy-4 has lower tin (1.3%) and higher iron (0.22%) than the standard grade. Zr-2.5Nb (Grade R60904) is a binary alloy with niobium to increase the strength. The alloy has been utilized for pressure tubes in CANDU reactors. Non-reactor grade Zirconium 702 (Grade R60702) has 4.5% maximum hafnium and is also available from Wah Chang.

Zirconium alloys have superior thermal properties compared to other traditional materials in consideration for spent nuclear fuel containers. Zirconium alloys have a thermal conductivity more than 30% higher than stainless steel alloys. The linear coefficient of thermal expansion for Zirconium alloys is nearly one-third the value for stainless steel giving zirconium alloys superior dimensional stability at elevated temperatures. This is an advantage in nuclear waste containers where temperatures could exceed 200°C for hundreds of years.

Zircaloy-2 and Zircaloy-4 have a hexagonal close-packed (HCP) crystal structure at room temperature as an alpha phase. The beta phase is body centered cubic (BCC) and begins to form upon heating to approximately 810°C. The fraction of beta phase increases with temperature until complete transformation to beta phase

ZrAlloy-019

Data are typical and should not be construed as maximum or minimum values for specification or for final design. Data on any particular piece of material may vary from those herein. Copyright Wah Chang 2003.

Page 1 of 4

PO Box 460 • 1600 Old Salem Road NE • Albany, Oregon 97321 • (888) 926-4211 ext. 6977 • Fax (541) 967-6994  
Custserv@wahchang.com • www.alleghtechtechnologies.com/wahchang

Page F3 of F6





## Design Analyses and Calculation



### TECHNICAL DATA SHEET

occurs at approximately 980°C. Zircaloy exhibits anisotropy as a result of the HCP crystal structure. The hexagonal crystal deforms by both slip and twinning to produce a strong preferred orientation of the crystals (texture) during cold working. Typically, cold rolled Zircaloy strip will have a strong normal texture where most of the basal poles of the hexagonal crystals are orientated about 35 degrees to the transverse plane of the strip. The anisotropic properties of Zircaloy strip results in significantly higher yield strength values in the transverse direction. The control of crystallographic orientation allows designers to optimize material properties.

### ZIRCONIUM ALLOY PROPERTIES

Zirconium resists corrosive attack in most organic and mineral acids, strong alkalis, and some molten salts. Solutions of nitric acid ( $\text{HNO}_3$ ), sulfuric acid ( $\text{H}_2\text{SO}_4$ ), and hydrochloric acid ( $\text{HCl}$ ) with impurities of ferric, cupric and nitrate ions generally result in corrosion rates of less than 0.13 mm/a (5 mpy) even at temperatures well above the boiling point curve. A tightly adherent and protective oxide film protects the metal-oxide interface to provide corrosion resistance. An additional benefit for zirconium alloys in long-term geological disposal options is the inert nature of zirconium oxide. Application of zirconium alloys alleviates the concern of nickel and chromium contamination in the ground water in severely corroded spent fuel containers.

Zirconium alloys produced by Wah Chang are available in a wide variety of sizes and shapes including plate, strip, sheet, foil, tubular products, rod, and wire. Wrought products are typically supplied in an annealed and conditioned form. One of our specialties at Wah Chang is the ability to develop alloys to meet your specifications. If you have an unusual alloy or size requirement, call us and we will be happy to help in the developmental process.

### THERMAL NEUTRON CROSS SECTIONS (BARNs)

Magnesium	0.059
Lead	0.17
Zirconium	0.18
Zircaloy-4	0.22
Aluminum	0.23
Iron	2.56
Austenitic Stainless Steel	3.1
Nickel	4.5
Titanium	6.1
Hafnium	104
Boron	750
Cadmium	2,520
Gadolinium	48,890

ZirAlly-019

Data are typical and should not be construed as maximum or minimum values for specification or for final design. Data on any particular piece of material may vary from those herein. Copyright Wah Chang 2003.

Page 2 of 4

PO Box 460 • 1600 Old Salem Road NE • Albany, Oregon 97321 • (888) 926-4211 ext. 6977 • Fax (541) 967-6994  
Custserv@wahchang.com • www.alleghtechtechnologies.com/wahchang





## Design Analyses and Calculation



### TECHNICAL DATA SHEET

#### COMPOSITION (WEIGHT PERCENT)

Name	Zircaloy-2	Zircaloy-4	Zr-2.5Nb
UNS Grade	R60802	R60804	R60904
Tin	1.20-1.70	1.20-1.70	---
Iron	0.07-0.20	0.18-0.24	---
Chromium	0.05-0.15	0.07-0.13	---
Nickel	0.03-0.08	---	---
Niobium	---	---	2.40-2.80
Oxygen	Per P.O.	Per P.O.	Per P.O.
Iron + Chromium + Nickel	0.18-0.38	---	---
Iron + Chromium	---	0.28-0.37	---

#### MAXIMUM IMPURITIES, WEIGHT %

Name	Zircaloy-2	Zircaloy-4	Zr-2.5Nb
Aluminum	0.0075	0.0075	0.0075
Boron	0.00005	0.00005	0.00005
Cadmium	0.00005	0.00005	0.00005
Carbon	0.027	0.027	0.027
Chromium	---	---	0.010
Cobalt	0.0020	0.0020	0.0020
Copper	0.0050	0.0050	0.0050
Hafnium	0.010	0.010	0.005
Hydrogen	0.0025	0.0025	0.0010
Iron	---	---	0.150
Magnesium	0.0020	0.0020	0.0020
Manganese	0.0050	0.0050	0.0050
Molybdenum	0.0050	0.0050	0.0050
Nickel	---	0.0070	0.0070
Nitrogen	0.0080	0.0080	0.0065
Phosphorus	---	---	0.0020
Silicon	0.0120	0.0120	0.010
Tin	---	---	0.0050
Tungsten	0.010	0.010	0.005
Titanium	0.0050	0.0050	0.0050
Uranium (total)	0.00035	0.00035	0.00035

ZrAlly-019

Data are typical and should not be construed as maximum or minimum values for specification or for final design.  
Data on any particular piece of material may vary from those herein. Copyright: Wah Chang 2003.

Page 3 of 4

PO Box 460 • 1600 Old Salem Road NE • Albany, Oregon 97321 • (888) 926-4211 ext. 6977 • Fax (541) 967-6994  
Custserv@wahchang.com • www.alleghtenrytechnologies.com/wahchang





## Design Analyses and Calculation



### TECHNICAL DATA SHEET

#### PROPERTIES OF ZIRCALOY-4

Density	6.55 g/cc (0.237 lbs/cu.-in.)
Coefficient of Thermal Expansion at 25°C	6 µm/m °C (3.3 µin/in.-°F)
Heat Capacity	0.285 J/g-°C (0.07 BTU/lb.-°C)
Thermal Conductivity	21.5 Watts/m-K (149 BTU-in/hr-ft² -°F)
Melting Point	1850°C (3,362°F)
Alpha→Alpha + Beta Phase Transformation	-810°C
Alpha + Beta→Beta Phase Transformation	-980°C
Hardness	89 Rb average
Modulus of Elasticity	99.3 Gpa (14,402 ksi)
Poisson's Ratio	0.37
Shear Modulus	36.2 Gpa (5,249 ksi)

#### MECHANICAL PROPERTIES OF ZIRCALOY-4 ANNEALED 2 MM THICK STRIP

Orientation	Longitudinal		Transverse	
Test Temperature	Room Temp.	288°C	Room Temp.	288°C
<b>Ultimate Tensile Strength,</b>				
MPa	541	271	515	241
(ksi)	(78.4)	(39.3)	(74.6)	(34.9)
<b>Yield Strength,</b>				
MPa	80	152	468	170
(ksi)	(55.2)	(22.0)	(67.8)	(25.6)
<b>Elongation, %</b>	<b>28</b>	<b>43</b>	<b>29</b>	<b>44</b>

#### CORROSION RATE DATA FOR ZIRCALOY-4

Corrosive Media	Concentration %	Temperature °C	Corrosion Rate mm/a (MPY)
HCl	70	160	0.36 (14)
HNO <sub>3</sub>	70	120	0.05 (2)
H <sub>2</sub> SO <sub>4</sub>	70	150	<0.13 (<5)
CuCl <sub>2</sub>	0.1	144	0.03 (1)
FeCl <sub>3</sub>	1	135	0.18 (7)
NaCl	25	250	nil

ZrAljy-019

Data are typical and should not be construed as maximum or minimum values for specification or for final design.  
Data on any particular piece of material may vary from those herein. Copyright Wah Chang 2003.

Page 4 of 4

PO Box 460 • 1600 Old Salem Road NE • Albany, Oregon 97321 • (888) 926-4211 ext. 6977 • Fax (541) 967-6994  
Custserv@wahchang.com • www.alleghenytechnologies.com/wahchang